University of Mosul

College of Engineering

Performance of Reinforced Concrete Beams Retrofitted by Sustainable Ferrocement Mortar

John Mazin Faraj Abbosh

Master's Degree in the Science of Civil Engineering/ Structural Engineering

Supervised by

Assist. Prof. Dr.

Salwa Mubarak Abdullah

Lec. Dr.

Muna Mubarak Abdullah

2025 A.D

1447 A.H

University of Mosul

College of Engineering

Performance of Reinforced Concrete Beams Retrofitted by Sustainable Ferrocement Mortar

A Thesis Submitted by

John Mazin Faraj Abbosh

to

The Council of the College of Engineering, University of Mosul in Partial Fulfillment of the Requirements for the Degree of Master of Science in Civil Engineering/ Structural Engineering

Supervised by

Assist. Prof. Dr.

Salwa Mubarak Abdullah

Lec. Dr.

Muna Mubarak Abdullah

2025 A.D 1447 A.H

Supervisor Certification

We certify that the thesis titled " **Performance of Reinforced Concrete Beams Retrofitted by Sustainable Ferrocement Mortar** " was prepared under our supervision at the University of Mosul as a partial requirement for Master of Science in civil engineering / structures.

Signature:
Name: **Assist. Prof. Dr. Salwa Mubarak Abdullah**
Date: / / 2025

Signature:
Name: **Lec. Dr. Muna Mubarak Abdullah**
Date: / / 2025

Report of the Linguistic Advisor

I certify that the thesis titled " **Performance of Reinforced Concrete Beams Retrofitted by Sustainable Ferrocement Mortar** " is linguistically reviewed and corrected by me and it is ready for discussion from the language point of view.

Signature:
Name: **Assist. Prof. Dr. Ali Hamada Mgallad**
Date: / / 2025

Chairman of the postgraduate studies certification

According to the recommendations presented by supervisors and the Linguistic Corrector, I nominate this thesis for discussion.

Signature:
Name: **Prof. Dr. Moataz A. Al-Obaydi**
Date: / / 2025

Head of the Civil Engineering Department certification

According to the recommendations presented by supervisors, the Linguistic Corrector and the Chairman of the postgraduate studies, I nominate this thesis for discussion.

Signature:
Name: **Assist. Prof. Dr. Baraa J. Mahmood**
Date: / / 2025

Certification of the Examining Committee

We certify, as an examining committee, that we have read the thesis entitled **"Performance of Reinforced Concrete Beams Retrofitted by Sustainable Ferrocement Mortar"** for student (John Mazin Faraj Abbosh) and we discussed it in content on 1 / 9 / 2025 and decide it meets the standard of a thesis for the Degree of Master of science in Civil Engineering / Structures.

Chief of the Committee

Signature:

Name: Assist. Prof. Dr. Sofyan Y. Ahmed

Member

Signature:

Name: Assist. Prof. Dr. Omar M. Abdulkareem

Member

Signature:

Name: Lec. Dr. Eman Kh. Ibrahim

Member (Supervisor)

Signature:

Name: Assist. Prof. Dr. Salwa M. Abdullah

Member (Supervisor)

Signature:

Name: Lec. Dr. Muna M. Abdullah

Certification of the Council of the Engineering College

Approved by the Council of the College of Engineering in its session ( ) which was held on / / 2025 and recommended the following:

Awarding the candidate the M.Sc. degree in Civil Engineering/structures, together with all honors, rights, privileges and responsibility pertaining there.

Signature:

Assist. Prof. Dr. Ayman T. Hameed

Reporter of the Council

/ / 2025

Signature:

Assist. Prof. Dr. Omar M. Hamdoon

Dean of the Engineering College

/ / 2025

Acknowledgements

First of all, I would like to express my thanks and gratitude to God Almighty for his countless blessings and for enabling me to complete this work.

Then, I would like to express my gratitude to **Assist. Prof. Dr. Salwa Mubarak Abdullah** and **Lec. Dr. Muna Mubarak Abdullah**, for their continuous support and advising. Without their great care and scientific honesty, this work would not have been possible.

Also, I would like to extend my sincere thanks to **Assist. Prof. Omar Mohammed Hamdoun**, Dean of the College of Engineering, and **Assist. Prof. Baraa Jabbar Mahmoud**, Head of the Civil Engineering Department. Furthermore, I would like to extend my sincere gratitude to the faculty, who have guided me throughout my studies, especially **Dr. Khalaf Ibrahim**, **Prof. Mutaz Al-Obaidi, Asst. Prof. Dr. Sofyan Younis Ahmed**, and the staff of the Materials Testing Laboratory in the Civil Engineering Department for their invaluable support.

Special thanks to my dear father, my esteemed mother, and my dear brothers and sister for their endless encouragement and support during my academic journey.

I would like to express my love and special thanks to my wonderful wife and daughters, I am so grateful to have you by my side. Your patience, understanding, and great support made this journey possible.

To my dear friends, who have been by my side every step of the way: Your kindness and support mean the world to me, and I truly appreciate highest every one of you.

Abstract

This study aims to investigate the effect of using sustainable ferrocement mortar and assess its efficacy compared to traditional mortar, and also to examine the effect of using different types of mesh reinforcement (welded steel wire mesh and glass fiber mesh) in ferrocement for retrofitted beams with full or U-shape wrapping. The experimental program consisted of three sections: The first section includes the experimental program adapted to study the impact of using supplementary cementitious materials such as silica fume, waste tire rubber, and waste plastic bottles fiber on the mechanical properties of sustainable ferrocement mortar. The results indicated that incorporating 8% silica fume, 5% crumb rubber, and 0.75% plastic fiber provided the optimal mixture. Compared to the traditional mixture at age 28 days, the compressive strength was reduced by 42.7%, flexural strength by 25.26%, and splitting tensile strength by 1.97%.

The second section covered the preloaded beams. Two beams served as reference beams tested to failure under center point loading. The remaining eight beams were preloaded to 70% of the failure load obtained from the reference beams. In the third section, experimental work was conducted to investigate the performance of reinforced concrete beams retrofitted using either traditional or sustainable mortar, reinforced with (welded steel wire mesh or glass fiber mesh). Wrapping configuration (full and U-shape wrapping).

The major results showed that using ferrocement effectively improved the ultimate capacity and delayed the appearance of first crack in the retrofitted beams compared to the reference beams. The highest increase in the ultimate load was (13.6) % for the beam retrofitted on full wrapping, using traditional mortar and reinforced with welded wire mesh. For beams reinforced with glass fiber mesh, the increase was (10.3) % compared to reference beams.

However, the ductility of beams retrofitted using sustainable mortar was higher compared to traditional mortar by (3.6 and 5.4) %. Toughness also increased by (11.9 and 10.6) % for full wrapping beams reinforced with welded wire and glass fiber mesh, respectively.

The stiffness of beam retrofitting, using sustainable mortar reinforced with welded wire mesh on full and U-shape wrapping decrease by (20.3, 15.45) % compared to the traditional mortar. Also, the stiffness for beam reinforcement with glass fiber mesh decreased by (18.75, 13.8) % compared to traditional respectively.

The deflection of the beam retrofitted, using traditional mortar, for both types of reinforcement, was lower than deflection in the references beams and beams retrofitted, using sustainable mortar.

Table of Contents

Abstract I

Table of Contents II

List of Tables VI

List of Figures VIII

List of Abbreviations XI

1. Chapter One: Introduction 1

1.1 Introduction 1

1.2 Retrofitting 2

1.3 Ferrocement 2

1.4 Composite and Construction of Ferrocement 4

1.4.1 Basic Matrix Components 4

1.4.2 Reinforcements 4

1.5 Environmentally Construction Materials 6

1.5.1 Silica Fume 6

1.5.2 Scrap Tires/Crumb Rubber 7

1.5.3 Plastic Bottle Waste 8

1.6 Objectives of Research 9

1.7 Thesis Layout 10

2. Chapter Two: Litreture Review 11

2.1 Introduction 11

2.2 Ferrocement with Metallic Wire Mesh 11

2.3 Ferrocement with Glass Fiber Reinforced Polymer 21

2.4 Environmentally Cement Mortar 23

2.5 Research Gap 26

3. Chapter Three: Experimental Program 27

3.1 Introduction 27

Materials Used 28
3.2 Traditional Materials 28
3.2.1 Cement 28
3.2.2 Fine Aggregate 29
3.2.3 Natural Coarse Aggregate 30
3.2.4 Water 31
3.3 Sustainable Materials 31
3.3.1 Silica Fume 31
3.3.2 Waste Tire Rubber (Crumb Rubber) 33
3.3.3 Waste Plastic Bottle Fiber 34
3.4 Reinforcement Used 35
3.4.1 Steel Reinforcement 35
3.4.2 Mesh Reinforcement 36
Section One: Preparation of Sustainable Mortar 38
3.5 Research Methodology 38
3.5.1 Mixing Procedure 40
3.6 Equipment Used to Measure Strength of Mortar 42
3.6.1 Universal Compressive Test Equipment 42
3.6.2 Universal Tensile Testing Equipment 42
3.6.3 Flexural Testing Machine 42
Section Two: Preloaded Reinforced Concrete Beams 43
3.7 Specimen Details 43
3.8 Wooden Formwork 44
3.9 Installation of Steel Reinforcement 44
3.10 Installation of Strain Gauges 45
3.11 Preparation of Specimens 47
3.11.1 Concrete Mixture Proportion 47
3.11.2 Casting of Reinforced Concrete Beams 47

3.12 Mechanical Properties of Hardened Concrete 49
3.12.1 Concrete Compressive Strength 49
3.12.2 Concrete Splitting Tensile Strength 49
3.12.3 Concrete Flexural Tensile Strength Test 49
3.13 Testing Procedure of Beams 50
3.14 Preloading of Specimens 51
Section Three: Retrofitting Reinforced Concrete Beams 52
3.15 Specimen Details 52
3.16 Wrapping of Mesh Reinforcement 55
3.17 Application of Retrofitting Mortar 56
3.17.1 Retrofitting Beams Using Traditional Mortar 56
3.17.2 Retrofitting Beams Using Sustainable Mortar 57
3.18 Fixing the Strain Gauges on Ferrocement Surface 58
3.19 Curing and Painting 59
3.20 Testing Set-Up 60
3.21 Prediction of Failure Load for Retrofitted Beams 60
4. Chapter Four: Result and Discussion 61
4.1 Introduction 61
4.2 Results of Traditional and Sustainable Mortar 62
4.2.1 Test Results of Cement Replacement by Silica Fume 62
4.2.2 Test Results of Sand Replacement by Crumb Rubber 64
4.2.3 Test Result of Adding Waste Plastic Bottle Fiber 66
4.2.4 Optimum Mixture 69
4.2.5 Cost Comparison 69
4.3 Results of Preloaded Specimens 70
4.3.1 Mechanical Properties of Concrete Mixture 70
4.3.2 Results of the Control and Preloaded Beams 70
4.3.3 Load-Deflection Curve of the Preloaded Beams 71

4.3.4 Load-Strain Curve of the Preloaded Beams 72
4.3.5 Mode of Failure of the Preloaded Beams 73
4.4 Results of Retrofitted Specimens 74
4.4.1 Load - Midspan Deflection Curve 75
4.4.2 Comparison and Discussion of Load-Deflection Curves 77
4.4.3 Load-Strain Curves in Steel Reinforcement 80
4.4.4 Comparison and Discussion of Load Strain Curve 81
4.4.5 Strain in Concrete 82
4.4.6 Crack Pattern and Mode of Failure 83
4.4.7 Ductility 87
4.4.8 Toughness 88
4.4.9 Stiffness 90
4.5 Effect of Key Parameters on Beam Behavior 91
4.5.1 Effect of Wrapping Types: 91
4.5.2 Effect of Mortar Types: 93
4.5.3 Effect of Reinforcement Types: 95
4.6 Experimental and Theoretical Calculation of Ultimate Load 97
4.7 Estimating Stresses by Experimental Calculations 98
5. Chapter Five: Conclusion and Recommendations 99
5.1 Introduction 99
5.2 Recommendation for Future Works 101
References 102
Appendix- A: Analysis of Simply Supported Beams A-1
Appendix- B: Mix Design B-1
Appendix- C: Estimate the Ultimate Load by Theoretical Calculations C-1
الخلاصة ١

List of Tables

Table (3.1): Chemical Properties of Cement 28
Table (3.2): Physical Properties of Cement 29
Table (3.3): Sieve Analysis of the Fine Aggregate 30
Table (3.4): Physical Properties of Fine Aggregates 30
Table (3.5): Sieve Analysis of Coarse Aggregate 30
Table (3.6): Physical Properties of Coarse Aggregate 31
Table (3.7): Physical Properties of Silica Fume 31
Table (3.8): Chemical Composition of Silica Fume 31
Table (3.9): Sieve Analysis of Waste Tire Rubber 33
Table (3.10): Physical Properties of Waste Plastic Bottle Fiber 34
Table (3.11): Properties of Reinforcing Steel Bars 35
Table (3.12): Properties of Welded Steel Wire Mesh and Glass Fiber Mesh 36
Table (3.13): Mix Proportion of Silica Fume (SF) Mortar 40
Table (3.14): Mix Proportion of Crumb Rubber (CR) Mortar 40
Table (3.15): Mix Proportion for Adding Plastic Fiber (PF) to Mortar 40
Table (3.16): Properties of Strain Gage According to Manufacturer . 46
Table (3.17): Concrete Mix Proportion 47
Table (3.18): Definition of the Symbol Used in Ferrocement 53
Table (3.19): Groups of Specimens 54
Table (3.20): Properties of Concrete Strain Gages 59
Table (3.21): Theoretical Ultimate Load of Retrofitted Beams 60
Table (4.1): Strength of Mortar at 7 and 28 Days for Different Silica Fume Replacement Ratios 63

Table (4.2): Strength of Mortar at 7 and 28 Days for Different Crumb Rubber Replacement Ratios 64
Table (4.3): Strength of Mortar at 7 and 28 Days for Different Plastic Fiber Addition Ratios 67
Table (4.4): Cost Comparison 69
Table (4.5): Mechanical Properties of Concrete Mixture 70
Table (4.6): Experimental and Theoretical Results of All Preloaded Beams 70
Table (4.7): Test Results for the Retrofitted Beams 75
Table (4.8): Strain of Longitudinal Reinforcement at Yield and Ultimate Loading of Retrofitted Beams 81
Table (4.9): Mode of Failure of All Tested Beams 84
Table (4.10): Stiffness of All Tested Beams 90
Table (4.11): Comparison Between Theoretical and Experimental Ultimate Loads 97
Table (4.12): Result of Experimental Strain and Stress in Steel Bars 98
Table (B.1): Properties of Aggregate B-1

List of Figures

Figure (1.1): Mortar Being Applied to Wire Mesh 3
Figure (1.2): Types of Metallic Wire Mesh 5
Figure (1.3): Types of Non-Metallic Mesh 5
Figure (1.4): Silica Fume 7
Figure (1.5): Rubber Waste 8
Figure (1.6): Type of Plastic Waste 9
Figure (2.1): Method of Application Ferrocement Laminate 12
Figure (2.2): Variation of First Crack Load and Ultimate Loads 13
Figure (2.3): Load Versus Deflection Curves for the (RC) Beams 14
Figure (2.4): Mid-Span Load Versus Strain Curve for Control Beam and Ferrocement Beam 15
Figure (2.5): Shear Reinforcement Using Wire Mesh Layer 16
Figure (2.6): Details of Beam Specimens 17
Figure (2.7): Load-Deflection Curve for Each Case 18
Figure(2.8): First Crack and Ultimate Load for Strengthened Beams ...19
Figure (2.9): Cross Sections of Control and Strengthened Beams 20
Figure (2.10): Load-Deflection Curve of All Test Specimens 21
Figure (2.11): Ultimate Load of All Tested Beams 22
Figure (2.12): Density of Hardened Cement Mortar 24
Figure (2.13): Strength at 90 Days for Reinforced HPM Mortar 25
Figure (3.1): Tests of Physical Properties of Cement 29
Figure (3.2): Activity Index Process 32
Figure (3.3): Silica Fume Activity Index Process 32
Figure (3.4): Waste Tire Rubber 33
Figure(3.5): Process to Produce Waste Plastic Fiber and its Dimension 34
Figure (3.6): Steel Reinforcement Specimens and Testing Machine 35

Figure (3.7): Stress-Strain Relationship of Steel 36
Figure (3.8): Testing for the Wire Mesh Reinforcement 37
Figure (3.9): Stress – Strain Curve for Welded Steel Wire Mesh and Glass Fiber Mesh 37
Figure (3.10): Dimension of Bracket 38
Figure (3.11): Research Methodology 39
Figure (3.12): Weighing, Casting and Curing of Specimens 41
Figure (3.13): a. Universal Compressive Test Equipment, b. Universal Tensile Testing Machine, c. Flexural Testing Machine 42
Figure (3.14): Longitudinal and Cross Section Details of the Beam 43
Figure (3.15): Wooden Formworks 44
Figure (3.16): Fixing Steel Reinforcement 45
Figure (3.17): Strain Gauges Location and Orientation 46
Figure (3.18): Strain Gauges Installation Process 46
Figure (3.19): Casting of the (RC) Beams 48
Figure (3.20): a. Testing of Compressive Strength, b. Splitting Tensile Machine Test, c. Flexural Tensile Strength Test 49
Figure (3.21): Test Setup 51
Figure (3.22): Preloaded Beams 51
Figure (3.23): Types of Wrapping Beams 53
Figure (3.24): Wrapping of Beams with Welded Steel and Glass Fiber Mesh for Fully Wrapped (A) and U-Shape Wrapped (B) 56
Figure (3.25): Details of Fixing Wire Mesh 56
Figure (3.26): Process of Retrofitting Using Traditional Mortar 57
Figure (3.27): Process of Retrofitting Using Sustainable Mortar 58
Figure (3.28): Concrete Strain Gauges and Installation Process 59
Figure (3.29): Curing and Painting the Beams 59

Figure (4.1): Strength of Mortar at 7 and 28 Days for Different Silica Fume Replacement Ratios.....64
Figure (4.2): Strength of Mortar at 7 and 28 Days for Different Crumb Rubber Replacement Ratios.....65
Figure (4.3): Strength of Mortar at 7 and 28 Days for Different Plastic Fiber Addition Ratios.....67
Figure (4.4): Load-Midspan Deflection Curves for Control Beams.....71
Figure (4.5): Load-Midspan Deflection Curves for Preloaded Beams...72
Figure (4.6): Load-Strain (FS1) Curves for Control Beams.....72
Figure (4.7): Load-Strain Curves (FS1) for Preloaded Beams 73
Figure (4.8): Failure Modes and Crack Patterns of Control and All Preloaded Beams.....74
Figure (4.9): Load-Midspan Deflection Curves for All Groups with Control Beams.....77
Figure (4.10): Load-Midspan Deflection Curves of Various Groups and Control Beams.....79
Figure (4.11): Comparison of Load- Midspan Deflection Curves for All Beams with Control Beam 80
Figure (4.12): Comparison Between Load-Strain Curves of All Groups and Control Beam 82
Figure (4.13): Process of Propagation of Cracks in All Beams.....83
Figure (4.14): Crack Patterns and Modes of Failure for All Group 86
Figure (4.15): Ductility Index for the Tested Beams.....88
Figure (4.16): Calculation of Toughness 89
Figure (4.17): Toughness for the Tested Beams.....89
Figure (4.18): Ultimate Load for All the Tested Beams.....96
Figure (A-1): Details of Beam A-1
Figure (C-1): Stress-Strain Distribution Beam with Ferrocement.....C-2

List of Abbreviations

Abbreviation	Definition
ACI	American Concrete Institute
ASTM	American Standards for Testing Materials
FE	Finite Element
F.M	Fineness Modulus
GFRP	Glass fiber-reinforced polymer
WWM	Welded Wire Mesh
IQS	Iraqi Standards specifications
LVDT	Linear Variable Differential Transducer
M.A.S	Maximum Aggregate Size
RC	Reinforced Concrete
S.G	Specific Gravity
w/c	Water/Cement ratio
I.D	Iraqi Dinar
SBR	Styrene-butadiene rubber

Notations

Symbol	Definition
μ	Ductility Index
δ	Deflection
Ac	Area of the concrete section
As	Area of steel
$\beta 1$	Factor is reduced of strength above 28 MPa, but is not taken less than 0.65
h	Height
b	Width
d	Effective depth
εcu	Ultimate strain in concrete
$f'c$	Concrete compressive strength
fu	Ultimate strength of reinforcing steel

*f*y	Yield strength of reinforcing steel
E	Modulus of Elasticity
ρ	Reinforcement ratio
ρb	Balance reinforcement ratio
Mu	Ultimate moment
Mn	Nominal flexural strength at section
Pu	Ultimate Load
I	Moment of inertia
Vn	Nominal shear strength
Vc	Concrete shear strength
Vu	Factored shear force
σ	Stress of RC beam
M	Bending moment of RC beam
c	Distance from compression zone to neutral axis
*f*r	Modules of rupture
Mr	Cracking moment
a	Depth of equivalent rectangular stress block
Ø	Strength reduction factor
Pcr	First cracking load

Chapter 1

Introduction

Chapter One
Introduction

1.1 Introduction

Concrete is a widely used building material due to its strength and durability. However, its performance can deteriorate over time due to various factors. Improper design, critical loads, and environmental conditions cause a reduction in the load-carrying capacity of reinforced concrete structures. This issue can be addressed by strengthening techniques, addressing material degradation, or implementing additional safety procedures [1].

Most reinforced concrete structural members experience bending forces over their service life due to various types of sustained loads. Beam elements often exhibit failure due to their weak flexural performance [2]. To prevent the flexural failure of reinforced concrete beams, their performance can be improved by increasing tensile strength along the tension face (often the soffit), enhancing ductile deformation during bending. Among the various strengthening methods, Jacketing is the main technique employed to augment the flexural strength of reinforced concrete beams [3].

When choosing strengthening materials, it is important to consider their bonding capabilities to the existing structure, as well as their strength, durability, and cost sustainability. Currently, commonly used flexural strengthening materials include plates of steel, ferrocement, fiber-reinforced polymers, epoxy polymers, and textile fibers [4], [5].

1.2 Retrofitting

Retrofitting involves improving the load-bearing capacity of older structures that were initially designed for lower service loads than those they currently endure. Other applications include seismic retrofitting, alterations in building usage, modifications of codal provisions, enhancements in overloading capacity, improving wear and tear, and the repair of damaged structures. Severe weather conditions can accelerate the deterioration of concrete structures over time [6]. Retrofitting can be classified into two primary types: global and local. Global retrofitting procedures are carried out by the incorporation of shear walls, wing walls, wall thickening, bracing, and mass reduction. Local retrofitting focuses on strengthening of individual footings, such as beams, columns, and joints [7]. Retrofitting is performed using various materials, including ferrocement, fiber reinforced polymer (FRP) and steel [8].

1.3 Ferrocement

Ferrocement is a thin-walled reinforced concrete consisting of cement mortar reinforced by multiple layers of continuous, relatively small wire mesh, as shown in Figure (1.1). The mesh can be constructed from metal or any other material [9]. Ferrocement can be used in the construction of domes, boats, and water tanks. Ferrocement is a special type of reinforced concrete, with some differences between them. Unlike conventional reinforced concrete, which uses large steel bars, ferrocement uses fine reinforcing meshes, such as woven wire meshes, welded wire meshes, expanded metal meshes, or fine bars. These meshes are completely immersed in the mortar matrix. Ferrocement can

be produced with a thickness of (25 mm) and include a protective cover to prevent the reinforcement from corrosion [10].

Figure (1.1): Mortar Being Applied to Wire Mesh

Ferrocement jacketing is widely used due to its many benefits, including lesser dead load due to small thickness, high tensile strength, less crack width, low cost, water resistance, ease of use, and long durability. In structural repairing, different strengthening methods are used, but the plate bonding technique is the most common. For this method, plates made of Carbon Fiber-Reinforced Polymer (CFRP), Glass Fiber-Reinforced Polymer (GFRP), ferrocement, and other materials are glued to the exterior of the structural component to improve its strength.

Recently, Ferrocement sheets gained popularity as retrofitting materials owing due to their availability, cost-effectiveness, durability, and the ability to mold them into various shapes without need for formwork [11].

1.4 Composite and Construction of Ferrocement

1.4.1 Basic Matrix Components

Ferrocement matrix consists of a mixture of cement, well-graded sand, water, and potentially other admixtures, including silica fume and superplasticizer. Like concrete, the matrix must possess sufficient workability, high strength , and low permeability [12].

The properties of basic matrix according to ACI 549R-18 [9] were:

- Sand must pass through a No. 8 (2.36 mm) sieve.
- Ordinary Portland cement is commonly used.
- Water must meet potable quality standards.
- Sand cementitious materials ratio ranges from 3:1 to 3:2 by weight.
- The water to cementitious materials ratio (w/cm) ranges from 0.35 to 0.6, with the lower limit achievable only through admixtures.

1.4.2 Reinforcements

- **Skeletal Steel**

Skeletal steel is often used in ferrocement construction as welded wire fabric or meshes of steel wires, bars, or strands [13]. If an armature is employed, it is typically constructed from plain or corrugated steel bars with a diameter of (6 to 10 mm). However, in developing countries, bamboo or other natural materials have also been employed as an alternative [14].

- **Steel Wire Meshes**

The main part of ferrocement is the fine wire mesh reinforcement. The number of mesh layers determines the composite thickness and strength. The wire diameter ranged from (0.5 - 1.5) mm, and the mesh opening size was from (6 - 25) mm [13]. The main types

of wire meshes, include: a. welded wire mesh; b. Woven square mesh; c. Chicken wire mesh d. Expanded metal mesh; [15] as shown in Figure (1.2).

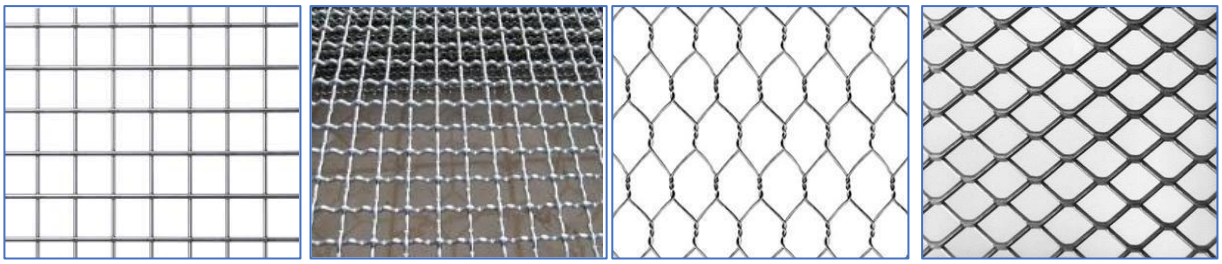

A. Weld Wire Mesh. B. Woven Wire Mesh. C. Chicken Mesh. D. Expanded Metal.

Figure (1.2): Types of Metallic Wire Mesh [15]

- **Non-Metallic Meshes**

Non-metallic meshes can be made from polypropylene mesh, glass fiber reinforced polymer sheet (GFRP), woven or knitted aramid fibers [9] as shown in Figure (1.3). GFRP materials are increasingly used for retrofitting and repairing deficient infrastructures, whose experienced significant strength and stiffness losses are due to harsh environmental conditions, including humidity, saltwater, and alkali solutions. GFRP exhibits a high modulus of elasticity, increased flexural and shear strength, as well as an increased resistance to corrosion, fatigue, and damping [16].

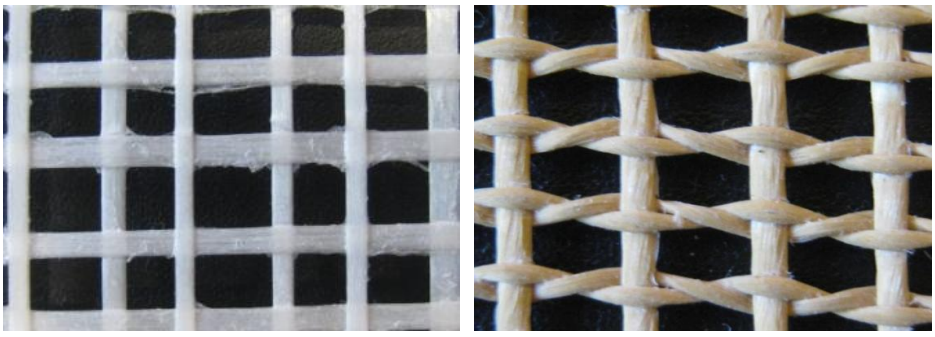

A. Glass Fiber Mesh. B. Woven or Knitted Aramid.

Figure (1.3): Types of Non-Metallic Mesh [17]

1.5 Environmentally Construction Materials

Concrete is widely utilized in construction. The decreasing amount of conventional concrete mix resources is a significant concern. The demand for these products also increases construction costs. The cement manufacturing process has a negative impact on the environment due to the decline in non-renewable natural resources. The cement manufacturing process also leads to the emission of dust and carbon dioxide into the atmosphere, the cement production process results in the release of approximately 0.8 ton of carbon dioxide to the atmosphere which increases pollution rates [18]. Incorporating recycled materials into concrete reduce resources consumption, reducing energy consumption resulting from cement production, also reducing harmful emissions, and reduce the amount of landfill waste. Recycled plastic, rice husk ash, waste glass, and wood ash can be used as a sustainable alternative to the conventional material. Among these, the disposal of automobile tires has a significantly positive impact on the environment [19].

1.5.1 Silica Fume

Silica fume is a byproduct of silicon metallic or ferrosilicon alloys production consists of spherical particles approximately one-hundredth the size of cement particles (0.1 μm) as shown in Figure (1.4). Fineness particle of silica fume was from (13000-30000) m^2/kg. It is fine particles significantly increase concrete compressive strength, improve its durability, and reduce its permeability due to pozzolanic reaction between silica fume and calcium hydroxide ($Ca(OH)_2$), creates additional calcium-silicate hydrate (C-S-H) that forms in the voids

within hardened cement paste, producing a very dense structure. Silica fume particles have a high surface area and require more water for a given workability than Portland cement, which can be offset by using a water-reducing admixture [20].

Figure (1.4): Silica Fume

1.5.2 Scrap Tires/Crumb Rubber

Waste recycling is a sustainable alternative, and the civil construction sector provides a promising opportunity to incorporate these materials as fine or coarse aggregate [21]. Waste tire, as shown in Figure (1.4) can be used as blocks in the formation of concrete and mortars. Tires serve as a prime example of the abundance of waste commonly found in both landfills and rivers. They can cause serious problems such as soil and river pollution [22]. The performance of rubber concrete is significantly affected by the rubber content. The use of rubber particles improves workability, ductility, and toughness. Crumb rubber can replace up to 50% of aggregate; however, using it results in a reduction of strength. This is because crumb rubber has lower strength and modulus of elasticity than natural aggregate [23].

Figure (1.5): Rubber Waste [24]

1.5.3 Plastic Bottle Waste

Waste plastics are utilized as fibers, aggregates, and binders in concrete and mortar components as shown in Figure (1.5) [25].

Many polyethylene terephthalate (PET) bottles utilized for beverage containers are discarded after a single use, with the disposed bottles being sent to landfills and burned, resulting in significant environmental issues. PET is a transparent polymer characterized by high mechanical properties and strong chemical resistance [26].

Researchers have investigated the reuse of waste plastics as construction materials, which offers significant economic and environmental advantages. Studies have demonstrated the feasibility of incorporating waste plastics, such as polypropylene (PP), shredded and recycled plastic waste [27], and polyethylene terephthalate (PET) [28], into concrete and mortar. Based on the previous studies, the proportions of plastic fiber that can be used ranged between 0.25% and 1.5% of the volume of the concrete mix or cement matrix in different shapes and

sizes. Fibers made from polyethylene terephthalate bottles can improve the mechanical properties of concrete, such as its tensile strength, compressive strength, and flexural strength [29]. In mortars, these fibers act as uniformly distributed reinforcements, reducing crack formation caused by plastic shrinkage [30].

A. Plastic Particles [26]. B. (PET) Recycled Fibers [30].

Figure (1.6): Type of Plastic Waste

1.6 Objectives of Research

The main objectives of this study are as follows:

1. To investigate the effect of incorporating sustainable materials into ferrocement mixes and to assess their efficacy compared to traditional ferrocement matrices. This includes adding recycled waste materials, such as silica fume, waste tire rubber and waste plastic bottle fiber.
2. To study the performance of using two layers of various mesh reinforcement, including welded wire mesh and glass fiber mesh in ferrocement mortar for retrofitting reinforced concrete beams.
3. To examine the role of externally applied ferrocement layers (full wrapping on four sides and U-shape wrapping on three sides) in retrofitting damaged RC beams by evaluating the improvement in ultimate load and deflection compared to the control beams.

1.7 Thesis Layout

Chapter One includes a general introduction to the problems experienced by reinforced concrete beams that lead to reducing their resistance, along with methods for strengthening them. It also presents a brief explanation of the strengthening method by using ferrocement composed of traditional or sustainable materials. Additionally, this chapter introduces the objectives of this study and the thesis layout.

Chapter Two reviews the most relevant studies related to using ferrocement reinforced with metal wire mesh and glass fiber wire mesh to retrofit reinforced concrete beams. It also includes studies of sustainable ferrocement mortar. In addition, this chapter introduce the knowledge gap.

Chapter Three presents the experimental program adopted in this study. It includes the results of the laboratory tests on the materials used, identifying the optimal ferrocement mixture containing sustainable materials, and the process of specimen preparation, casting, curing, and testing.

Chapter Four presents test results in details through providing the necessary tables and figures, along with a discussion of the main findings.

Chapter Five presents the conclusions, recommendations, and suggestions for future work.

Chapter 2

Literature Review

Chapter Two
Literature Review

2.1 Introduction

This chapter reviews some of the most relevant studies on using ferrocement reinforced with metal wire mesh and glass fiber mesh to retrofit or strengthen reinforced concrete beams. It also highlights studies of sustainable cement mortar. Additionally, this chapter introduces the research gap that needs further investigation.

2.2 Ferrocement with Metallic Wire Mesh

Khan et al. [31] studied the effectiveness of ferrocement reinforcement technologies by changing the number of layers of wire mesh, development length, and application method. Three different application methods were conducted: cast in situ, precast ferrocement laminate A, and precast ferrocement laminate B, as shown in Figure (2.1). Two-point load tests were carried out on ten reinforced concrete beams. The results show that strengthening the beams with a cast in situ ferro-mesh layer was the most effective method, while precast ferrocement laminate B is not only simple but also promising. It helped improve the stiffness, ductility, and load-carrying capacity. Also, Ferro-mesh's three layers were stiffer and capable of supporting a larger load compared to the two layers.

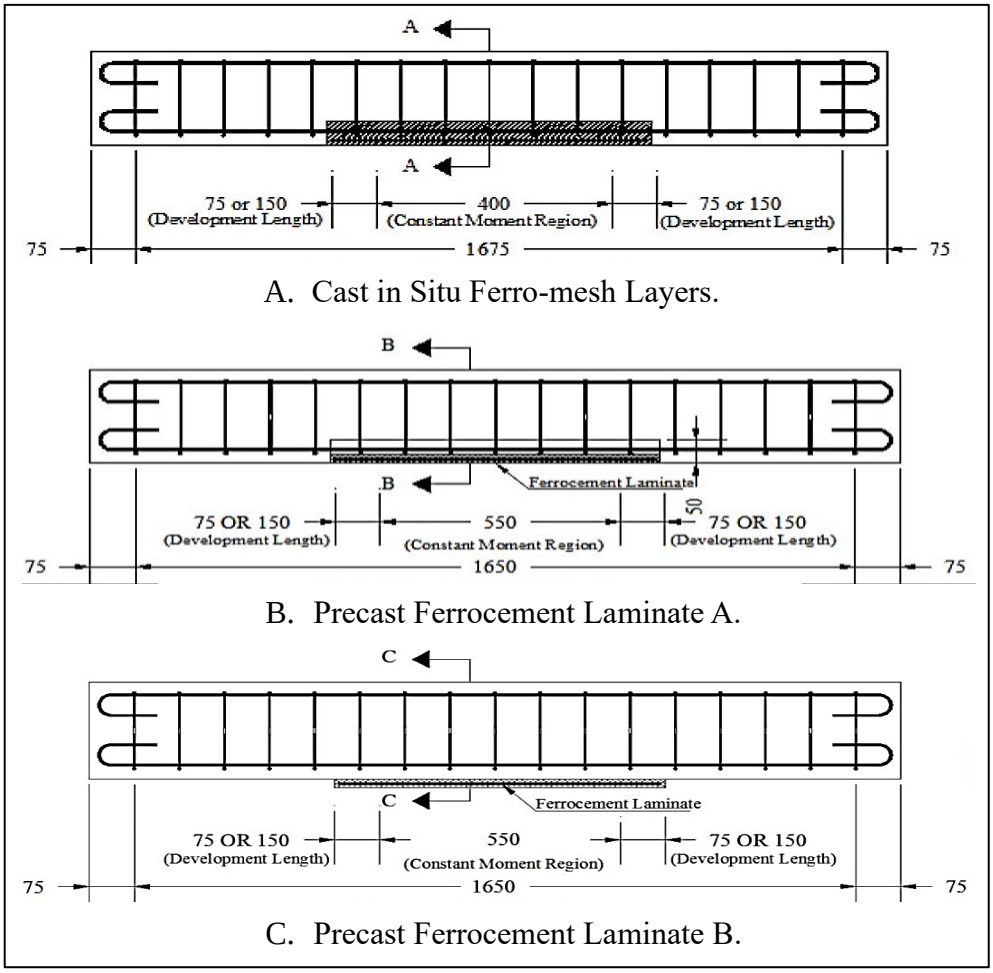

Figure (2.1): Method of Application Ferrocement Laminate [31]

Alam et al. [32] studied the effect of using ferrocement materials with different numbers of wire mesh to retrofit reinforced concrete beams (RC). A total of sixteen (RC) beams were cast and tested under a three-point bending flexural test. Four beams were designated as control beams while the remaining twelve beams were divided into three categories; FRB1 (one layer of wire mesh with 12mm thickness), FRB2 (two layers of wire mesh with 16mm thickness), and FRB3 (three layers of wire mesh with 20mm thickness). The beams were retrofitted on three sides. The study concludes that the first cracking load and ultimate load increase with the increase of both the number of mesh layers and the thickness as shown in Figure (2.2). The study revealed that the

deflections and crack widths of the beams retrofitted with ferrocement were less compared to the control beams.

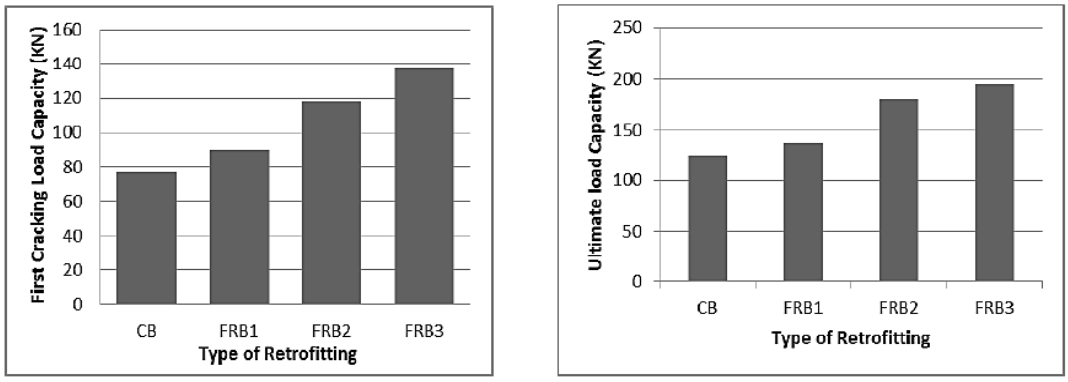

A. First cracking Load. B. Ultimate Failure Load.

Figure (2.2): Variation of First Crack Load and Ultimate Loads [32]

Fahmy et al. [33] investigated the development of conventional (RC) beams by casting and testing beams containing different core materials (normal concrete, recycled concrete, and concrete brick). These beams were made of U-shaped ferrocement. The experimental program included thirty beams. Both expanded and welded steel mesh were utilized with single layers and double layers. Two forms of shear connectors were used: Mechanical and adhesive bonding. The results show that the tested beams exhibited high ultimate loads and crack resistance compared with control beams. Figure (2.3) shows the load-deflection curve for the reinforced beam. The results showed that the specimen with concrete core (WSC) and recycled concrete core (WSR) reinforced with a single-layer welded wire mesh have comparable stiffness. Both specimens reached a deflection of around 20 mm at their ultimate load. Specimens of concrete core (ESC) and recycled concrete core (ESR) with single-layer expanded wire mesh also showed similar stiffness. They reached deflections of approximately 20.1 and 19.6 mm at their ultimate loads, respectively.

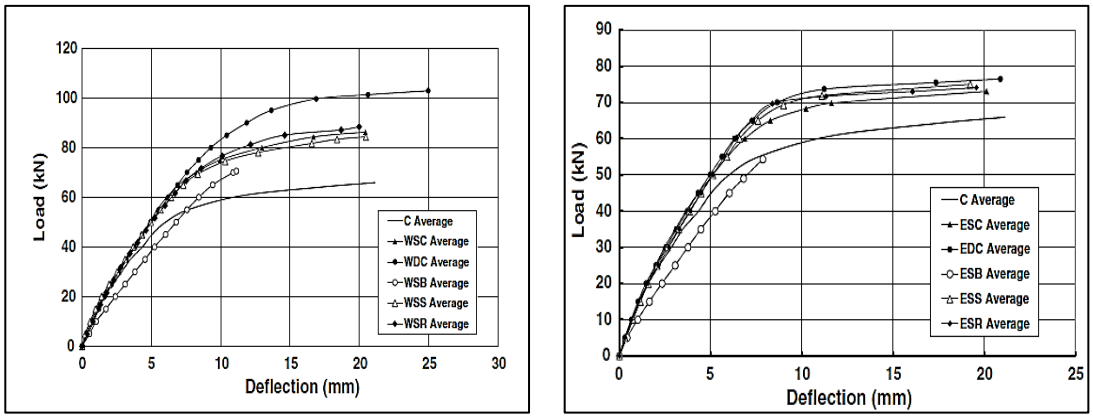

A. Welded Wire Mesh. B. Expanded Wire Mesh.

Figure (2.3): Load Versus Deflection Curves for the (RC) Beams [33]

Makki [34] studied the performance of RC beams strengthened with ferrocement. Ten RC beams were cast and tested. This study examined various characteristics, including shear reinforcement, different diameters of wire mesh, and two rehabilitation techniques: repairing and strengthening. The beams were subjected to a load of 50% and 70% of their ultimate load. The wire mesh was attached mechanically with bolts. The results exhibited an increase in the ultimate load by 50.94% to 125% using the repairing technique and 69.8% to 175% using the strengthening technique. Also, increasing the diameter of the wire mesh caused an increase in the ultimate load for beams with or without shear reinforcement.

Vijayalakshmi et al. [35] investigated the behavior of reinforced concrete beams modified with ferrocement to improve beam strength in flexural and shear. Three beams were cast and tested under a four-point load. Ferrocement mix (1:1.5/0.35) with 25mm thickness was used. The results showed that ferrocement is an efficient and cost-effective technique for strengthening reinforced concrete beam and to support

sustainable development. The results also showed that the deflection in the ferrocement beam was less compared to the control beam. Also, the strain in the ferrocement beams was less than the control beam. Under 16 kN load the strain value was (33.78×10^{-6}) for the control beam and (11×10^{-6}) in the ferrocement beam as shown in Figure (2.4).

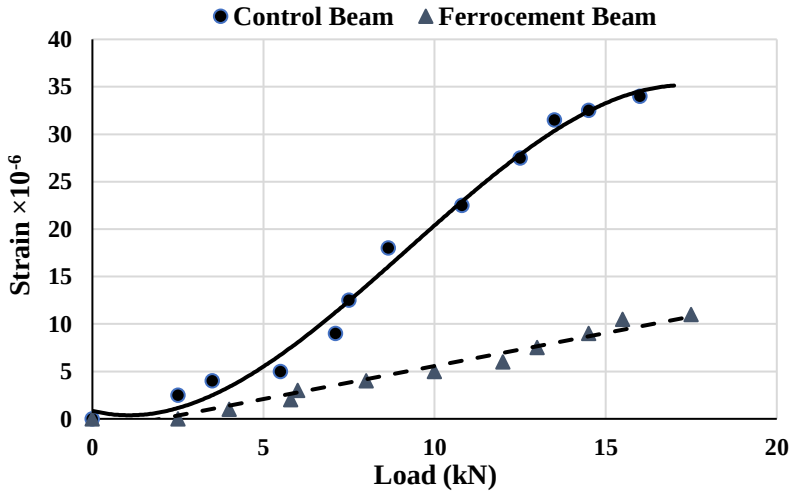

Figure (2.4): Mid-Span Load Versus Strain Curve for Control Beam and Ferrocement Beam [35]

El-Sayed et al. [36] investigated the shear behavior of beams reinforced with ferrocement. The primary parameters studied were stirrups (shear reinforcement) and wire mesh. The wire mesh was replaced with stirrups due to weight considerations as shown in Figure (2.5). The experimental program consisted of seven beams, one of them represent control beam, three beams used shear reinforced expanded wire mesh and the last three beams used welded wire mesh. These beams were tested under two-point loading. The results showed that the beam with welded wire mesh exhibited an increase in shear capacity compared to the reference beam and expanded wire mesh. Adding layers of wire meshes enhanced the ultimate load and shear capacity, also the results exhibited an increase in the stiffness and a decrease in the deflection of

the ferrocement beams. Beams reinforced with steel meshes exhibited a higher quantity of cracks with narrower widths compared to those strengthened with traditional steel reinforcement.

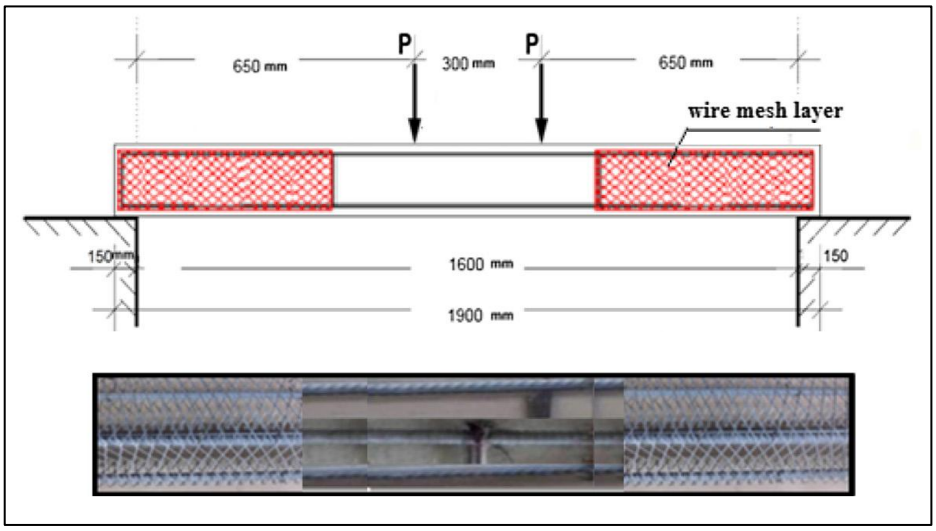

Figure (2.5): Shear Reinforcement Using Wire Mesh Layer [36]

Miah et al. [37] investigated the effectiveness of ferrocement technology in enhancing the performance of reinforced concrete beams constructed with low-strength concrete. The beams were constructed, using nontraditional concrete (burned clay bricks were used as a coarse aggregate). The ferrocement mortar mix was 1:2/0.45 with a thickness of 25mm. Several load configurations were utilized: (a) two-point loads were placed at one-third of the span, (b) two-point loads were located near the support, (c) two-point loads were located near the midpoint of the span, (d) one load was adjacent to the support and one load was in the middle of the span. Experimental results showed that asymmetric loading decreases overall strength capacity and increases deformation. Reinforced ferrocement beams incorporating welded wire mesh demonstrate augmented ultimate load capacity and improved ductility.

Sirimontree et al. [38] investigated the flexural performance of beams enhanced with ferrocement. Three beams were prepared to carry out the experiments. The initial beam serves as a reference (BR), the second beam (BF) was reinforced with ferrocement without shear connectors, and the third beam (BFS) was reinforced with ferrocement and shear connectors. The details of these beams are illustrated in Figure (2.6). All specimens undergo four-point bending test. The results showed that the flexural strengths of the second and third beams exceed that of the reference specimen by about 79%. The ductility of the specimen (BFS) with shear connectors was considerably more than that of the reference beams. The results also showed an enhancement in the ultimate load for beams strengthened with ferrocement without and with shear connectors by 72.5% and 79%, respectively. In addition, the deflection decreased in the specimen with shear connectors (BFS) by 26%.

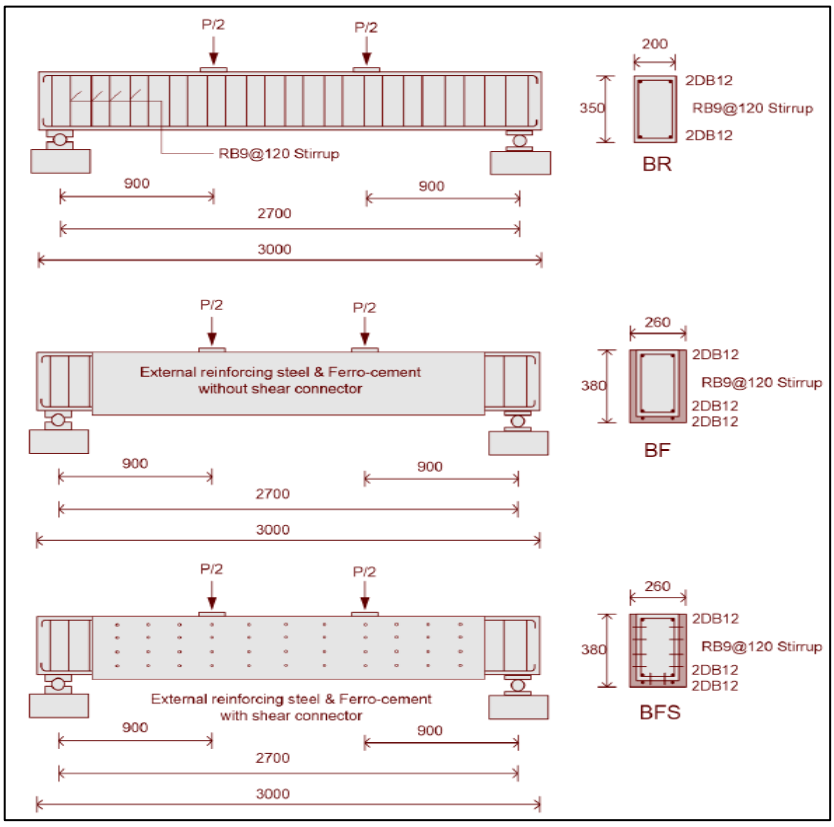

Figure (2.6): Details of Beam Specimens [38]

Pragadhish et al. [39] examined the flexural performance of pre-damaged beams with various ferrocement layouts. Total of five beams were constructed and tested. Four beams were pre-damaged when subjected to two-point loads at one-third of beam length and equal to 60% of the ultimate load. Epoxy resin was applied to the surfaces of both the laminate and the beam. The strengthening of compromised beams was executed with ferrocement laminates composed of chicken and welded mesh, incorporating 2 and 3 layers accordingly. A numerical model was created with ANSYS. The beam reinforced with 3 and 2-layer welded and chicken wire mesh improved first crack and ultimate load. Also, they exhibited an increase in both stiffness and ductility compared to reference beams. The analytical findings agree with the experimental investigation as shown in Figure (2.7).

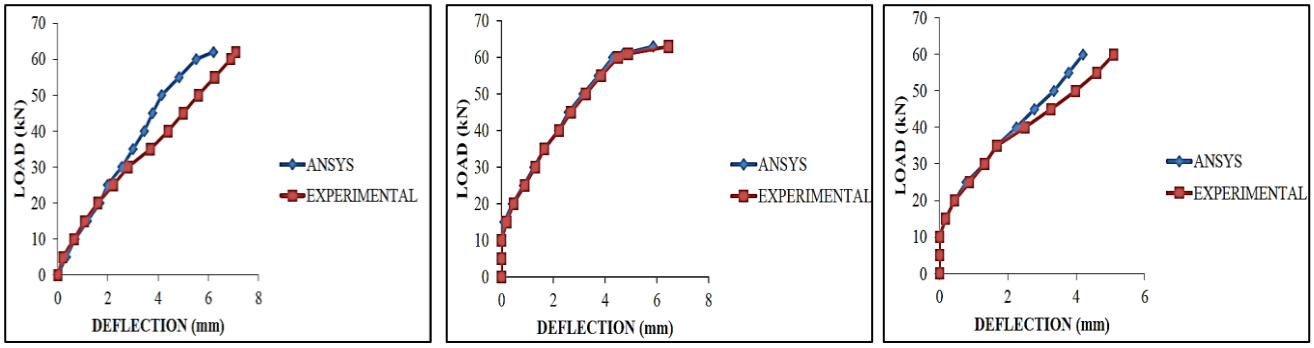

A. Comparison of Conventional Beam.

B. Comparison of 3-Layer Weld Mesh.

C. Comparison of 3-Layer Chicken Mesh.

Figure (2.7): Load-Deflection Curve for Each Case [39]

Soundararajan et al. [40] investigated ten reinforced concrete beams strengthened with ferrocement utilizing a galvanized square weld wire mesh, volume fractions of 1.76% and 2.35% for beams (RCSF01, RCSF03) respectively. Ferrocement mortar mix 1:2/0.4 was used. Slag replacement ratios of 0% and 30% by weight of fine aggregate were

also used. Beams (RCSF02, RCSF04) were strengthening using ferrocement with 30% steel slag and mesh volume fraction 1.76% and 2.35 respectively. The results showed that the first crack load and the ultimate load were higher in reinforced concrete beams augmented with ferrocement of a volume fraction of 2.35% (Vr) and a 30% replacement of steel slag, as illustrated in Figure (2.8).

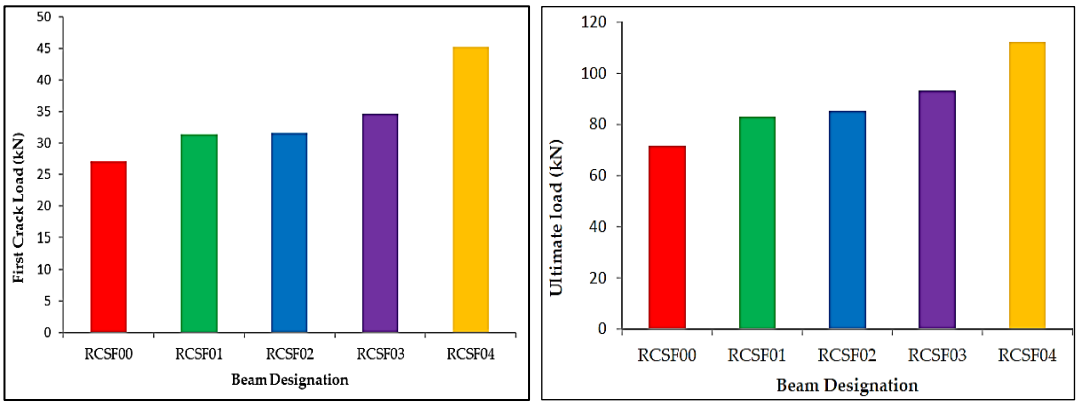

A. First Crack Load. B. Ultimate Load.

Figure (2.8): First Crack and Ultimate Load for Strengthened Beams [40]

Živkovic et al. [41] examined the flexural capacity of reinforced concrete beams strengthened with glued ferrocement strips. The research involved fifteen (RC) beams subjected to two-point loads. Strengthening was implemented by utilizing four varieties of ferrocement (number of layers varied from (8-14) and thickness varied from (17-23) mm) on the tension side, each with varying wire mesh layers and thickness. A numerical analysis was also conducted, using the finite element method. According to this study, the increase in the capacity of strengthened beams was about 21.4% compared to the reference due to increase the number of layer and thickness. The difference in failure load between numerical and experimental results was about 3.94%.

Taha et al. [42] evaluated different wrapping forms in terms of angle of rotation, torsional strength, and crack development. Six beams were cast. Designed two beams as control beams (BN) while four beams were divided into two groups, strengthening (B1) from three sides and (B2) for two sides by using ferrocement as shown in Figure (2.9). The construction of ferrocement by using wire mesh was necessary for the implementation of strengthening system. To maintain cohesiveness across reinforced beams, the mortar mixture was made with a ratio of 1:2.5/0.3 and styrene-butadiene rubber (SBR) replacement at 20% from cement weight. The study found that the three-sided wrapping form is a viable approach to improving torsional behavior. Small improvement in stability was observed as a result of the beam's reinforcement on two sides. Application of the U-shaped wrapping resulted in increased stability, which was accompanied by a decrease in both the ultimate twist and crack formation.

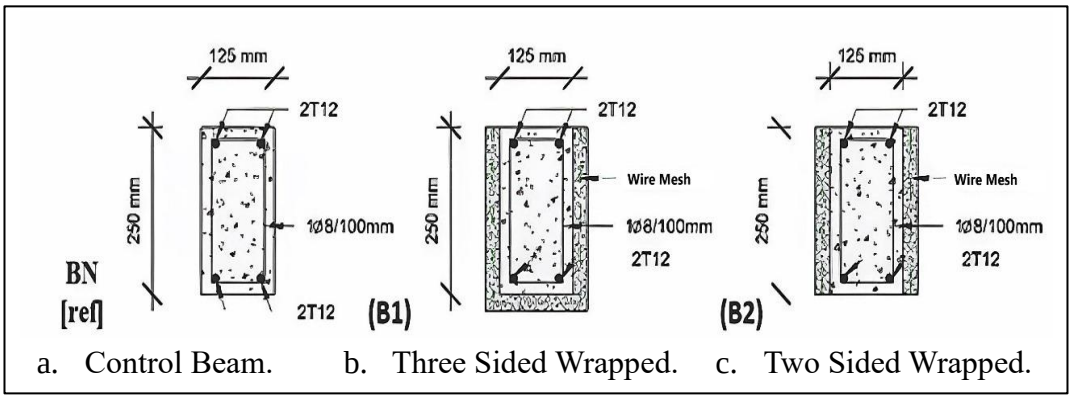

a. Control Beam. b. Three Sided Wrapped. c. Two Sided Wrapped.

Figure (2.9): Cross Sections of Control and Strengthened Beams [42]

2.3 Ferrocement with Glass Fiber Reinforced Polymer

Shaheen et al. [43] examined the efficacy of ferrocement beams augmented with composite materials. Several types of mesh, including welded (WWM), expanded (ESM), polypropylene (PEM), and glass fiber wire mesh (FGM) were utilized for the reinforcement with different layers and different volume fraction. Twelve beams were cast and tested under a three-point load. The results showed that the beams that were reinforced using glass fiber had lower values for both the ultimate and the first cracking load. Ferrocement beams reinforced with four layers of welded wire mesh were characterized by high performance compared to other types of wire mesh. In addition, the beams strengthened with metal wire mesh have a lower crack width compared to those strengthened with non-metal wire mesh as shown in Figure (2.10). Figure (2.10) shows the load versus deflection curves for all the tested beams.

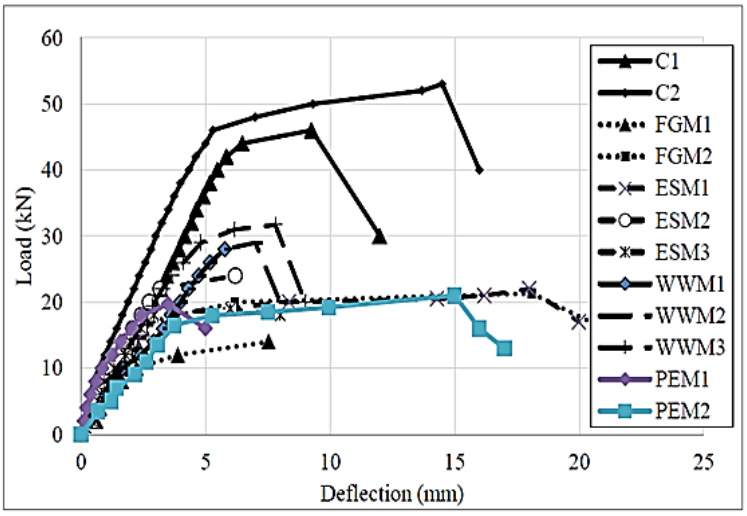

Figure (2.10): Load-Deflection Curve of All Test Specimens [43]

Tilekar et al. [44] investigated the flexural behavior of reinforced concrete beams strengthened by glass fiber polymer (GFRP) wraps. RC beams with dimensions of (200×200×2000) mm and concrete

compressive strength of 30 MPa and a mixing ratio of 1:2.56:2.48/0.45 were cast and tested under center point load. The beams were reinforced using glass fiber sheets with a thickness of 1.2 mm, which were attached to the beams using epoxy. Three beams were tested for flexural strength. The results showed that the utilization of (GFRP) sheets with full and partial (half) wrapping increases the ultimate load-bearing capability of RC beams by 34.48% and 10.35%, respectively, as illustrated in Figure (2.11).

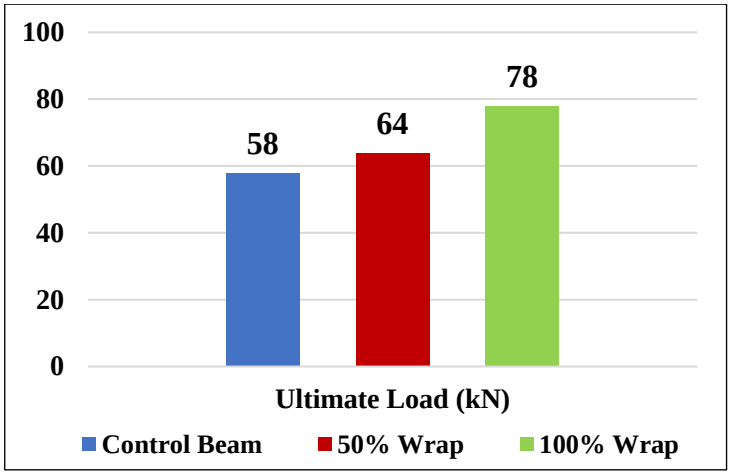

Figure (2.11): Ultimate Load of All Tested Beams [44]

Kumar et al. [45] studied the structural performance of reinforced concrete beams reinforced with glass fiber reinforced polymer (GFRP), ferrocement laminates, and carbon fiber reinforced polymers (CFRP). A total of 24 beams measuring (1500×200×150) mm were cast and tested. Ferrocement mortar was made with a mixing ratio of 1:2/0.4 and reinforced with square wire mesh. The beams underwent load testing for bending and shear failure modes. Each failure mode comprised four sets of beams: control beams, beams strengthened with (CFRP), beams strengthened with (GFRP), and beams strengthened with ferrocement. Beams reinforced with GFRP, ferrocement, and CFRP exhibited increases in the first crack load by 33.1%, 9.4%, and 17.3%,

respectively. The ultimate load-carrying capacities improved by 31%, 10.4%, and 19%, respectively.

Al-Rawe et al. [46] examined the rehabilitation of reinforced concrete columns exposed to biaxial load, using improved ferrocement jacketing. The experimental work consisted of fifteen columns with brackets at both ends. The columns were preloaded to 65% and 85% of the ultimate loads. The specimens were separated into three groups. In the first group, the specimens were retrofitted using conventional ferrocement and reinforced with steel wire mesh. In the second group, the specimens were retrofitted with high-performance mortar and reinforced with steel wire mesh. In the third group, the specimens were retrofitted with improved mortar and strengthened with fiberglass mesh. All columns were subjected to biaxial loading until failure. The results showed that when the preloading percentage increased, the load-bearing capacity decreased. Furthermore, ferrocement jacketing with conventional and high-performance mortar improves columns' ductility, failure behavior, and fracture resistance.

2.4 Environmentally Cement Mortar

Boiny et al. [47] studied the aim of using recycled plastic bottles as fibers to strengthen cement mortar. Fibers made of polyethylene terephthalate (PET) plastic bottles were used with different volume fraction and size. The plastic fibers were incorporated into the mixture by weight percentages of 0%, 0.5%, 1.0%, 1.5%, 2.0%, and 3.0% of the total weight. The primary objective was to examine the impact of (PET) incorporation on the mechanical characteristics of cement mortar. The

impact of (PET) on cement mortar was examined through split tensile strength, compressive strength, and Schmidt tests at 7 and 28 days. The results indicated that the inclusion of plastic fibers enhances the splitting tensile strength of the cement mixture by 18% compared to the control sample when adding 0.5% plastic fiber. The addition of (PET) leads to a slight reduction in density compared to the hardened cement mortar due to the low density of (PET) as shown in Figure (2.12).

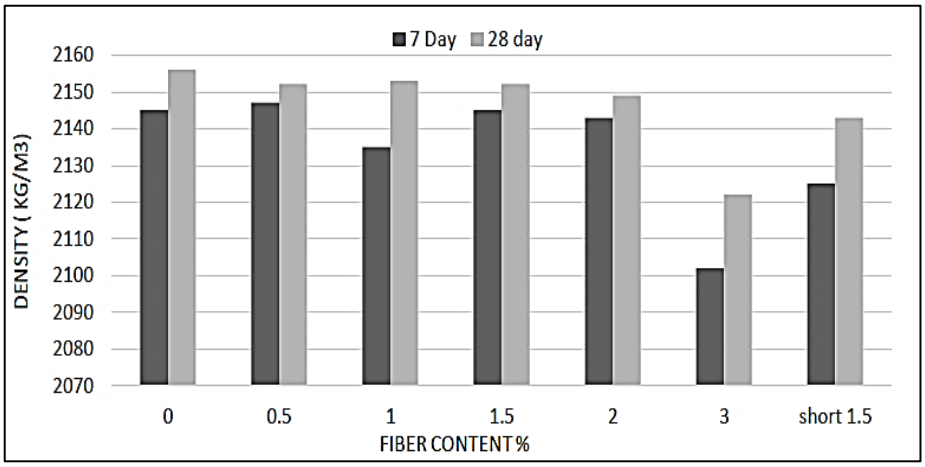

Figure (2.12): Density of Hardened Cement Mortar [47]

Shukur et al. [48] examined the quality of concrete utilizing polyethylene terephthalate (PET) and polypropylene pipe (PEP) as aggregate replacements. PET and PEP substituted up to 15% of the aggregates in concrete compositions. This study demonstrates that two varieties of plastic waste can effectively serve as partial substitutes for fine or coarse aggregate in concrete mixes. PEP diminishes workability due to irregular shapes and may enhance the interaction among the mixed components, causing a decrease in slump, while PET improves this material characteristic. The concrete density was lower than control mixes by 10%. The use of recycled plastic diminished the compressive strength, tensile strength, and flexural strength by as much as 31%, 22%, and 60%, respectively, in comparison to conventional concrete.

Dawood et al. [49] investigated the properties of green high-performing mortar (HPM) utilized in the manufacturing of ferrocement. The program consisted of four different phases. The initial phase involved the analysis of non-reinforced high-performance mortar (HPM) including 20% supplementary cementitious materials (SCM). The second phase examined the behavior of HPM reinforced with varying amounts of natural sisal fibers (NSF). The third phase evaluated the performance of ferrocement made from both non-reinforced and reinforced high-performance materials under bending loads. The final phase examined the economic viability of the research program. The results indicated that the incorporation of 9% silica fume and 11% metakaolin enhanced the characteristics of HPM. The use of NSF resulted in an improvement in flexural strength and splitting tensile strength, as shown in Figure (2.13).

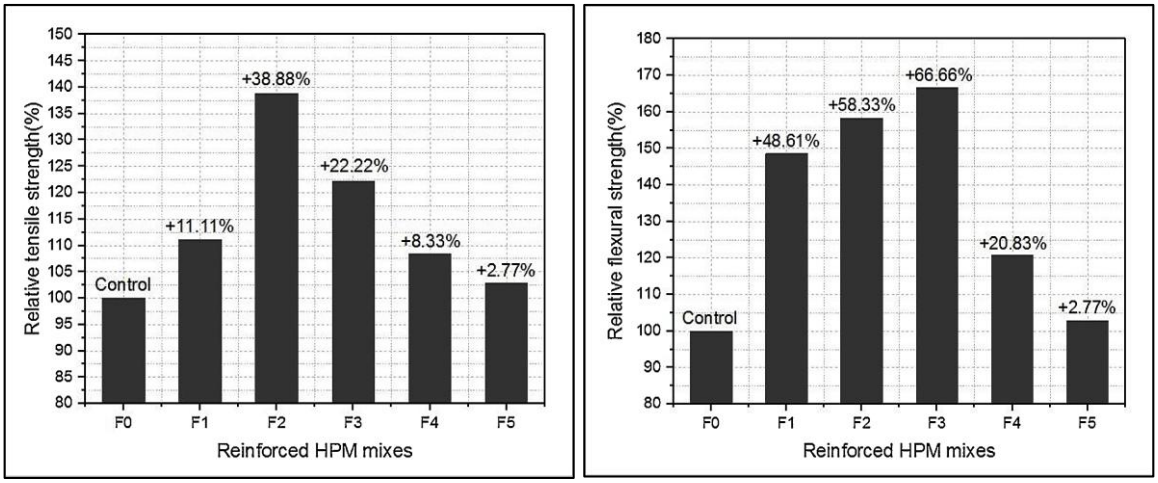

A. Splitting Tensile Strength. B. Flexural Strength.

Figure (2.13): Strength at 90 Days for Reinforced HPM Mortar [49]

Sumanth et al. [50] examined the characteristics of the mortar mix produced by partially substituting fine aggregate with waste rubber tires in ferrocement. The mix proportions utilized were 1:2, 1:3, and 1:4 with a water-to-cement ratio of 0.5 and reinforced with two layers of

hexagonal wire mesh. Waste tire rubber was incorporated into the concrete by a replacement volume ratio of 0%, 1%, 2%, 3%, 4%, 5%, and 6% of fine aggregate. The dimensions of the specimen were specified as (900×250×50) mm for the bending test and (100×100×100) mm for the compression test. The results indicated that including crumb rubber in cement mortar as partial substitute for fine aggregate in varying volume fractions led to a decrease in flexural and compressive strength as increase crumb rubber content. Adding crumb rubber to ferrocement improves the ductility and energy absorption capacity and contributes to a reduction in weight.

2.5 Research Gap

Previous studies have explored various aspects of ferrocement use. Some focused on the effect of conventional ferrocement materials on beam strength, while others investigated the impact of different numbers of mesh layers on the initial cracking load and deflection. Researchers also studied how the ferrocement mortar thickness influences strength. In addition, few studies examined the effects of incorporating environmental components in ferrocement mortar. However, the use of environmentally friendly materials in retrofitting reinforced concrete beams is still under investigation. This study examined an integrated sustainable ferrocement mixture containing silica fume, waste tire rubber, and waste plastic bottle fiber, unlike previous studies that examined each material separately. The current study aims to address this gap.

Chapter 3

Experimental Program

Chapter Three

Experimental Program

3.1 Introduction

This chapter consists of three sections. The first section outlines the experimental program designed to identify an optimal mixture incorporating sustainable materials, including silica fume (SF), waste tire rubber (crumb rubber) (CR), and waste plastic bottle fibers waste (PF). Various mortar mixtures were prepared using silica fume (as a replacement ratio for the weight of cement) and waste tire rubber (as a replacement ratio for the weight of sand). Additionally, waste plastic bottle was incorporated as fiber into the mixture at specific volumetric ratios.

The second section outlines the experimental program of the preloaded beams. A total of ten reinforced concrete beams were cast, including two control specimens tested until failure and eight preloaded specimens tested up to 70% of the ultimate load. Also, it covers materials used in casting, their properties, reinforced steel, strain gauges, and wood formwork.

The third section covers the retrofitting process of the preloaded beams. The preloaded beams were retrofitted using ferrocement. The used ferrocement consists of traditional mortar and the optimal sustainable mortar mix found in the first section. Two types of reinforcement were used: steel wire mesh and glass fiber mesh. In addition, two different configurations were used: full and U-shape wrapping. The retrofitted beams were then tested to failure.

Materials Used

3.2 Traditional Materials

3.2.1 Cement

Ordinary Portland cement (OPC) of grade 30 MPa type I (Sinjar) manufactured in Iraq was used in this study. The chemical and physical properties of used cement, meeting the IQS: No. 5/2015 [51], are listed in Table (3.1) and Table (3.2), respectively, conducted at Environmental Engineering Laboratory and Construction Material Laboratory, University of Mosul for chemical and physical properties respectively, as shown in Figure (3.1).

Table (3.1): Chemical Properties of Cement

Chemical Compounds	**Result %**	**Limits of Iraqi Specification** [51]
Cao	65.1	-
SiO_2	19.6	-
Al_2O_3	5.2	-
Fe_2O_3	3.13	-
MgO	1.83	≤ 5%
So_3	2.19	≤ 2.5% if C_3A≤ 5% ≤2.8% if C_3A≤ 5%
Free lime	0.86	0.66-1.02
Loss on ignition	0.17	≤ 4%
Insoluble residue	0.84	≤ 1.5
Solid solution	16.25	-
C_2S	29.4	-
C_3S	40.5	-
C_3A	6.48	-
C_4AF	10.68	-
LSF	88	-

Table (3.2): Physical Properties of Cement

Properties	**Results**	**Limits of Iraqi Specification** [51]
Consistency	0.295	--
Initial Setting Time (minutes)	120	≥ 45
Final Setting Time (hr.)	5	≤ 10
3 days Compressive Strength (MPa.)	20	≥ 15
7 days Compressive Strength (MPa.)	30.6	≥ 23
Fineness Sieve No. 170(%)	2.2	≤ 10
Specific Gravity	3.15	--

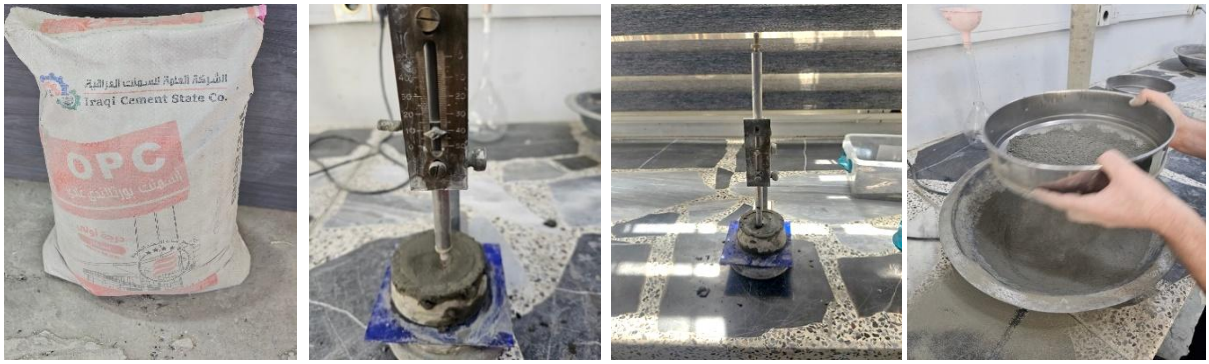

A. Cement Type. B. Vicat Test for Setting Time. C. Fineness Test.

Figure (3.1): Tests of Physical Properties of Cement

3.2.2 Fine Aggregate

Locally available natural river sand from Kanhash passing sieve No. 4 was used. Sieve analysis following the IQS: 45/2016 [52] was conducted at the Construction Material Laboratory, University of Mosul, and the results are listed in Table (3.3). The physical properties of the fine aggregate were measured following ASTM C128-22 for specific gravity and water absorption [53], and ASTM C566-19 for evaporable moisture content [54], as shown in Table (3.4).

Table (3.3): Sieve Analysis of the Fine Aggregate

Sieve Size	**% passing**	**Limits- Zone II Iraqi Specification** [52]
No. 4	95.20	90-100
No. 8	87.00	75-100
No. 16	78.40	55-90
No. 30	57.90	35-59
No. 50	17.10	8-30
No. 100	3.10	0-10
Pan	0.0	----

Table (3.4): Physical Properties of Fine Aggregates

Physical Properties	**Test Result**
Specific Gravity (S.S.D)	2.6
Water Absorption %	2.46
Fineness Modulus	2.61
Unit Weight (kg/m^3)	1600

3.2.3 Natural Coarse Aggregate

Locally available gravel with (0.75") maximum aggregate size was used as a coarse aggregate. The results of sieve analysis following the IQS: 45/2016 [52] and the physical properties following the American Standard ASTM C127-15 [55] for specific gravity and water absorption and ASTM C29-17 [56] for unit weight. These tested were conducted at the Construction Material Laboratory, University of Mosul, and are listed in Table (3.5) and Table (3.6) respectively.

Table (3.5): Sieve Analysis of Coarse Aggregate

Sieve Size	**% Passing**	**Limits Iraqi Specification** [52]
1.5"	100.00	100
1"	100.00	95-100
3/4 "	95.96	95-100
1/2 "	53.36	-----
3/8 "	32.84	30-60

Table (3.6): Physical Properties of Coarse Aggregate

Physical Properties	Test Result
Specific Gravity (S.S.D)	2.69
Water Absorption %	0.66
Compact unit weight (kg/m^3)	1626

3.2.4 Water

Potable water was used following IQS: No.1703/2016 [57].

3.3 Sustainable Materials

3.3.1 Silica Fume

Micro silica (SF) is a byproduct of the manufacture of silicon metal and ferro-silicon alloys from CONMIX Company. The physical and chemical properties of silica fume are given in Tables (3.7) and (3.8) according to the manufacture [58]. The pozzolanic activity index (P.A.I.) of silica fume, based on a test conducted at the Construction Material Laboratory, University of Mosul, was 107% at 28 days, which meets ASTM C1240-20 [59]. Figure (3.2) shows the activity index process.

Table (3.7): Physical Properties of Silica Fume

Property	Value	Limit of Specification
Color	Gray powder	---
Specific Gravity	2.17	2.1 to 2.4
Surface Area m^2	21	Minimum 15 m^2/g
Particles retained on sieve 45 μm	7	Maximum 10%

Table (3.8): Chemical Composition of Silica Fume

Property	Value	Limit of Specification
Silicon Dioxide (SiO_2)	90.65%	Minimum 85%
Moisture Content (H_2O)	0.68%	Maximum 3%
Loss on Ignition (LOI)	2.86%	Maximum 6%

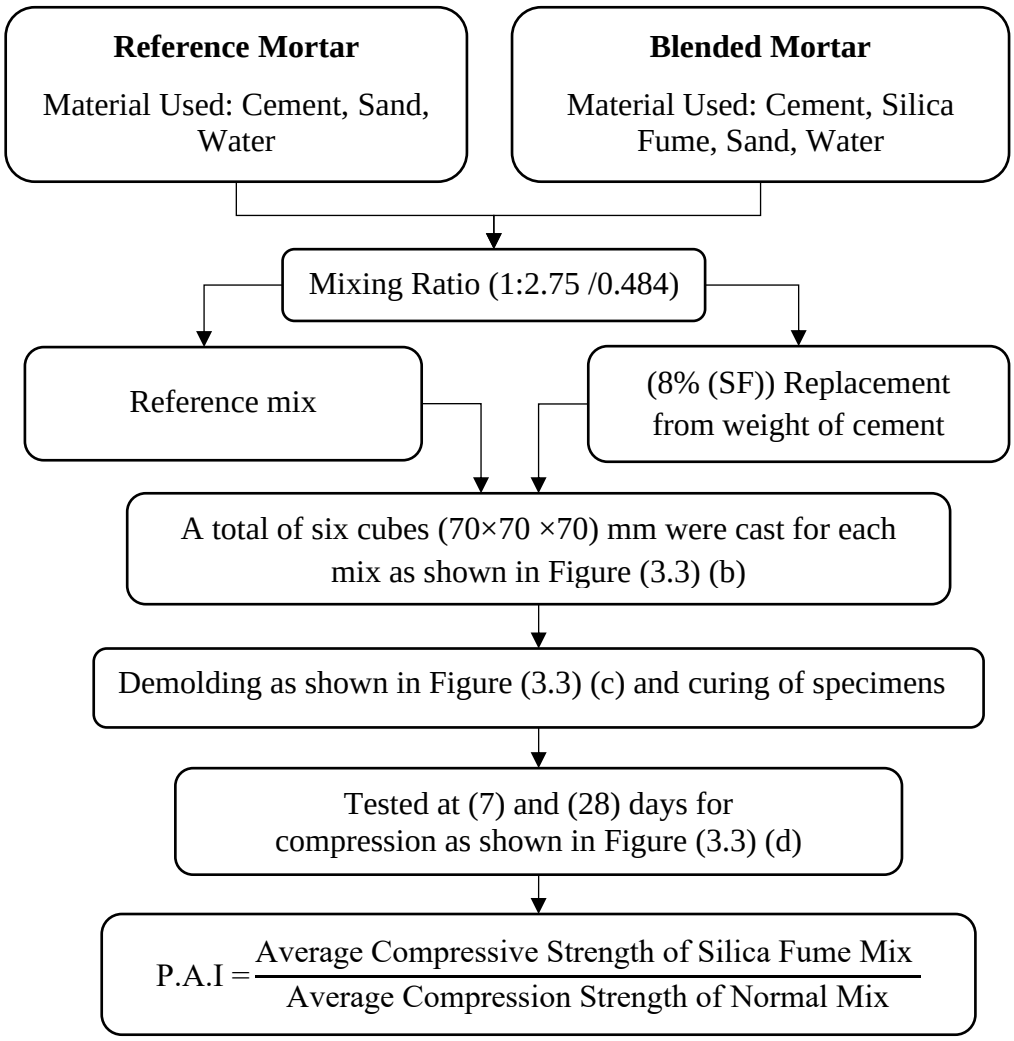

Figure (3.2): Activity Index Process

a. Silica Fume. b. Casting. c. Demolding. d. Testing the Specimens.

Figure (3.3): Silica Fume Activity Index Process

3.3.2 Waste Tire Rubber (Crumb Rubber)

Crumb rubber (CR) is generated from recycled tires and processed by removing metal and fiber components, followed by mechanical shredding of discarded vehicle tires (See Figure (3.4)). The particle sizes of crumb rubber used in this study ranged from 0.3mm to 3.5mm. Sieve analysis of crumbs rubber is listed in Table (3.9), and the fineness modulus of crumb rubber is 3.82. Table (3.9) shows that the sieve analysis results do not meet the standard specification (IQS: 45/2016 [52]) for sieve number (30 to 100). This is because of the non-spherical shape and low specific gravity of the crumbs rubber, preventing them from quickly passing through the fine sieves. These result match the results found by Sulaiman T. et. al [60].

Figure (3.4): Waste Tire Rubber

Table (3.9): Sieve Analysis of Waste Tire Rubber

Sieve Size	% passing	Limits- Zone I Iraqi Specification
No.4	100.0	90-100
No.8	81.53	60-95
No.16	29.32	30-70
No.30	6.43	15-34
No.50	0.00	5-20
No.100	0.00	0-10

3.3.3 Waste Plastic Bottle Fiber

The waste plastic bottle fiber (PF), which is locally available (also known as polyethylene terephthalate), is used in this study. The plastic bottles were first washed with water to remove dust, then each bottle was shaped as a sheet by removing the neck and base as shown in Figure (3.5). Finally, the sheet was hand-cut into strips using scissors. The dimensions and physical properties of (PF) are given in Table (3.10).

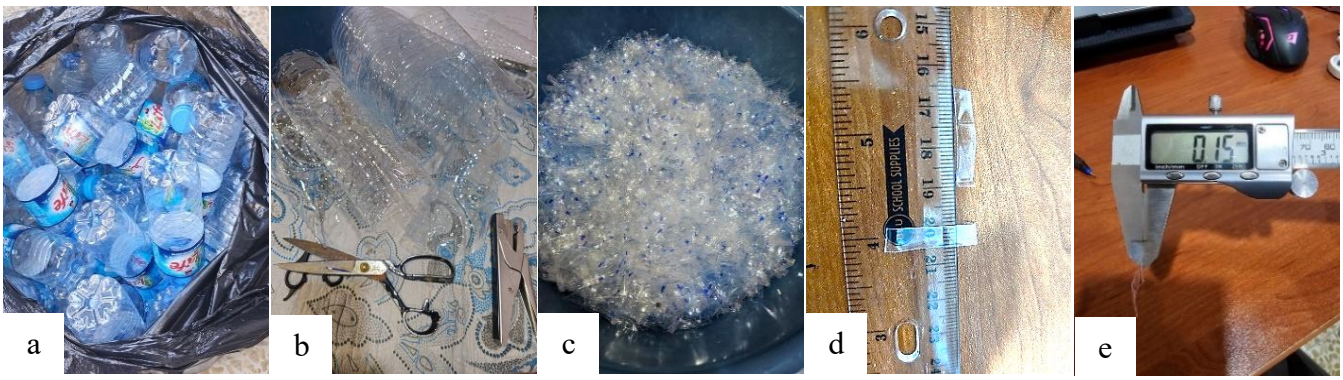

a. Waste Bottles. b, c. Hand-Cut into Strips Using Scissors. d, e. Fiber Dimension Measurement.

Figure (3.5): Process to Produce Waste Plastic Fiber and its Dimension

Table (3.10): Physical Properties of Waste Plastic Bottle Fiber

Property	Description
Type	Polyethylene terephthalate
Average Length (mm)	25
Average Width (mm)	5
Average Thickness (mm)	0.15
Aspect Ratio	25.588
Density (kg/m^3) *	1375
Water absorption	0.0

*According to previous studies [61].

3.4 Reinforcement Used

3.4.1 Steel Reinforcement

Deformed reinforcing steel bars were supplied from "Mass Company", and used to reinforce the beams. The main longitudinal bars for tension, compression, and stirrups were (10) mm in diameter. Samples of the three bars were tested to specify their properties of yield strength, ultimate strength, and elongation as given in Table (3.11) and as shown in Figure (3.6). Their results conform to the specifications of ASTM A615M-22 [62] of grade 80. The relation between stress and strain was shown in Figure (3.7).

Table (3.11): Properties of Reinforcing Steel Bars

Properties	**Value**	**Requirements ASTM** [62]
Nominal Bar Diameter (mm)	10	
Actual Diameter (mm)	9.75	
Yield Stress (MPa)	580	Min. 550 MPa
Ultimate Stress (MPa)	695	Min. 690 MPa
Elongation (%)	9.4	Min. 7%

Figure (3.6): Steel Reinforcement Specimens and Testing Machine

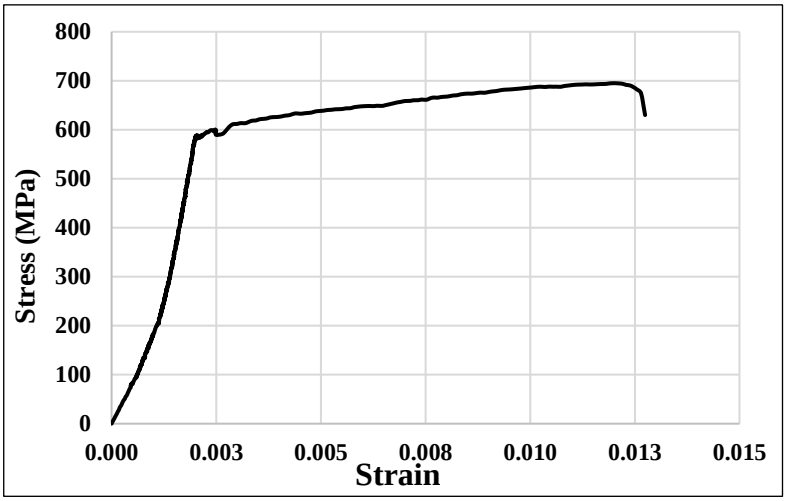

Figure (3.7): Stress-Strain Relationship of Steel

3.4.2 Mesh Reinforcement

The two types of mesh reinforcement used in this study include,

- Welded steel wire mesh with a diameter of (0.6) mm.
- Glass fiber mesh with a cross-section dimension of (0.3×0.3) mm in longitudinal direction and (0.3×1.5) mm in transverse direction.

Their specifications were experimentally tested as shown in Table (3.12). Figure (3.8) shows type of mesh and testing process conducted at Construction Material Laboratory, University of Mosul. The reinforcement wire mesh ratio (ρ_{wire}) is defined as the cross-sectional area of one wire divided by the cross-sectional area of the ferrocement accommodating it [46], [63]. The stress-strain relation for welded steel wire and glass fiber mesh are shown in Figure (3.9) (A) (B).

Table (3.12): Properties of Welded Steel Wire Mesh and Glass Fiber Mesh

Properties	Welded Steel Wire Mesh	Glass Fiber Mesh
Opening Size (mm)	12.5 × 12.5	4 × 4
Size of Wire (mm)	0.6	0.3 × 0.3
Ultimate Load (N)	518	340
Yield Strength (MPa)	395	---
Ultimate Strength (MPa)	610	540
ρ_{wire} (Two Layer)	0.00181	0.0018
Weight (g/m^2)	340	160

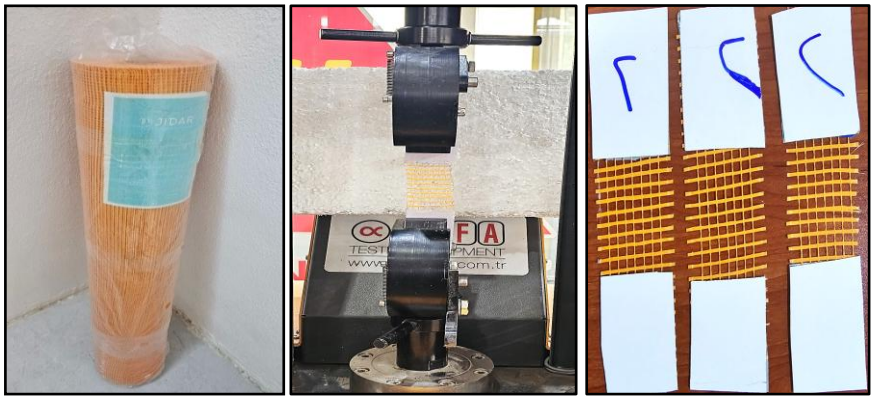

A. Glass Fiber Mesh. B. Test of Glass Fiber Mesh.

C. Welded Wire Mesh. D. Test of Welded Wire Mesh.

Figure (3.8): Testing for the Wire Mesh Reinforcement

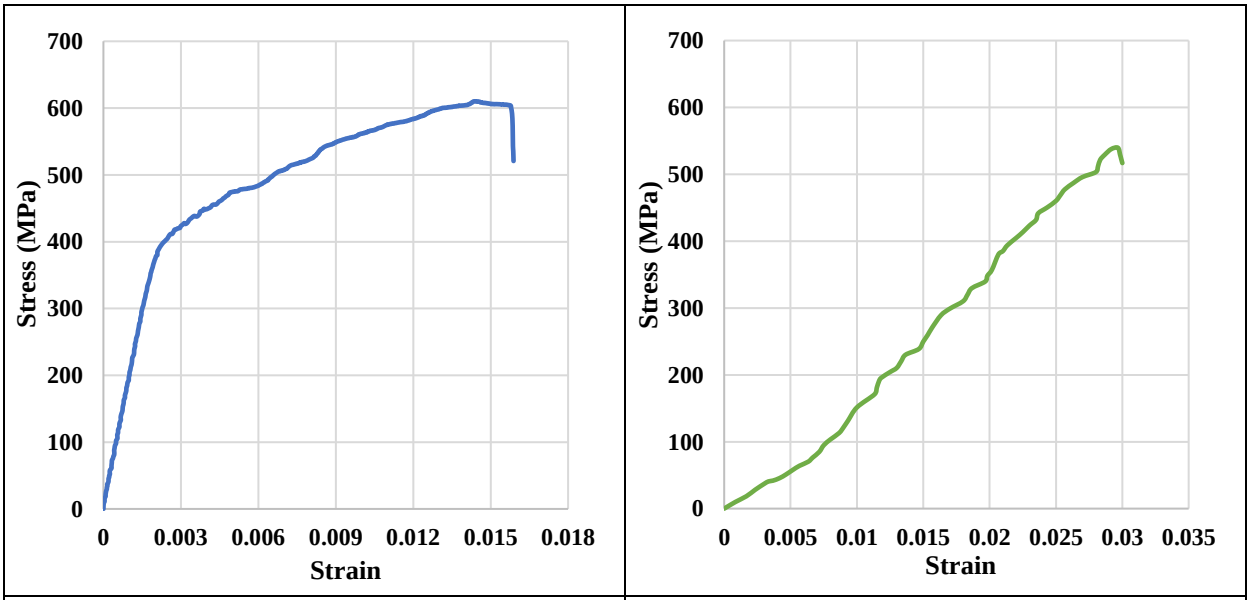

A. Welded Steel Wire Mesh. B. Glass Fiber Mesh.

Figure (3.9): Stress – Strain Curve for Welded Steel Wire Mesh and Glass Fiber Mesh

Section One

Preparation of Sustainable Mortar

3.5 Research Methodology

A total of (234) specimens were cast and tested for compressive, flexural, and splitting tensile strengths. These included (78) cubes (70×70×70 mm), (78) prisms (40×40×160 mm), and (78) brackets (See Figure (3.10). The experimental work consisted of three primary phases. The first phase involved evaluating of silica fume (SF) as a partial replacement of cement weight by (0, 8, 9, 10, 12, and 15) %. In the second phase, waste tire rubber (crumb rubber (CR)) was incorporated as a partial replacement of sand weight by (0, 5, 10, and 15) %. Note that the mix with (0) % crumb rubber is identical to the mix with (0) % silica fume. In the third phase, the optimal percentages of silica fume from Phase 1 and crumb rubber from Phase 2 were incorporated with a volumetric ratio of waste plastic fibers (PF) at (0, 0.5, 0.75, and 1.0) % to determine the best-performing mixture. Figure (3.11) shows the research methodology.

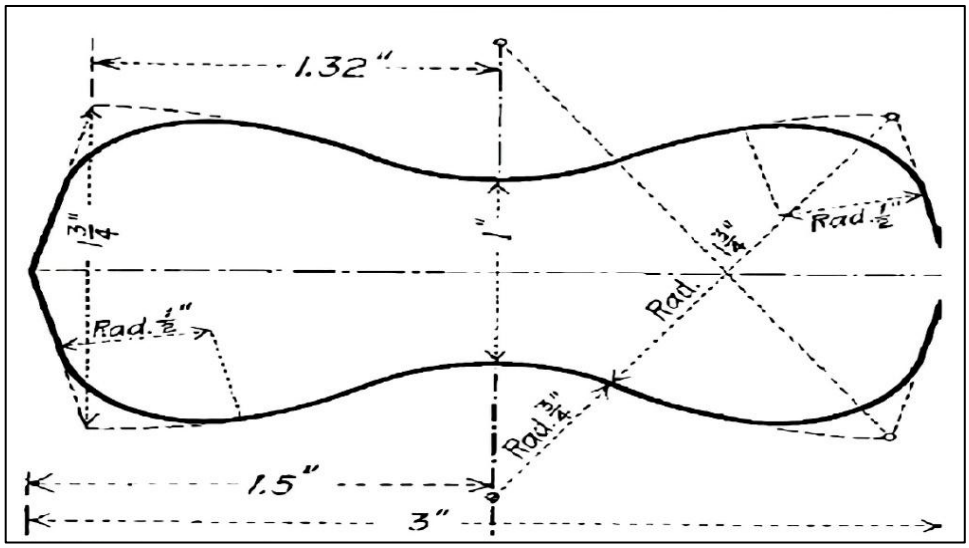

Figure (3.10): Dimension of Bracket

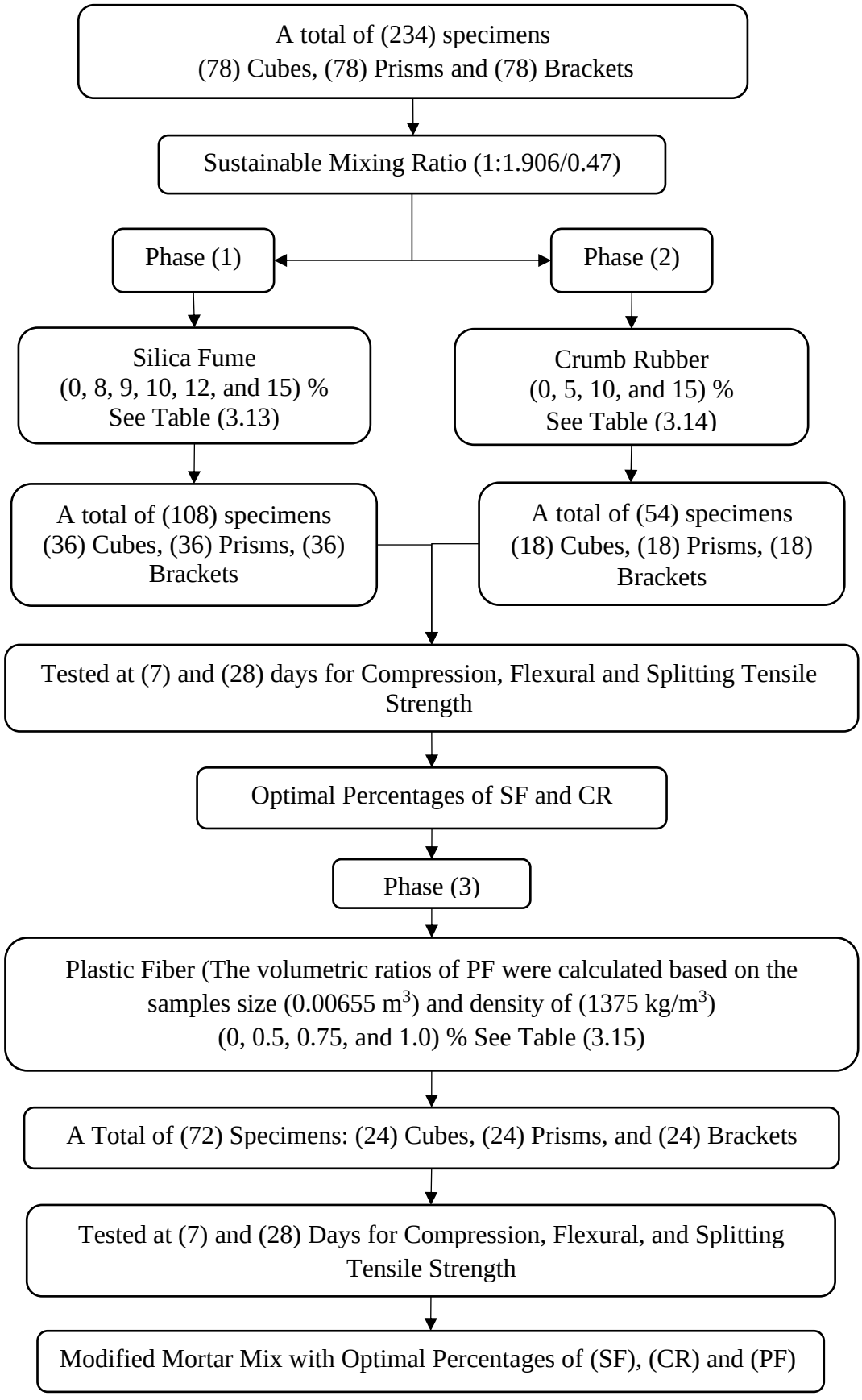

Figure (3.11): Research Methodology

Table (3.13): Mix Proportion of Silica Fume (SF) Mortar

Mix Code	Cement (gm)	% Silica Fume Replacement	Silica Fume (gm)	Sand (gm)	Water (gm)
Traditional Mix	2500	0	0	4765	1175
SF 1	2300	8	200	4765	1175
SF 2	2275	9	225	4765	1175
SF 3	2250	10	250	4765	1175
SF 4	2200	12	300	4765	1175
SF 5	2125	15	375	4765	1175

Table (3.14): Mix Proportion of Crumb Rubber (CR) Mortar

Mix Code	Cement (gm)	Sand (gm)	% Replacement Sand with (CR)	Crumb Rubber (gm)	Water (gm)
Traditional Mix	2500	4765	0	0	1175
CR 1	2500	4527	5	238	1175
CR 2	2500	4288	10	477	1175
CR 3	2500	4050	15	715	1175

Table (3.15): Mix Proportion for Adding Plastic Fiber (PF) to Mortar

Index	Cement (gm)	Silica Fume (gm)	Sand (gm)	Tire (gm)	Water (gm)	% of Plastic Fiber	Plastic Fiber Content (gm)
Traditional Mix	2500	0	4765	0	1175	0	0
Control Mix	2300	200	4527	238	1175	0	0
PF 1	2300	200	4527	238	1175	0.5	45
PF 2	2300	200	4527	238	1175	0.75	68
PF 3	2300	200	4527	238	1175	1	90

3.5.1 Mixing Procedure

The materials were mixed manually at Construction Material Laboratory, University of Mosul for three minutes as shown in Figure (3.12) (A), then water was added and mixed for another three minutes to get a homogenous mixture according to [49] . After that, the prepared mix was used to pour in the molds. The molds included six cubes (70×70×70 mm) to test the compressive strength according to ASTM C 109 [64], six prisms (40×40×160 mm) to test the flexural strength

ASTM C 348 [65], and six brackets to test the splitting tensile strength based on ASTM C 260 [66], as shown in Figure (3.12) (B). After pouring all of the specimens in a single layer, they were compacted by vibration for approximately 15 to 30 seconds, or until the surface of the mortar was freed from air bubbles. After casting, the specimens were left at room temperature for 24 hours, then demolded and cured by being placed in a water tank according to ASTM C192 [67], as shown in Figure (3.12) (C). After curing, the specimens were tested at ages 7 and 28 days to determine the ideal sustainable mortar.

Silica Fume Mix. Crumb Rubber Mix. Plastic Fiber Mix.

A. Mixed Dry Material.

B. Casting Specimens.

C. Demolding and Curing the Specimens.

Figure (3.12): Weighing, Casting and Curing of Specimens

3.6 Equipment Used to Measure Strength of Mortar

3.6.1 Universal Compressive Test Equipment

This device has a capacity of 200 tons and a load rate of 0.5 MPa/Sec. It is utilized to evaluate the compressive strength of the mortar cubes according to ASTM C 109 [64], as illustrated in Figure (3.13) (a). The compressive strength was determined as an average strength of three specimens.

3.6.2 Universal Tensile Testing Equipment

It is a device with a carrying capacity of 100 tons used to test bracket specimens for tensile strength tests according to ASTM C 260 [66], as shown in Figure (3.13) (b). The tensile strength was determined as an average strength of three specimens.

3.6.3 Flexural Testing Machine

It is a device with a carrying capacity of 30 tons with two channels used to test the compressive strength of the cube in channel (1) and the flexural strength of the prism in channel (2) according to ASTM C 348 [65], as shown in Figure (3.13) (c). The flexural strength was determined as an average strength of three specimens.

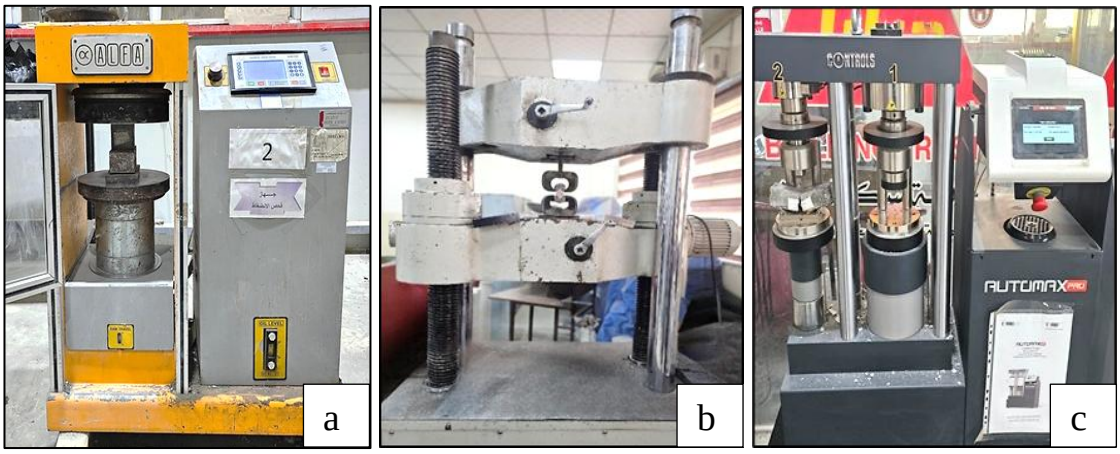

Figure (3.13): a. Universal Compressive Test Equipment, b. Universal Tensile Testing Machine, c. Flexural Testing Machine

Section Two

Preloaded Reinforced Concrete Beams

3.7 Specimen Details

The reinforced concrete beams had the following dimensions: a height of 250 mm, a width of 150 mm, and a length of 1800 mm. These beams were tested by applying center-point loading as shown in Figure (3.14).

The concrete cover to the stirrups was 20 mm. The longitudinal and transverse reinforcements were analyzed to failure in flexural mode according to the Building Code Requirements for Structural Concrete (ACI 318M-19) [68] as mention in appendix (A). The longitudinal reinforcement consists of (3Ø10 mm) bars in tension zone, (2Ø10 mm) bars in compression zone and (Ø10 mm @ 100 mm c/c) stirrups, as shown in Figure (3.14). A total of ten reinforced concrete beams were cast, including two control specimens tested to failure and the other eight specimens were preloaded to 70% of the ultimate load.

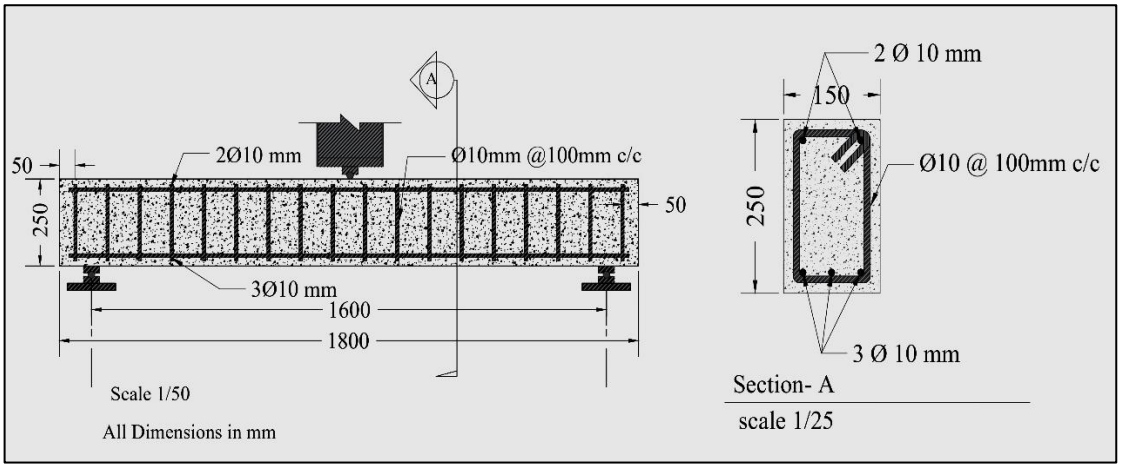

Figure (3.14): Longitudinal and Cross Section Details of the Beam

3.8 Wooden Formwork

Two formworks were built for casting specimens; each form consists of five connected parts, as shown in Figure (3.15). The formworks were built using plywood sheets with a thickness of (18) mm. The internal dimensions were (150 × 250) mm (width × height) and (1800) mm in length. Each side of the form was secured with a nail, and wooden clamps were placed at the top of each mold for additional support. Before casting, all the forms were oiled to ensure easy removal of the concrete.

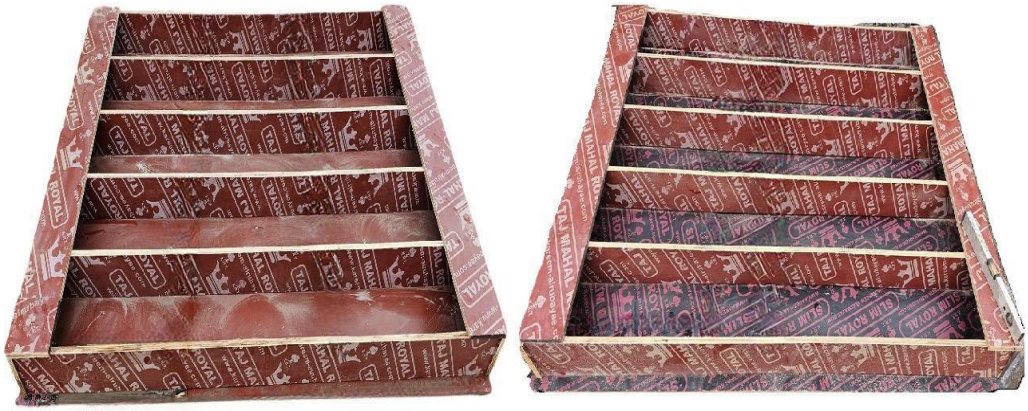

Figure (3.15): Wooden Formworks

3.9 Installation of Steel Reinforcement

The specimens were reinforced using longitudinal steel bars (3Ø10) mm at the tension zone, and (2Ø10) mm at the compression zone. In addition, shear reinforcement (stirrups) (Ø10 @ 100 mm c/c) was provided. The details of reinforcement are shown in Figure (3.16). Concrete spacers were placed under the bottom bars and along the sides before casting. These spacers were used to ensure the required concrete cover for reinforcement in beams.

Fixing Reinforcement.

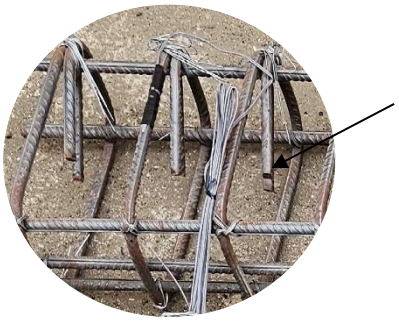

Details of Reinforcement.

Figure (3.16): Fixing Steel Reinforcement

3.10 Installation of Strain Gauges

All beams were instrumented with strain gauges to measure the strain in the steel reinforcement. The properties of the gauges are listed in Table (3.16). Three strain gauges were mounted on each beam:

- FS1: mounted horizontally on the longitudinal reinforcing bars at the section of the maximum bending moment, as shown in Figure (3.17).
- (SS2) and (SS3): mounted vertically in the middle of the second stirrups from each side of the beam, as shown in Figure (3.17).

The process of installing gauges is shown in Figure (3.18)

Table (3.16): Properties of Strain Gage According to Manufacturer

Type	**FLAB-6-11-3LJC-F**
Gage Length	6 mm
Gage Factor	2.08 ±1%
Gage Resistance	118.5 ±0.5
Transverse Sensitivity	0.4%

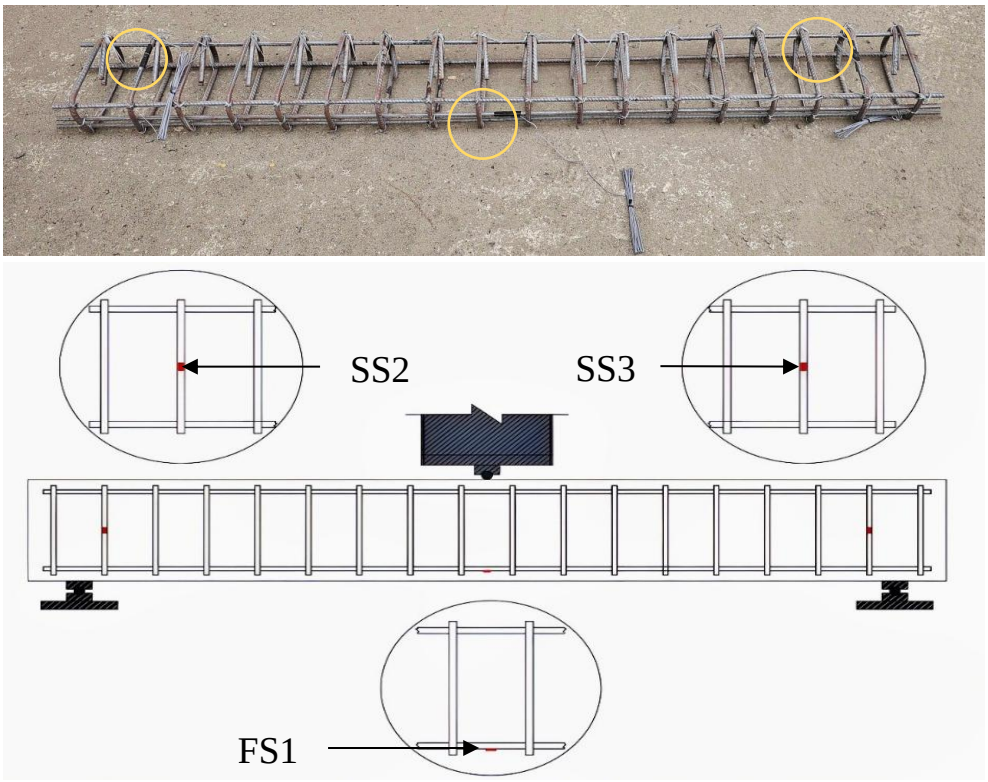

Figure (3.17): Strain Gauges Location and Orientation

a. Strain Gauge. b. Grinding Surface. c. Attaching Strain Gauge. d. Appling Rubber Tape.

Figure (3.18): Strain Gauges Installation Process

3.11 Preparation of Specimens

3.11.1 Concrete Mixture Proportion

The concrete mix was designed according to (ACI 211.1-22) [69] as mentioned in appendix (B) to achieve the target compressive strength of (30) MPa. The mix proportions were (1: 1.906: 2.787 / 0.47). The details of the concrete mix are provided in Table (3.17). The slump values were between (75-130) mm measured according to ASTM C143/C143M-20 [70].

Table (3.17): Concrete Mix Proportion

Description	Quantities (kg/m^3)
Cement	381
Fine aggregate	726
Coarse aggregate	1062
Water	179

3.11.2 Casting of Reinforced Concrete Beams

All the specimens were prepared and cast at Construction Material Laboratory, University of Mosul. A total of ten reinforced concrete beams were cast in the same period. The casting process is as follow:

1. The forms were placed on the ground in equilibrium status, cleaned, and sealed with silicone to the outer edges. The reinforcement was then placed inside the wood forms.
2. The concrete materials were weighted according to the mixing ratio. Cement, sand, and gravel were saturated surface dry aggregate, mixed manually. Then, water was added, and the mixing continued until the concrete was homogeneous, as shown in Figure (3.19) (A).
3. Slump test equipment was prepared, as shown in Figure (3.19) (B).

4. The concrete was poured into the forms and compacted using an electrical vibrator to get minimum voids. Then, smooth the top surface of the concrete as shown in Figure (3.19) (C).
5. Additional specimens were cast including, three cubes of concrete (150×150×150) mm, three-cylinder (Ø150×300) mm, and two prisms (100×100×500) mm, as shown in Figure (3.19) (D).
6. After 24 hours, outer side of the wooden formwork was removed. Then, the specimens were cured for (28) days using wetted jute bags and covered with plastic sheets as shown in (3.19) (E).

A. Mixing the Material.

B. Slump Test.

C. Remove Air Voids.

D. Casting the Specimens.

E. Curing the Specimens.

Figure (3.19): Casting of the (RC) Beams

3.12 Mechanical Properties of Hardened Concrete

3.12.1 Concrete Compressive Strength

The compressive test is performed for three cubes with dimensions (150×150×150) mm, for mixture at the age of (28) days according to B.S 1881, part 116: 1983 [71]. Figure (3.20) (a) shows the testing machine.

3.12.2 Concrete Splitting Tensile Strength

Three standard cylinders (150×300) mm were tested at the age of (28) days to measure the splitting tensile strength of concrete according to ASTM C496-17 [72]. Figure (3.20) (b) shows the testing machine.

3.12.3 Concrete Flexural Tensile Strength Test

The test was carried out on two prism specimens (100×100×500) mm used to measure the flexural strength (modulus of rupture (f_r)) following ASTM C293-18 [73]. Figure (3.20) (c) shows the testing machine

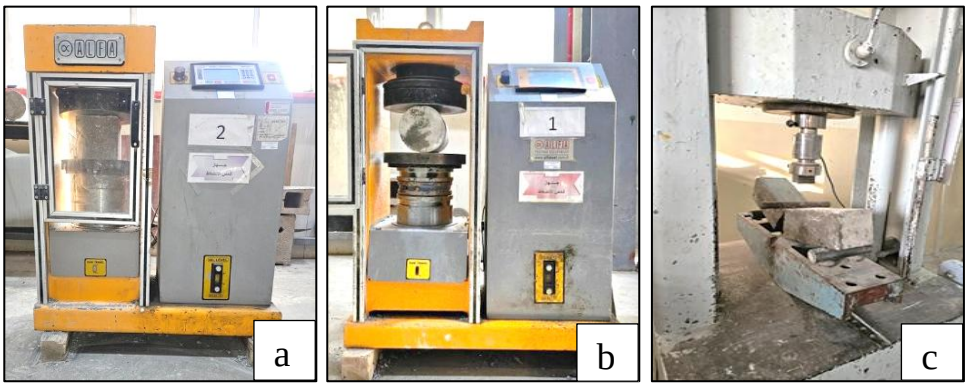

Figure (3.20): a. Testing of Compressive Strength, b. Splitting Tensile Machine Test, c. Flexural Tensile Strength Test

3.13 Testing Procedure of Beams

The frame shown in Figure (3.21) was used to test the specimens. The load was applied using hydraulic piston and transferred by H-section column through load cells to the specimen. The capacity of the used load cell was 100 tons. It was placed under the hydraulic piston as shown in Figure (3.21) and attached to a data logger device to measure the transformed load. Linear Variable Differential Transformer (LVDT) is an electromechanical transducer capable of converting the rectilinear motion of a structure member into a corresponding electrical signal that a data logger linked to it can read. LVDT linear position sensors are readily available that can measure displacement of structural members, as shown in Figure (3.21). All of the strain gauges, LVDT, and load cell were connected to the data logger (Type: TDS-530) in order to record the required information during the testing process as shown in Figure (3.21) and extracts it as an excel sheet file.

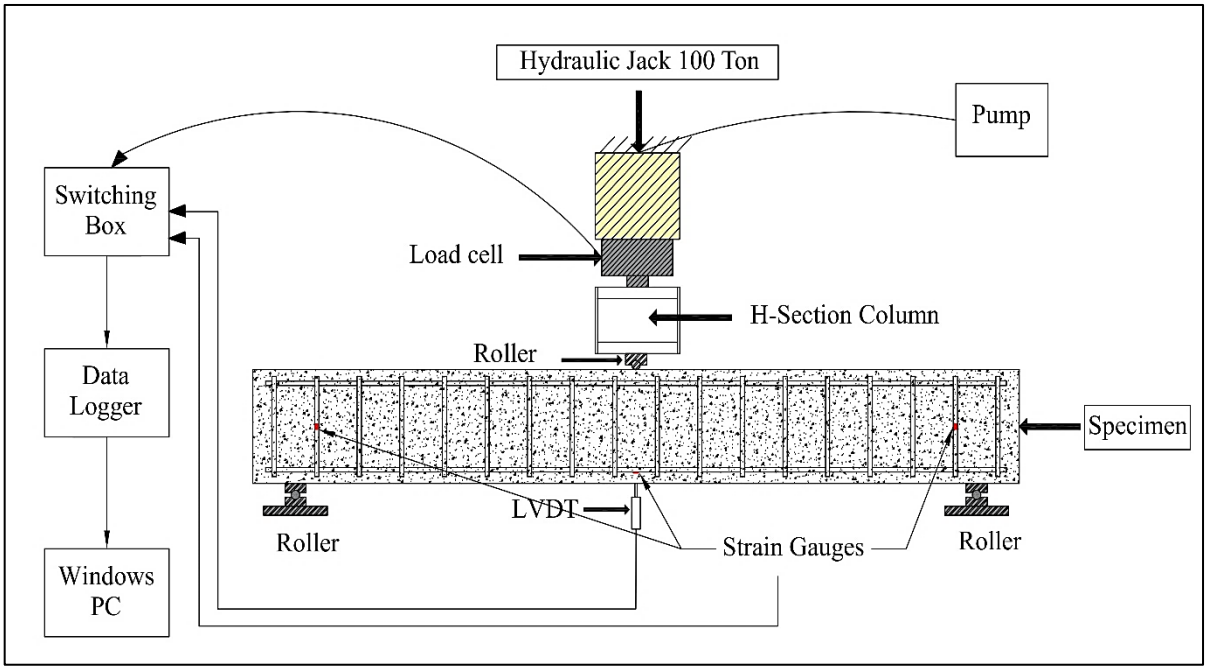

A. Measuring Tools Setup Testing.

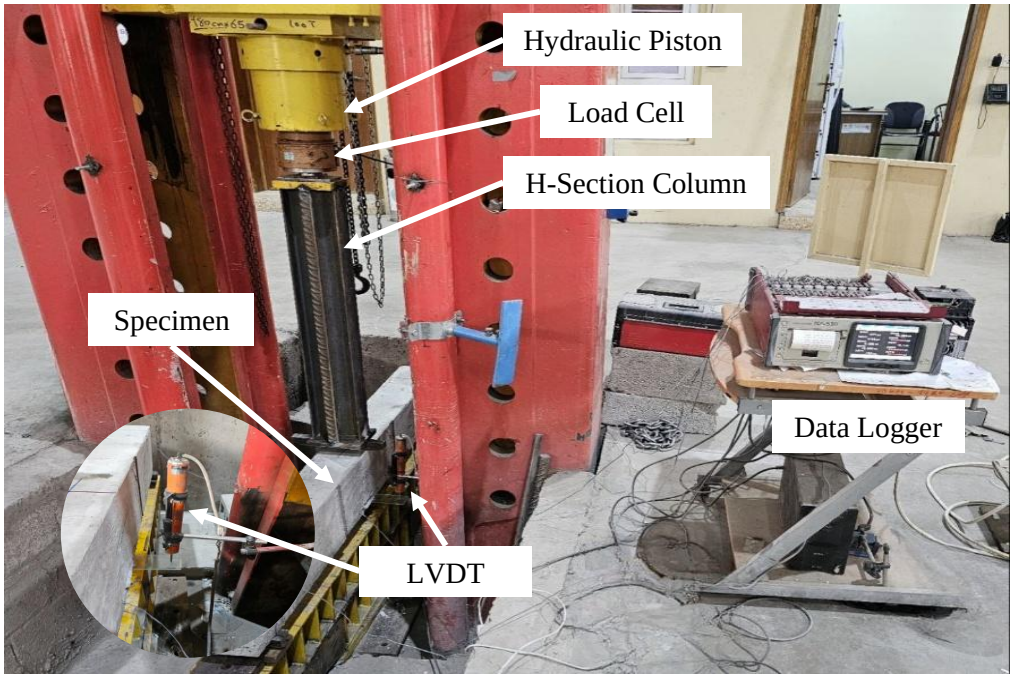

B. Experimental Setup for the specimens.

Figure (3.21): Test Setup

3.14 Preloading of Specimens

The beam tests were carried out at 28 days after moist curing. The specimens were tested under center-point loading as shown in Figure (3.21). Two specimens (CB1 and CB2) were tested to failure and considered as a reference beams. The load was applied at a constant rate of (0.1) kN/Sec. The remaining eight specimens were loaded up to (70) % of the ultimate load of the reference beams as shown in Figure (3.22).

Figure (3.22): Preloaded Beams

Section Three

Retrofitting Reinforced Concrete Beams

3.15 Specimen Details

Ten reinforced concrete beams were tested. Two beams served as reference and were tested to failure without any jacketing. The remaining eight beams were preloaded to 70% of the failure load. These eight beams were divided into four groups, each containing two beams, based on their retrofitting materials and wrapping method, as shown in Figure (3.23) (A, B).

- **Group 1** contains two beams, both retrofitted using traditional mortar and reinforced with welded steel wire mesh. One of them was retrofitted from all four sides (full wrapping), while the other was retrofitted from three side (U-shape wrapping).
- **Group 2** contains two beams, both retrofitted using traditional mortar and reinforced with glass fiber mesh. One of them was retrofitted from all four sides (full wrapping), while the other was retrofitted from three side (U-shape wrapping).
- **Group 3** contains two beams, both retrofitted using sustainable mortar and reinforced with welded steel wire mesh. One of them was retrofitted from all four sides (full wrapping), while the other was retrofitted from three side (U-shape wrapping).
- **Group 4** contains two beams, both retrofitted using sustainable mortar and reinforced with glass fiber mesh. One of them was retrofitted from all four sides (full wrapping), while the other was retrofitted from three side (U-shape wrapping).

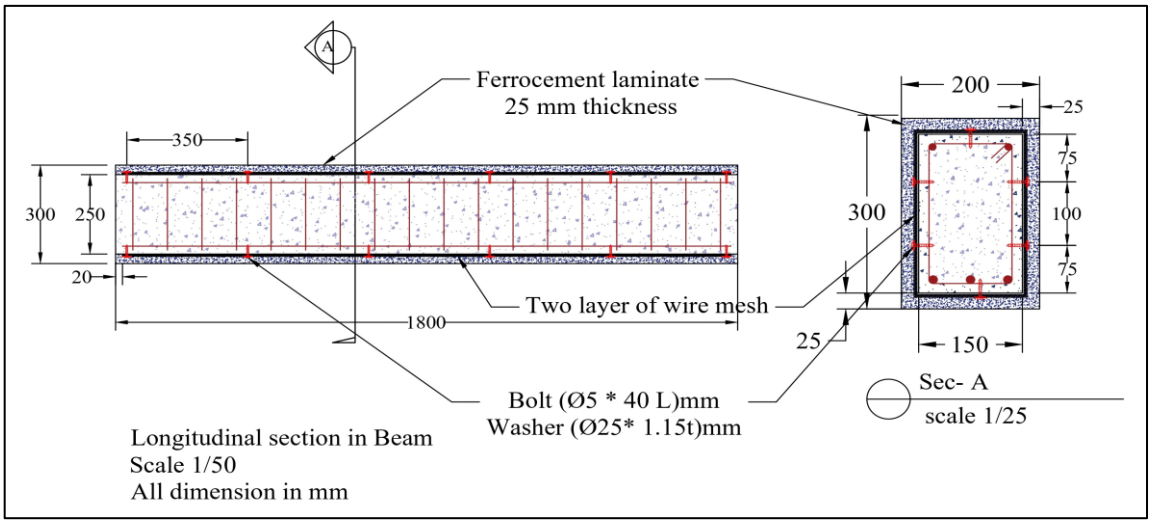

A. Longitudinal and Cross Section of Beam Shows Full Wrapping.

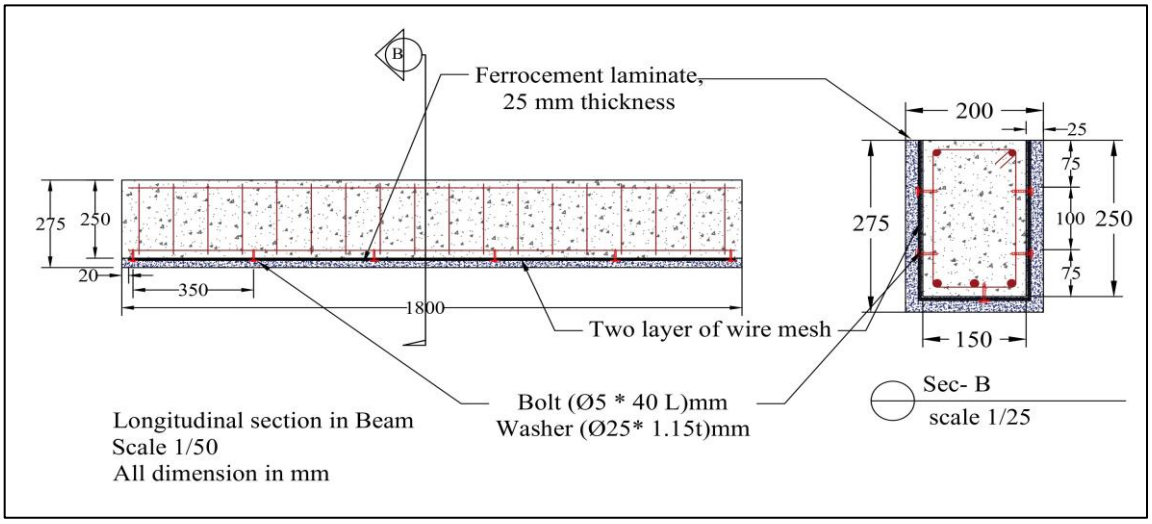

B. Longitudinal and Cross Section of Beam Shows U-Shape Wrapping.

Figure (3.23): Types of Wrapping Beams

The symbols that are used in this study are represented in Table (3.18).

Table (3.18): Definition of the Symbol Used in Ferrocement

Symbol	Definition
C	Control
B	Beam
T	Traditional mortar
E	Eco-friendly (sustainable) mortar
F	Full wrapping (four sides)
U	U-shape wrapping (three sides)
W	Welded wire mesh
G	Glass fiber mesh

The variables that were studied in this research were:

1. **Mortar:** Ferrocement made of sustainable mortar with (silica fume, waste tire rubber, and waste plastic bottle fiber), as well as traditional mortar.
2. **Reinforcement:** Welded steel wire mesh and glass fiber mesh.
3. **Wrapping Configuration:** Two different configurations were used: Full wrapping of the beam on four sides and U-shape wrapping on three sides.
4. **Reinforcement Layers:** All beams were reinforced with two layers of welded steel wire mesh or glass fiber mesh with a ferrocement thickness of 25mm.
5. **Sustainable Mortar Optimization:** Several mixtures were conducted and tested to determine the optimum mixture.

Table (3.19) shows the details of the four specimen groups.

Table (3.19): Groups of Specimens

Groups	Specimen's Code	Type of Mortar	Type of Mesh	Type of Wrapping	Preloaded Percentage	No. of Specimens
CB	CB	Beams without any jacketing			100%	2
Group 1	BTWF	T	W	F	All these beams were preloading to 70% of the ultimate load	1
	BTWU	T	W	U		1
Group 2	BTGF	T	G	F		1
	BTGU	T	G	U		1
Group 3	BEWF	E	W	F		1
	BEWU	E	W	U		1
Group 4	BEGF	E	G	F		1
	BEGU	E	G	U		1

3.16 Wrapping of Mesh Reinforcement

The preloaded beams were wrapped on four sides (full wrapped) and three sides (U-shape) using two layers of two types of mesh reinforcement: welded steel wire mesh and glass fiber mesh, as shown in Figure (3.24). Each layer exhibits an overlap of at least two mesh opening sizes [9] or 50 mm, as shown in Figure (3.25) (A). Two layers of mesh, as shown in Figure (3.25) (B), with dimension of (850×1800) mm on full wrapping, (650 ×1800) mm on U-shape wrapping and cover of (2) mm were fixed using bolts with dimension (Ø5×40 length) mm and washers (Ø25×1.15 thickness) mm to prevent debonding and achieve the maximum tensile strength of these meshes.

The glass fiber mesh was placed in the longitudinal direction to achieve reinforcement ratios approximately similar to those of the welded steel wire mesh and to avoid mesh overlap in mid span of beam when used in the transverse direction.

The fixing process involves

- Cleaning: Cleaning the beam surface.
- Drilling the holes: Each hole measuring (8) mm, equal to the fischer diameter.
- Spacing: Holes were placed at (350) mm interval at the top, bottom, and side of the beam, with two rows on each side, as illustrated in Figure (3.23).
- Bolt insulation: Bolts were inserted into each fischer with washers placed on the mesh, and the bolts were tightened to achieve a perfect fix of mesh on the beam's sides as shown in Figure (3.25) (C).

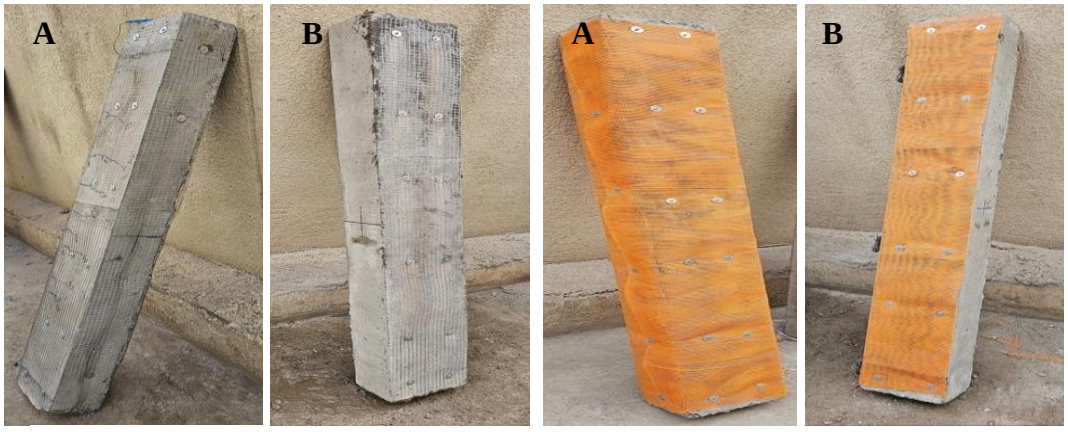

A. Welded Steel Wire Mesh. B. Glass Fiber Mesh.

Figure (3.24): Wrapping of Beams with Welded Steel and Glass Fiber Mesh for Fully Wrapped (A) and U-Shape Wrapped (B)

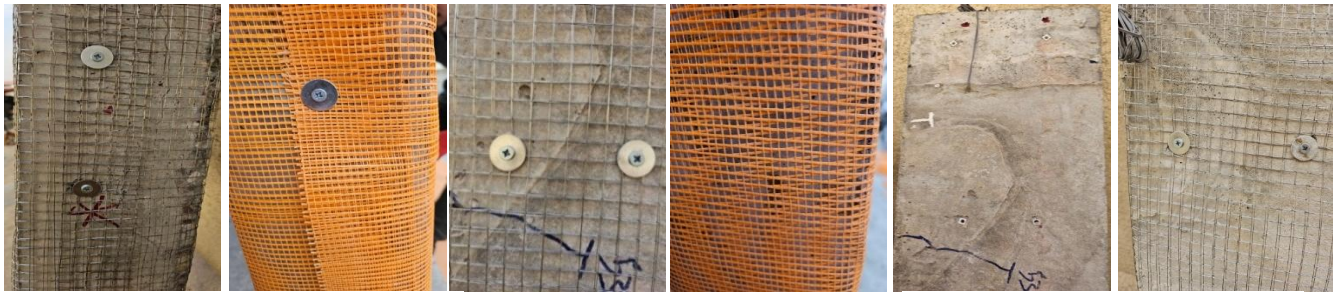

A. Overlapping the Meshes. B. Two Layers of Mesh. C. Holes, Fishers and

Figure (3.25): Details of Fixing Wire Mesh

3.17 Application of Retrofitting Mortar

3.17.1 Retrofitting Beams Using Traditional Mortar

The process of plastering the beams includes.

1. Surface Preparation: Preparing and cleaning surfaces of the beams from dust and dirt.
2. Material Weighing and Mixing: Measuring all the required materials (note that sand must pass through sieve No. 8 according to ACI 549R-18 [9]) and mix them with the ratio of (1:1.906) and water/cement ratio of (0.47) until the mortar are homogeneous.
3. Plastering Process: The plastering process includes,

- Filling the gaps of the mesh by mortars.
- Installing wooden rulers to maintain uniform thickness.
- Continuing the plastering process to achieve the final appearance of the beams with a thickness of 25 mm.

Figure (3.26) shows process of retrofitting the preloaded beams using traditional mortar reinforcement with welded steel wire mesh and glass fiber mesh, applied to the specimens (BTWF, BTWU, BTGF, BTGU).

A. Filling the Voids of Mesh. B. Fixing Wood Rule. C. Final Appearance of Beams.

Figure (3.26): Process of Retrofitting Using Traditional Mortar

3.17.2 Retrofitting Beams Using Sustainable Mortar

The optimal mixture of the sustainable materials, used in retrofitting the beams, contains 8% silica fume as replacement ratio from weight of cement, 5% crumb rubber replacement from weight of sand and 0.75% volumetric ratio from waste plastic fiber (obtained from the total volume of ferrocement used to retrofit the preloaded beams).

The optimal mixture within addition to the basic materials were used to prepare the sustainable mortar, reinforced with either welded steel wire mesh or glass fiber mesh. This mortar was applied on the specimens

(BEWF, BEWU, BEGF, BEGU) following the same process in section 3.17.1 as shown in Figure (3.27).

A. Mixing Materials. B. Filling the Voids of Mesh. C. Fixing Wood Rule. D. Final Appearance of Beams.

Figure (3.27): Process of Retrofitting Using Sustainable Mortar

3.18 Fixing the Strain Gauges on Ferrocement Surface

The strain gauge was used to monitor the behavior of the specimens under applied load and measure the strain in ferrocement mortar. The concrete strain gauges were used as shown in the Figure (3.28) and its properties listed in Table (3.20).

The process of fixing a concrete strain gauge includes smoothing and cleaning the surface from any impurities. Using a special type of glue, the strain gauge was fixed on the mortar at the midspan of the beams on a tension face as shown in Figure (3.28). The strain gauge was covered by a plastic sheet until finishing the preparation of the specimen to protect it due to its sensitivity. The strain wires were connected to a data logger equipment with a movable ram memory for saving data and then transporting it to the computer in excel form.

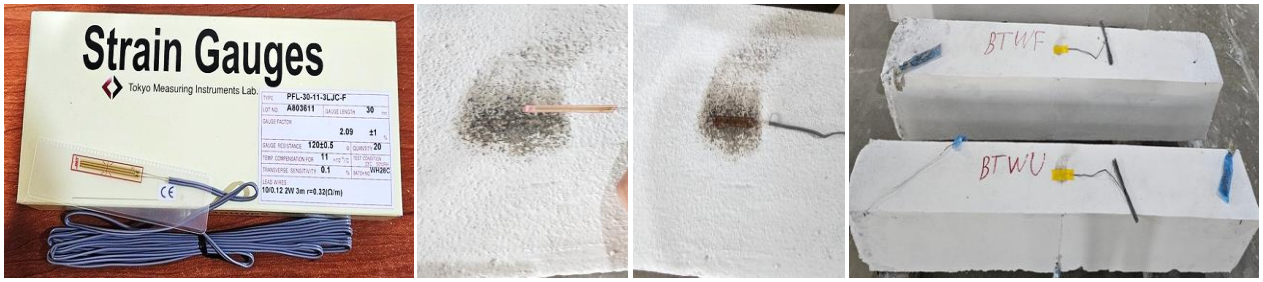

Figure (3.28): Concrete Strain Gauges and Installation Process

Table (3.20): Properties of Concrete Strain Gages

Type	PFL-30-11-3LJC-F
Gage Length	30 mm
Gage Factor	2.09 ±1%
Gage Resistance	120 ±0.5
Transverse Sensitivity	0.1%

3.19 Curing and Painting

The specimens were covered in burlap bags to retain moisture for 28 days, as shown in Figure (3.29) (A). The burlap was moistened daily. After the curing period, the specimens were dried and painted white, as shown in Figure (3.29) (B) to make the cracks visible, and then the beam code was recorded on it.

A. Curing of Specimens. B. Paint of Specimens.

Figure (3.29): Curing and Painting the Beams

3.20 Testing Set-Up

After the 28-day curing period, four groups of specimens containing eight retrofitted beams were tested under center point load up to failure using the same test setup and following the same process mentioned in section (3.13).

3.21 Prediction of Failure Load for Retrofitted Beams

The expected failure load of the retrofitted beams was estimated based on ACI 549R-18 [9]. All the calculation details are shown in Appendix C. Table (3.21) shows the predicted failure loads. This process considered the number of mesh layers, beam dimensions, and material properties. A full bond between the ferrocement layers and the beam was assumed. The predicted values were later compared to the test results.

Table (3.21): Theoretical Ultimate Load of Retrofitted Beams

Sample	Depth of Neutral Axis c (mm)	Theoretical Ultimate Load (kN)
CB	42.74	74.78
BTWF	34.36	91.52
BTWU	34.54	90.10
BTGF	33.42	88.31
BTGU	33.21	87.08
BEWF	44.80	88.31
BEWU	45.00	86.54
BEGF	42.93	83.96
BEGU	42.63	82.86

Chapter 4

Experimental Results and Discussion

Chapter Four

Results and Discussion

4.1 Introduction

The results obtained from the experimental program are analyzed and discussed in this chapter to study the effect of retrofitting reinforced concrete beams, using ferrocement with either traditional or sustainable mortar. The beams were reinforced with either welded steel wire mesh or glass fiber mesh on all four sides (full wrapping) or three sides (U-shaped wrapping).

Many samples of sustainable mortar containing silica fume, waste tire rubber, and waste plastic bottle fibers were tested to evaluate compressive strength, flexural strength, and splitting tensile strength. The selection of the optimum mix was based on the least reduction in these strengths compared to the other proportions and with the traditional mortar.

Ten reinforced concrete beams were tested under center-point loading. Two reference beams were tested to failure without any jacketing. The remaining eight beams were preloaded to 70% of the failure load, then they were retrofitted using ferrocement and tested to failure.

The first cracking load, ultimate load, failure modes, ductility ratio, stiffness, and toughness were all determined from the test for all beams. In addition, load-midspan deflection curves, load-strain curves for the longitudinal and shear reinforcement bars, and load-strain curves in concrete were plotted for all of the tested beams.

4.2 Results of Traditional and Sustainable Mortar

4.2.1 Test Results of Cement Replacement by Silica Fume

Table (4.1) presents the test results for compressive, flexural, and splitting tensile strength at 7 and 28 days with different percentages of cement replaced by silica fume (SF). Figures (4.1) (A and B) illustrate the variation of these strengths with SF replacement at 7 and 28 days, respectively. The results indicated that the use of silica fume at various replacement ratios for cement weight leads to an increase in compressive, flexural, and splitting tensile strength.

Figures (4.1) (A and B) show an increase in compressive strength by using silica fume. The percent increase in compressive strength at 28 days compared to the traditional mix are listed in Table (4.1). Observed from Table (4.1) that the greatest improvements occurred up to a 10% replacement. Beyond this point, the improvement was minimal. A similar behavior was observed at 7 days. The increase in strength was due to hydration of cement creates various compounds, such as calcium silicate hydrates (CSH) and calcium hydroxide (CH). The CSH gel is responsible for concrete strength. Adding SF to fresh mortar causes a chemical reaction with CH, resulting in more CSH gel. The fine SF powder operates as a micro filler, filling spaces between cement grains and reducing porosity [74], [75], [76].

A similar observation was detected in flexural strength. The greatest improvements were found to be between 8% and 12% silica fume replacement. Afterwards, the impacts decreased. These results are consistent with earlier studies [77] and [78], which showed that silica fume enhances the mortar's resistance to bending stresses.

The splitting tensile strength also increased by using silica fume. Table (4.1) shows the best increases in tensile strength at 28 days compared to the traditional mix were observed at 8%, 9%, and 10% replacement; beyond this range, the effect was smaller. These results match the earlier research [77], [79], [80]. Which showed that silica fume improves tensile strength, but the benefits gradually fall off with increasing replacement ratios due to the increase in water content and decrease in cement quantity.

Based on the results, the optimal silica fume content for improving strength is between 8 and 10%. Using more than this amount offers no additional benefit and may cause negative effects, like higher water demand and material lumping. This is due to the high surface area of silica fume. A trial mix with an 8% replacement was effective in enhancing the performance of sustainable mortar.

Table (4.1): Strength of Mortar at 7 and 28 Days for Different Silica Fume Replacement Ratios

Index	**% Rep. (SF) with Cement**	**Compressive Strength (Mpa)**			**Flexural Strength (Mpa)**			**Splitting Tensile Strength (MPa)**		
		7 days	**28 days**	**% Increase *f*cu 28 days**	**7 days**	**28 days**	**% Increase *f*r 28 days**	**7 days**	**28 days**	**% Increase *f*t 28 days**
Traditional Mix	0	33.59	43.48	---	8.65	9.54	---	3.34	3.54	---
SF1	8	35.64	46.33	6.6	8.71	9.89	3.66	3.51	4.28	20.9
SF2	9	35.52	45.22	4.0	8.70	9.72	1.90	3.45	4.14	16.95
SF3	10	33.93	44.75	2.9	8.72	9.65	1.20	3.43	4.12	16.38
SF4	12	33.77	43.75	0.6	8.69	9.69	1.58	3.41	3.63	2.54
SF5	15	33.69	43.65	0.4	8.66	9.56	0.25	3.36	3.57	0.85

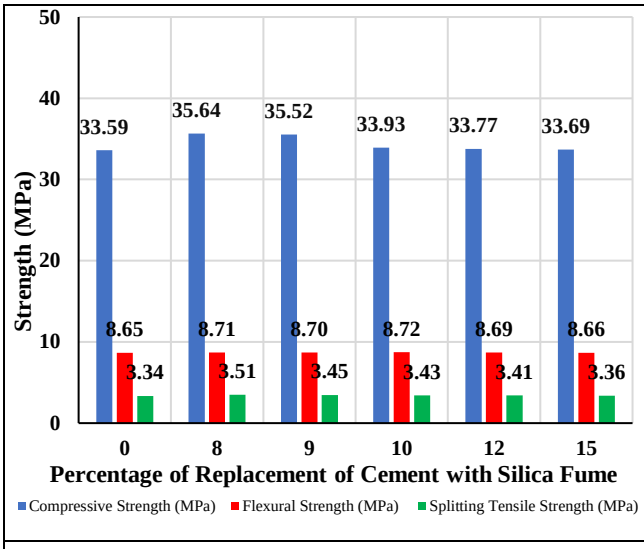

A. Strength at 7 days for Different Silica Fume Replacement Ratio.

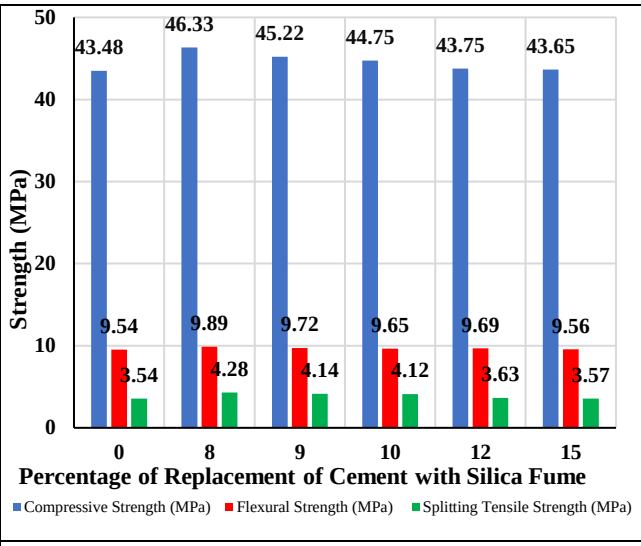

B. Strength at 28 days for Different Silica Fume Replacement Ratio.

Figure (4.1): Strength of Mortar at 7 and 28 Days for Different Silica Fume Replacement Ratios

4.2.2 Test Results of Sand Replacement by Crumb Rubber

The effect of waste tire rubber (crumb rubber (CR)) replacement on the compressive, flexural, and splitting tensile strength of the sustainable mortar at 7 and 28 days is shown in the Table (4.2) and Figures (4.2) (A and B).

Table (4.2): Strength of Mortar at 7 and 28 Days for Different Crumb Rubber Replacement Ratios

Index	% Rep. (CR) with Sand	Compressive Strength (Mpa)			Flexural Strength (Mpa)			Splitting Tensile Strength (MPa)		
		7 days	28 days	% Decrease *f*cu 28 days	7 days	28 days	% Decrease *f*r 28 days	7 days	28 days	% Decrease *f*t 28 days
Traditional Mix	0	33.59	43.48	---	8.65	9.54	---	3.34	3.54	---
CR1	5	24.10	28.32	34.87	6.63	8.58	10.0	2.91	3.20	9.6
CR2	10	17.04	22.82	47.51	5.75	7.13	25.2	1.67	2.53	28.5
CR3	15	14.28	18.57	57.29	4.77	6.14	35.6	1.58	2.10	40.6

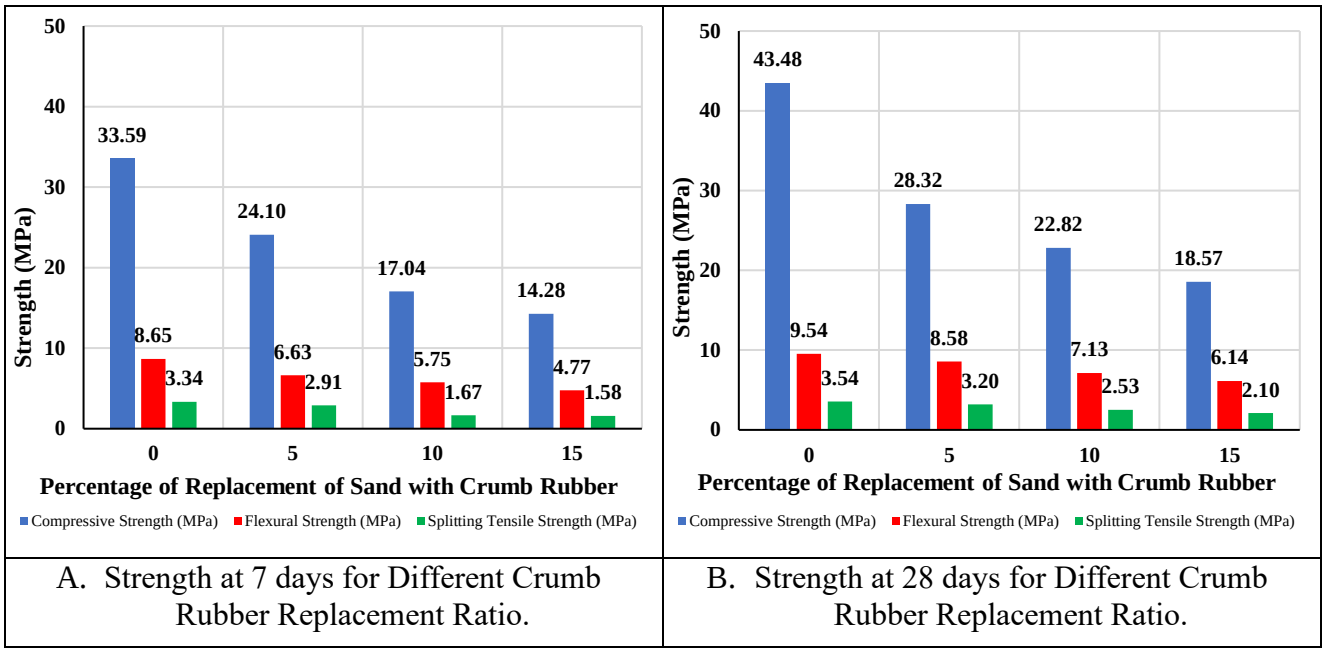

A. Strength at 7 days for Different Crumb Rubber Replacement Ratio.

B. Strength at 28 days for Different Crumb Rubber Replacement Ratio.

Figure (4.2): Strength of Mortar at 7 and 28 Days for Different Crumb Rubber Replacement Ratios

The compressive strength of mortar containing crumb rubber decreased as the crumb rubber replacement percentage increased. These results are consistent with previous studies [81], [82]. At 7 days, the compressive strength of crumb rubber mortar reduced by 28.25%, 49.24%, and 57.45% for 5%, 10%, and 15% rubber replacements, respectively. At 28 days, the reduction was listed in Table (4.2) compared to the traditional mix. The strength is reduced because of the weak bond between rubber particles and the cement matrix, which leads to micro-cracks and accelerates crack propagation under load [83].

The flexural strength of crumb rubber mortar also decreased as the replacement level increased. Table (4.2) shows the percent decrease in flexural strength at 28 days, compared to the traditional mix. This reduction was due to the weak adhesion between rubber particles and cement paste, the non-homogeneous distribution of rubber particles

inside the mortar mixture, and the hydrophobic characteristics of rubber particles. These factors caused more air bubbles in the mortar mixture and increased overall air content [84], [85].

The same pattern was observed in splitting tensile strength, which decreased with increasing crumb rubber content. From Table (4.2) observed the least decrease in tensile strength at 28 days was at 5% replacement ratio. This reduction is due to the loss of bonding material. Furthermore, the decrease in splitting tensile strength was lower than that of the compressive strength because the rubber particles bridge cracks and limit their progression, and the rubber particles are flexible and can stretch slightly [84], [86].

The optimum strength was achieved with 5% of crumb rubber replacement in the cement mortar as this proportion caused the least reduction in strength. A trial mix with this percentage was prepared to confirm the results.

4.2.3 Test Result of Adding Waste Plastic Bottle Fiber

The incorporation of waste plastic bottle fibers (PF) into sustainable mortar made with 8% silica fume as a cement replacement and 5% crumb rubber as a sand replacement had a clear impact on compressive, flexural, and splitting tensile strength at 7 and 28 days. The results are presented in Table (4.3) and Figures (4.3) (A and B).

Plastic fibers lead to a decrease in compressive, flexural, and tensile strength. The percentages of decrease in these strengths at 28 days compared to traditional mortar are shown in Table (4.3).

Table (4.3): Strength of Mortar at 7 and 28 Days for Different Plastic Fiber Addition Ratios

Index	% Addition of PF	Compressive Strength (Mpa)			Flexural Strength (Mpa)			Splitting Tensile Strength (MPa)		
		7 days	28 days	% Decrease *f*cu 28 days	7 days	28 days	% Decrease *f*r 28 days	7 days	28 days	% Decrease *f*t 28 days
Traditional Mix	0	33.59	43.48	---	8.65	9.54	---	3.34	3.54	---
Control Mix	0	26.42	32.52	25.2	6.82	7.45	21.9	3.07	3.33	5.95
PF1	0.5	19.75	24.69	43.2	6.57	7.05	26.1	3.16	3.39	4.32
PF2	0.75	20.32	24.90	42.7	6.62	7.13	25.3	3.22	3.47	1.98
PF3	1	19.27	22.89	47.4	6.39	6.80	28.8	3.10	3.37	4.75

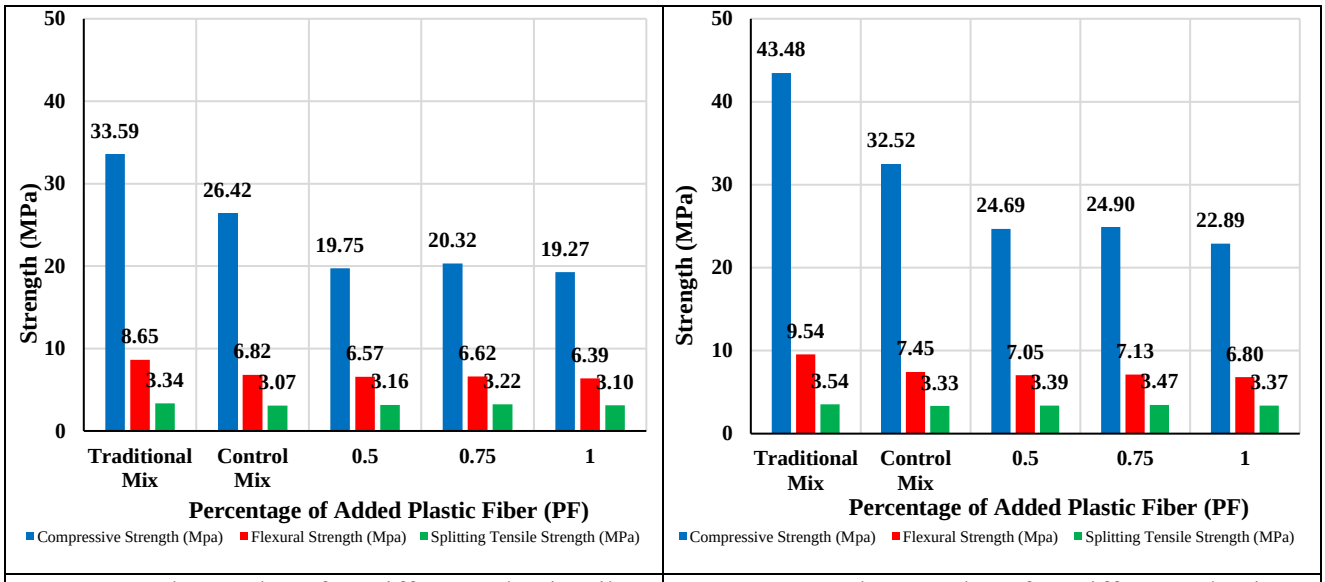

A. Strength at 7 days for Different Plastic Fiber Addition Ratio.

B. Strength at 28 days for Different Plastic Fiber Addition Ratio.

Figure (4.3): Strength of Mortar at 7 and 28 Days for Different Plastic Fiber Addition Ratios

Adding waste plastic fiber in the different volumetric proportions reduced the compressive strength of the sustainable mortar. The test results showed a reduction in the compressive strength, aligning with the previous study [87], [88]. At 28 days, the percentage decrease in the compressive strength of the sustainable mortar compared to the control

mix was 24%, 23.43%, and 29.61% for 0.5, 0.75, and 1% of plastic fiber, respectively. The lowest reduction was observed in specimens containing 0.75% fiber. The decrease in the strength was due to the high void ratio of the reinforced samples exceeding that of the non-reinforced sample and a weak interfacial bond between the fiber and the sustainable mortar [89].

The addition of waste plastic fiber to the mortar also negatively affected flexural strength, causing a reduction compared to the control mix. At 28 days, the reduction was 5.37%, 4.29% and 8.72% for 0.5%, 0.75%, and 1% of plastic fiber, respectively. This result is consistent with the previous study [90]. The reduction can be attributed to the fiber length and their random distribution in the matrix. Meddah and Bencheikh [91] reported that fiber length affects the flexural strength. The inclusion of short fibers (30 mm) slightly reduced the flexural strength, while longer fibers (50 and 60 mm) did not show a significant effect on the flexural strength.

Unlike compressive and flexural strength**,** splitting tensile strength exhibited an improvement with an increase in fiber content. At 28 days, the percentage increase in splitting tensile strength compared to the control mix was 1.8%, 4.2%, and 1.2% for 0.5%, 0.75%, and 1% of plastic fiber, respectively. These results agree with the previous studies [92], [93]. The most significant increase occurred at 0.75% fiber content. Plastic fibers significantly improve the mortar's resistance to crack propagation. The mechanism involves (PF) acting as a reinforcing material that prevents the formation and propagation of cracks within the mortar matrix [94]. This reinforcing effect is particularly significant at the 0.75% level, exhibiting a positive connection with the tensile strength of PF fiber.

4.2.4 Optimum Mixture

The optimum mix was obtained with 8% silica fume replacing cement, 5% crumb rubber replacing sand, and 0.75% plastic fiber added to the mortar. The modified mortar showed mechanical strengths of (24.9 MPa (compressive), 7.13 MPa (flexural), and 3.47 MPa (splitting tensile strength) at 28 days. The strength of the optimal mortar at 28 days is reduced compared to the traditional mortar by (42.7, 25.3, and 1.97) % for compressive, flexural, and splitting tensile strength, respectively.

4.2.5 Cost Comparison

The cost comparisons between traditional and sustainable mortar are calculated based on volume (0.02 m^3) and are shown in Table (4.4). Table (4.4) shows that using traditional mortar is less expensive and stronger than the sustainable mortar. The cost of sustainable mortar increased by 10.4% compared to the traditional mortar. This disparity is due to the lack of specialized facilities for recycling waste materials such as silica fume, crumb rubber, and waste plastic fiber in Iraq.

Table (4.4): Cost Comparison

Details	Unit	Estimation Cost and Quantities for Traditional Mortar			Estimation Cost and Quantities for Sustainable Mortar		
		Unit Price (I.D)	Amount	Total price (I.D)	Unit Price (I.D)	Amount	Total price (I.D)
Cement	Ton	150000	0.00762	1143	150000	0.00762	1143
Sand	m^3	30000	0.0091	273	30000	0.0086	258
Silica Fume	Kg	2500	0	0	2500	0.61	1525
Waste Tire Rubber	Kg	1000	0	0	1000	0.726	726
Waste Plastic Fiber	Kg	2500	0	0	2500	0.206	515
Labors	daily	25000	1	25000	25000	1	25000
Total Cost (I.D)				**26416**	**Total Cost (I.D)**		**29167**

4.3 Results of Preloaded Specimens

4.3.1 Mechanical Properties of Concrete Mixture

The mechanical properties of the concrete mix, which is used in this study, including compressive, flexural, splitting tensile strength, and the slump test, are listed in Table (4.5).

Table (4.5): Mechanical Properties of Concrete Mixture

No.	Mechanical Properties	Value
1	Average Cube Compressive Strength (MPa)	37.0
2	Average Splitting Tensile Strength (MPa)	2.36
3	Average Flexural Strength (MPa)	5.74
4	Slump (mm)	130

4.3.2 Results of the Control and Preloaded Beams

The experimental results of control beams and all preloaded beams, including first cracking load, ultimate load, and corresponding deflection are presented in Table (4.6).

Table (4.6): Experimental and Theoretical Results of All Preloaded Beams

Group	Code	1st Crack load (kN)	Theoretical 1st Cracking load (kN)	Def. at 1st crack load (mm)	Ultimate Load (kN)	Def. at Ultimate load (mm)
CB	CB	16.5	13.3	0.75	76.85	14.68
Group 1	BTWF	17.3	13.5	0.6	53.8	4.4
	BTWU	16.6	13.5	0.65	53.8	4.52
Group 2	BTGF	16.9	13.4	0.7	53.8	4.67
	BTGU	16.6	13.4	0.6	53.8	4.65
Group 3	BEWF	16.2	13.3	0.67	53.8	4.17
	BEWU	17.7	13.3	0.65	53.8	4.63
Group 4	BEGF	17	13.5	0.60	53.8	4.42
	BEGU	17	13.5	0.7	53.8	4.52

4.3.3 Load-Deflection Curve of the Preloaded Beams

Two unstrengthened beams (CB1, CB2) served as control beams and are coded as (CB). Figure (4.4) shows the load-deflection curve for the control beams. The ultimate load was (77.9 and 75.8) kN and the mid-span maximum deflection were (14.15, 15.21) mm, respectively. The average ultimate load and deflection of the control beam (CB) was 76.85 kN, 14.68 mm. These values were used for comparison with the other beams. The results of the control beams are listed in Table (4.6).

The eight preloaded beams are coded with the same symbols used for retrofitted beams. These beams were preloaded to 70% of the failure loads of the control beams (CB), which equals (53.8) kN. Figure (4.5) shows the load-midspan deflection curve for all preloaded beams. As shown in Figure (4.5), all the preloaded beams exhibited similar load and deflection curves because of their identical material property and load testing conditions. The results of the preloaded beams are listed in Table (4.6).

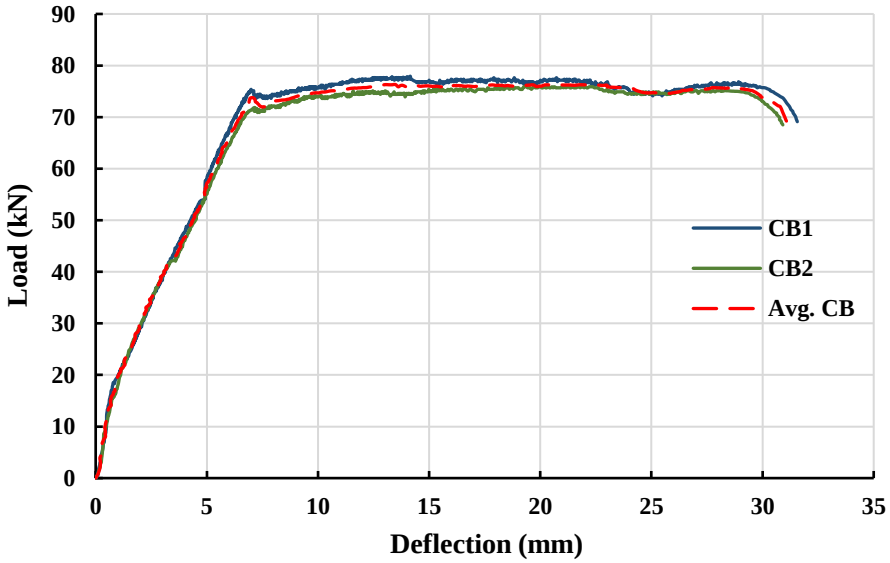

Figure (4.4): Load-Midspan Deflection Curves for Control Beams

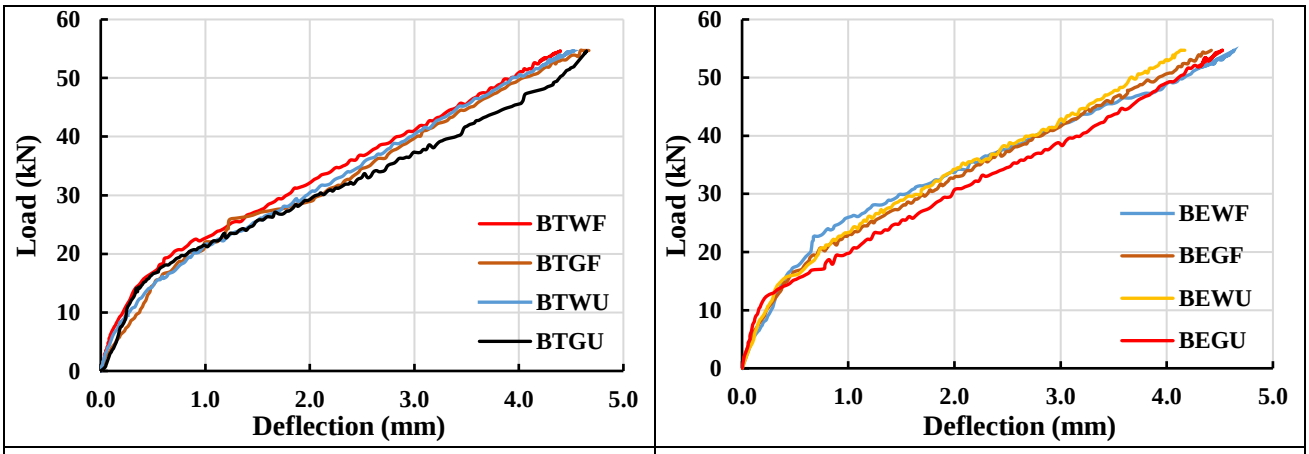

A. Load - Deflection Curve of Group 1 and 2. B. Load - Deflection Curve of Group 3 and 4.

Figure (4.5): Load-Midspan Deflection Curves for Preloaded Beams

4.3.4 Load-Strain Curve of the Preloaded Beams

The strains of control and preloaded beams were measured at three points (See Figure 3.17). Control beam (CB1) recorded a yield strain in longitudinal steel bars (FS1) equal to (6310×10^{-6}), while (CB2) had a yield strain equal to (6615×10^{-6}). The control beams exhibited strain values greater than yielding strain, which equals to (2000×10^{-6}), indicating that the longitudinal steel reached the yield strain as shown in Figure (4.6). The average strain for control beams (CB) equal to (6462×10^{-6}) at a yield load equal to 73.45 kN, as shown in Figure (4.6).

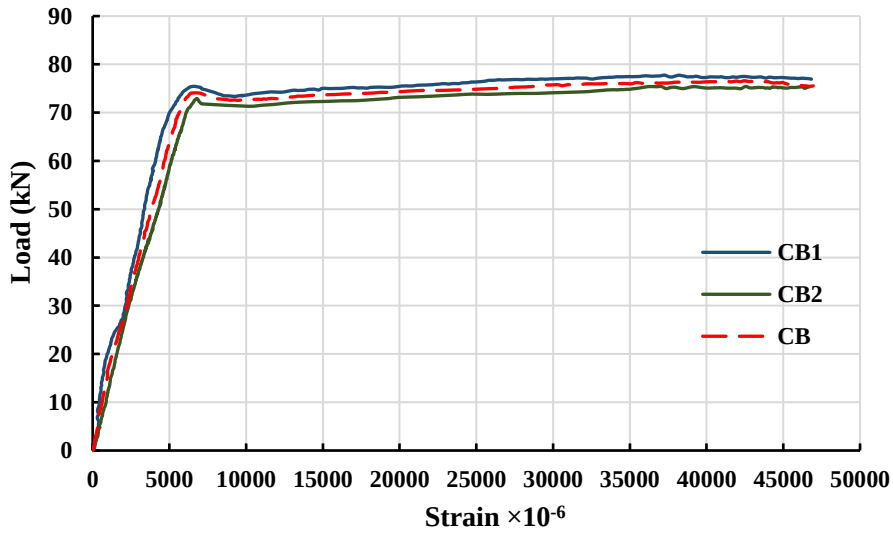

Figure (4.6): Load-Strain (FS1) Curves for Control Beams

The load strain curve in the longitudinal steel bars of all preloaded beams are shown in the Figure (4.7). Note that strain gauge in beam (BTGU) did not record the strain values due to a technical problem. The yield strain of these beams was set at 70% of the control beams yield strain, which is equal to (4523×10^{-6}). It was observed that the strain in preloaded beams reached the bar yield strain of (2000×10^{-6}).

The strain in the stirrups of both control and preloaded beams was not recorded due to technical issues.

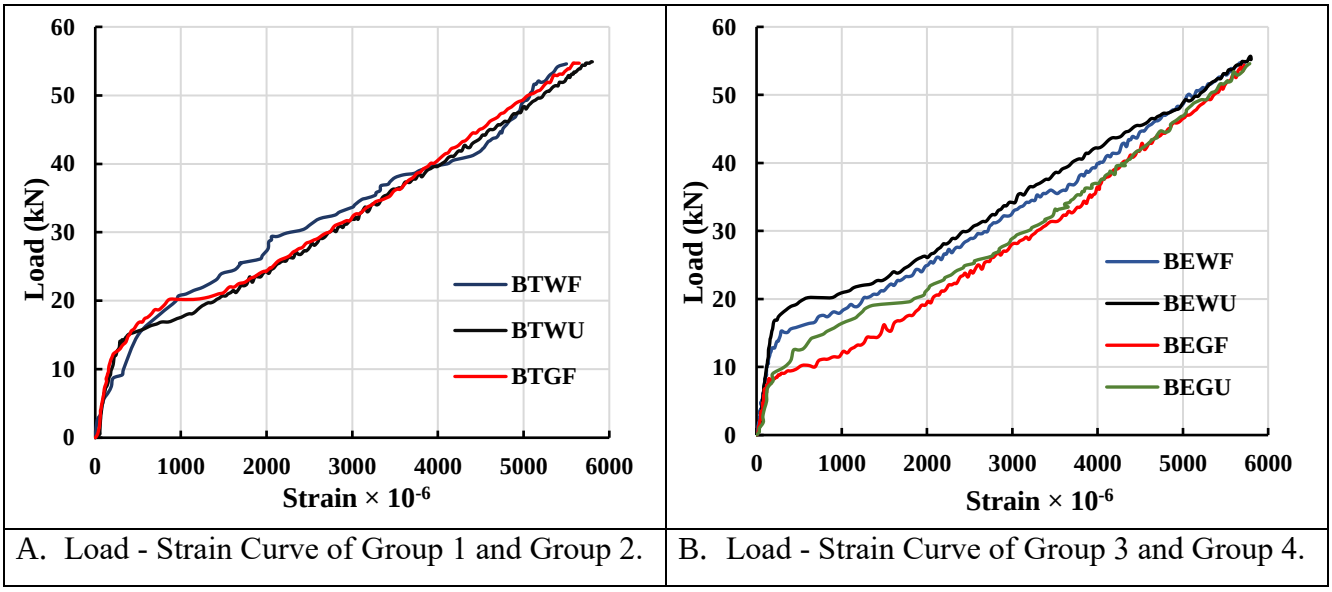

A. Load - Strain Curve of Group 1 and Group 2.

B. Load - Strain Curve of Group 3 and Group 4.

Figure (4.7): Load-Strain Curves (FS1) for Preloaded Beams

4.3.5 Mode of Failure of the Preloaded Beams

Figure (4.8) (A) shows the mode of failure and crack pattern of the control beams. Cracking initiated at the mid-span under applied load and then spread toward both ends. As the loads increased to the ultimate level, two wide cracks extended from tension to the compression zone. The control beams failed in flexural, followed by crushing of the concrete in the compression zone at the mid-span of the beams.

The eight beams preloaded to 70% of the failure load developed a few hairline cracks during loading, as shown in Figure (4.8) (B). They exhibited flexural cracks along their tension zone, which did not require any treatment prior to strengthening.

A. Failure Mode and Crack Pattern of Control Beams.

B. Crack Pattern of All Preloaded Beams.

Figure (4.8): Failure Modes and Crack Patterns of Control and All Preloaded Beams

4.4 Results of Retrofitted Specimens

Table (4.7) presents the experimental results of the retrofitted beams, including first cracking load, yield load, ultimate load, and the corresponding mid-span deflection.

Table (4.7): Test Results for the Retrofitted Beams

Group	Beam Code	At Cracking		At Yielding		At Ultimate		
		Load (kN)	Deflection (mm)	Load (kN)	Deflection (mm)	Load (kN)	Deflection (mm)	% Increase Ultimate Load
CB	**CB**	16.5	0.75	73.45	7.17	76.85	14.68	---
Group 1	**BTWF**	32.1	1.7	84.3	6.7	87.3	20.53	13.6
	BTWU	29	2.7	78.9	6.85	82.8	19.45	7.7
Group 2	**BTGF**	28	1.6	81	7.2	84.8	20.10	10.3
	BTGU	24.5	1.9	75.1	7.1	81.8	19.00	6.4
Group 3	**BEWF**	27	2.4	78.2	7.8	81.3	24.70	5.8
	BEWU	29.5	2.7	82.8	8.5	82.8	8.50	7.7
Group 4	**BEGF**	24	2.28	74	8.1	78.5	23.83	2.1
	BEGU	28	2.44	76.6	8.4	81.6	24.24	6.2

4.4.1 Load - Midspan Deflection Curve

Group 1 includes two beams (BTWF and BTWU). The results show that applying ferrocement with traditional mortar enhance the load-deflection behavior compared to the control beam as shown in Figure (4.9) (A). These results agree with results found by [32] and [34]. Full wrapping beam (BTWF) increases the ultimate load by (13.6 and 5.4) % as compared to the control and BTWU beams, respectively. At yield load, the deflection of the retrofitted beam (BTWF and BTWU) is reduced by (6.6 and 4.5) %, respectively, as compared to the control beam due to the increase in its effective depth. At ultimate load, the deflection increased by (39.8 and 32.5) %, respectively. This is due to the use of ferrocement, which allowed the beam to deform more before failure and improved its ductility.

Group 2 includes two beams (BTGF and BTGU). Figure (4.9) (B) shows the load-deflection curves of the specimens in Group 2 and control beam. Similar behavior to specimens in group 1 was observed, showing an increase in the ultimate load by 10.3% for BTGF and 6.4 % for BTGU compared to the control.

Group 3 includes two beams (BEWF and BEWU). For Beam BEWF, the ultimate load was (81.3) kN, and the maximum mid-span deflection was (24.7) mm. For beam BEWU, the ultimate load was (82.8) kN, with a maximum deflection of (8.5) mm. Beam BEWU exhibited a drop in load-carrying capacity as shown in Figure (4.9) (C), indicating failure or collapse. This behavior may be due to weak bonding between the sustainable mortar and beam surface, which leads to partial debonding of the ferrocement layer, resulting in sudden wide cracking in the beam and eventual failure. The ultimate load of beams BEWF and BEWU increased by 5.8 and 7.7 %, respectively, compared to the control. The ultimate load of beams BEWU increased by 1.85% compared to beam BEWF.

Group 4 includes two beams (BEGF and BEGU). Figure (4.9) (D) shows that the ultimate load of the beams (BEGF and BEGU) increased by (2.1 and 6.2) %, respectively, compared to the control beams. Also, the ultimate load of beams BEGU increased by (3.95) % compared to beam BEGF. Additionally, the deflection at ultimate load for both retrofitted specimens was higher compared to the control beam (See Table (4.7)).

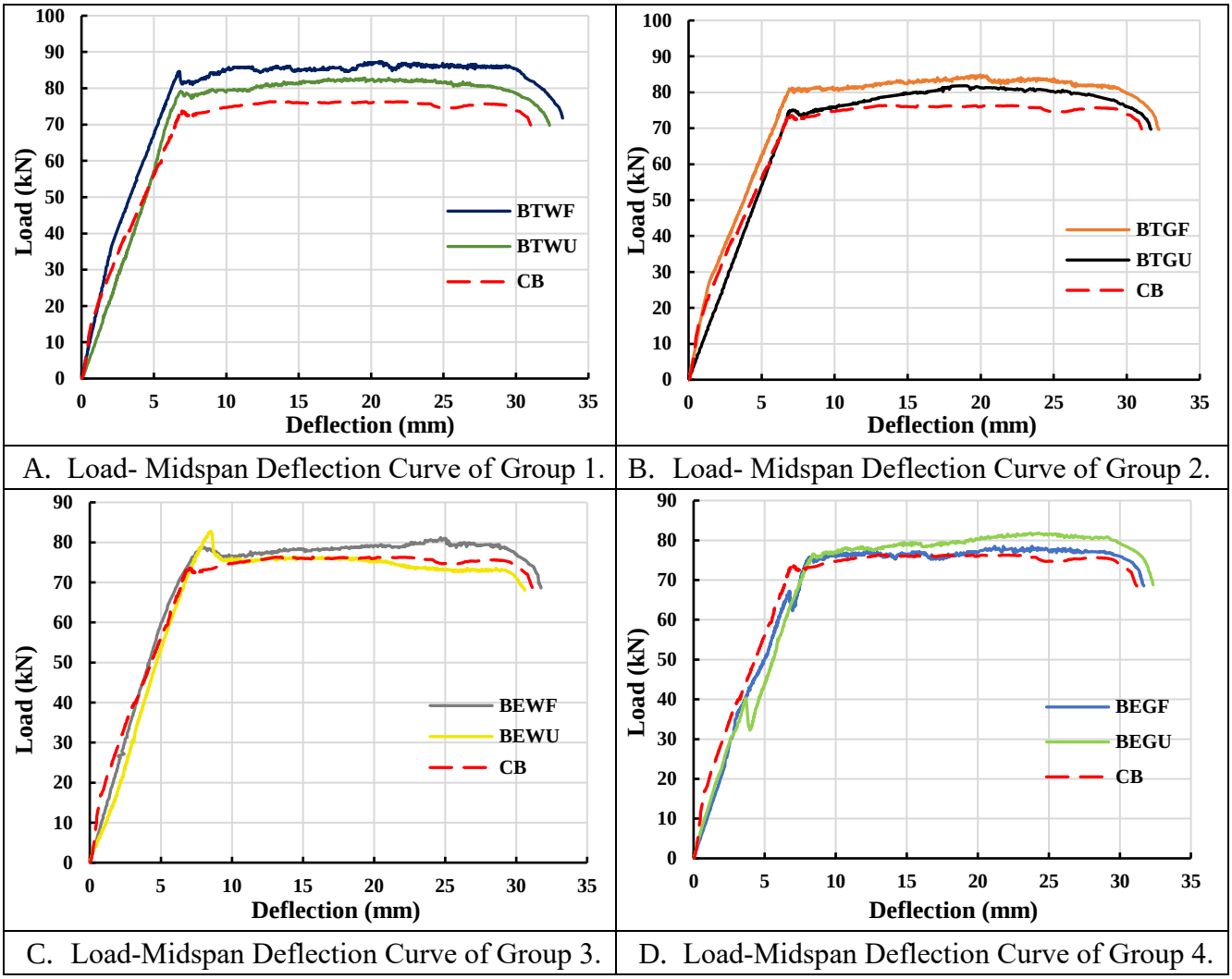

A. Load- Midspan Deflection Curve of Group 1.

B. Load- Midspan Deflection Curve of Group 2.

C. Load-Midspan Deflection Curve of Group 3.

D. Load-Midspan Deflection Curve of Group 4.

Figure (4.9): Load-Midspan Deflection Curves for All Groups with Control Beams

4.4.2 Comparison and Discussion of Load-Deflection Curves

Figure (4.10) (A) shows the load-deflection curve of the beams in Group 1 and Group 2, along with the control beam. Figure (4.10) (A) shows that the specimens in Group 1 (reinforced with welded steel wire mesh) exhibited higher ultimate load and lower deflection compared to the specimens in Group 2 (reinforced with glass fiber mesh). The reduction in ultimate load in Group 2 compared to Group 1 was (2.86 and 1.21) % for full and U-shape wrapping, respectively. These results agree with [43] and [95], showing that the steel wire mesh

provided a higher ultimate load and less deflection than glass fiber mesh.

Figure (4.10) (B) shows the load-deflection curve of beams in Group 1 and Group 3, in addition to the control beam. The ultimate load of the beams retrofitted with ferrocement using sustainable mortar (BEWF and BEWU) exhibited a reduction by (6.87 and 0) %, compared to the beams retrofitted with ferrocement using traditional mortar (BTWF and BTWU). The deflection values in sustainable mortar beams were more than those in Group 1. This increase is due to lower stiffness and weak bonding between the sustainable mortar and the beam surface.

Figure (4.10) (C) shows the load-deflection curves of beams in the Group 3, Group 4, and the control beam. The ultimate load of beams BEGF and BEGU decreased by (3.44 and 1.45) %, compared to beams BEWF and BEWU, respectively. Additionally, the beams in Group 3 exhibited lower deflection compared to those in Group 4. This behavior is due to the use of welded wire mesh, which resists deformation more than the glass fiber mesh. This difference was also observed when testing the mesh samples, as the welded wire mesh showed less deflection than the glass fiber mesh (see section 3.4.2).

Figure (4.10) (D) shows the load-deflection curves of beams in Group 2, Group 4, and the control beam. The ultimate load of beams BEGF and BEGU decreased by (7.43 and 0.24) %, compared to beams BTGF and BTGU, respectively. Additionally, beams in Group 4 exhibited higher deflection compared to the beams in Group 2 due to the use of sustainable mortar.

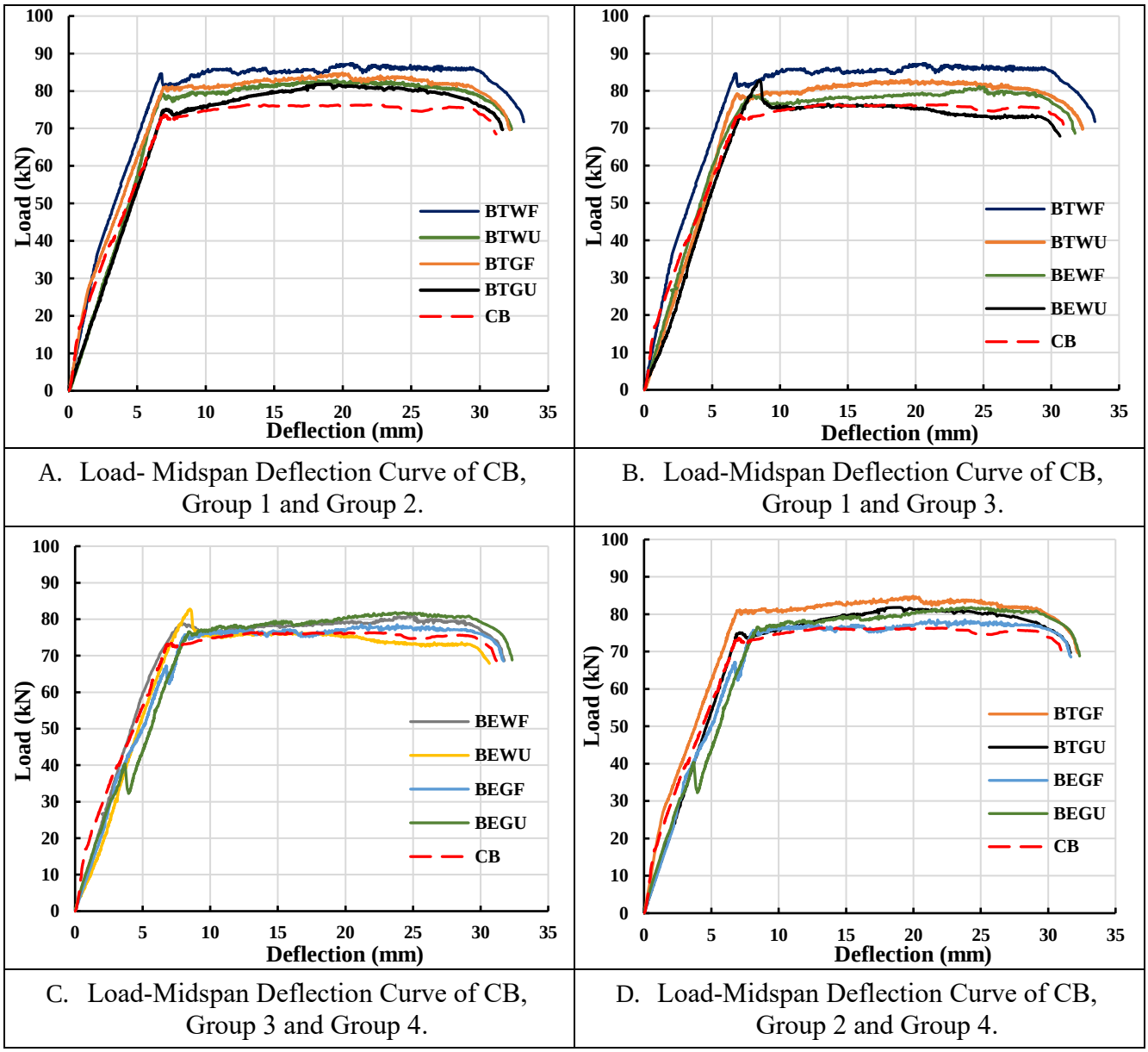

Figure (4.10): Load-Midspan Deflection Curves of Various Groups and Control Beams

Figure (4.11) shows the load-midspan deflection curve of all beams retrofitted using ferrocement with either (traditional and sustainable mortar) and reinforced with (welded steel wire or glass fiber mesh) for full wrapping (A) and U-shaped wrapping (B) in all groups, along with the control beam.

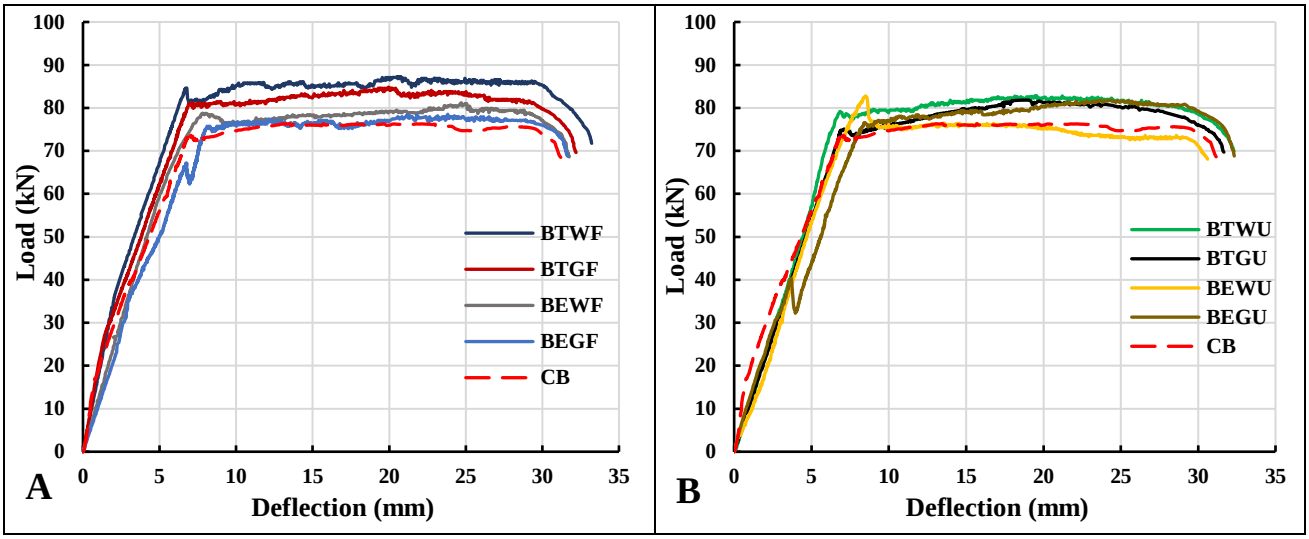

Figure (4.11): Comparison of Load- Midspan Deflection Curves for All Beams with Control Beam (A) Full Wrapping and (B) U-Shaped Wrapping

4.4.3 Load-Strain Curves in Steel Reinforcement

In this section, load-strain curves in the longitudinal bars are presented. Load-strain curves in the transverse reinforcement were not recorded due to technical problems. In general, all retrofitted beams exceed the yield strain value of (2000×10^{-6}). The yield strain values in the retrofitted beams were higher than strain in the control beam due to increased strength of the retrofitted beams. Table (4.8) presents the strain value of all retrofitted beams at yield and ultimate load. The yield load of these beams was the same yield load of load deflection curve and was obtained according to park [96], based on the method of reduced stiffness equivalent to an elasto-plastic yield.

Table (4.8): Strain of Longitudinal Reinforcement at Yield and Ultimate Loading of Retrofitted Beams

Group	Specimen's Code	Yielding Load (kN)	Strain at Yield $\times 10^{-6}$	Ultimate Load (kN)	Strain at Ultimate $\times 10^{-6}$
CB	**CB**	73.45	6462	76.6	42467
Group 1	**BTWF**	84.3	9792	85.8	132100
	BTWU	78.9	9500	81.2	88342
Group 2	**BTGF**	81	12588	81.2	80000
	BTGU*	---	---	---	---
Group 3	**BEWF**	78.2	10131	78.5	61495
	BEWU	82.8	9796	82.8	9796
Group 4	**BEGF**	74	13000	76.1	29411
	BEGU	76.6	11000	78.6	27723

* Beam BTGU was not recorded due to technical issues.

4.4.4 Comparison and Discussion of Load Strain Curve

Figure (4.12) (A) shows the load-strain curves of the beams in Group 1, Group 2, and control beam. The yield strain values (FS1) in Group 2 were higher by 28.55%, compared to Group 1 for the fully wrapped beam. This increase is due to the use of glass fiber mesh.

Figure (4.12) (B) shows the load-strain curve of beams in Group 1, Group 3, and the control beam. At yield load, the strain values in the longitudinal bars for Group 3 were higher than the strain in Group 1 by 3.46% for the fully wrapped beam and 3.1% for the U-shape wrapped beam. This increase is attributed to the use of sustainable mortar.

Figure (4.12) (C) shows the load-strain curves of the beams in Group 3, Group 4, and the control beam. The yield strain values (FS1) in the beams of Group 4 were higher than that in Group 3 by 28.3% for the fully wrapped beam and by 12.3% for the U-shaped wrapped beam. This increase is due to the glass fiber mesh, allowing more deformation, compared to the welded wire mesh.

Figure (4.12) (D) shows the load-strain curve of beams in Group 2, Group 4, and the control beam. The yield strain values (FS1) in the

longitudinal steel bars of beams in Group 4 were higher than those in Group 2 by 3.3% for the fully wrapped beam. This increase is again attributed to the use of sustainable mortar.

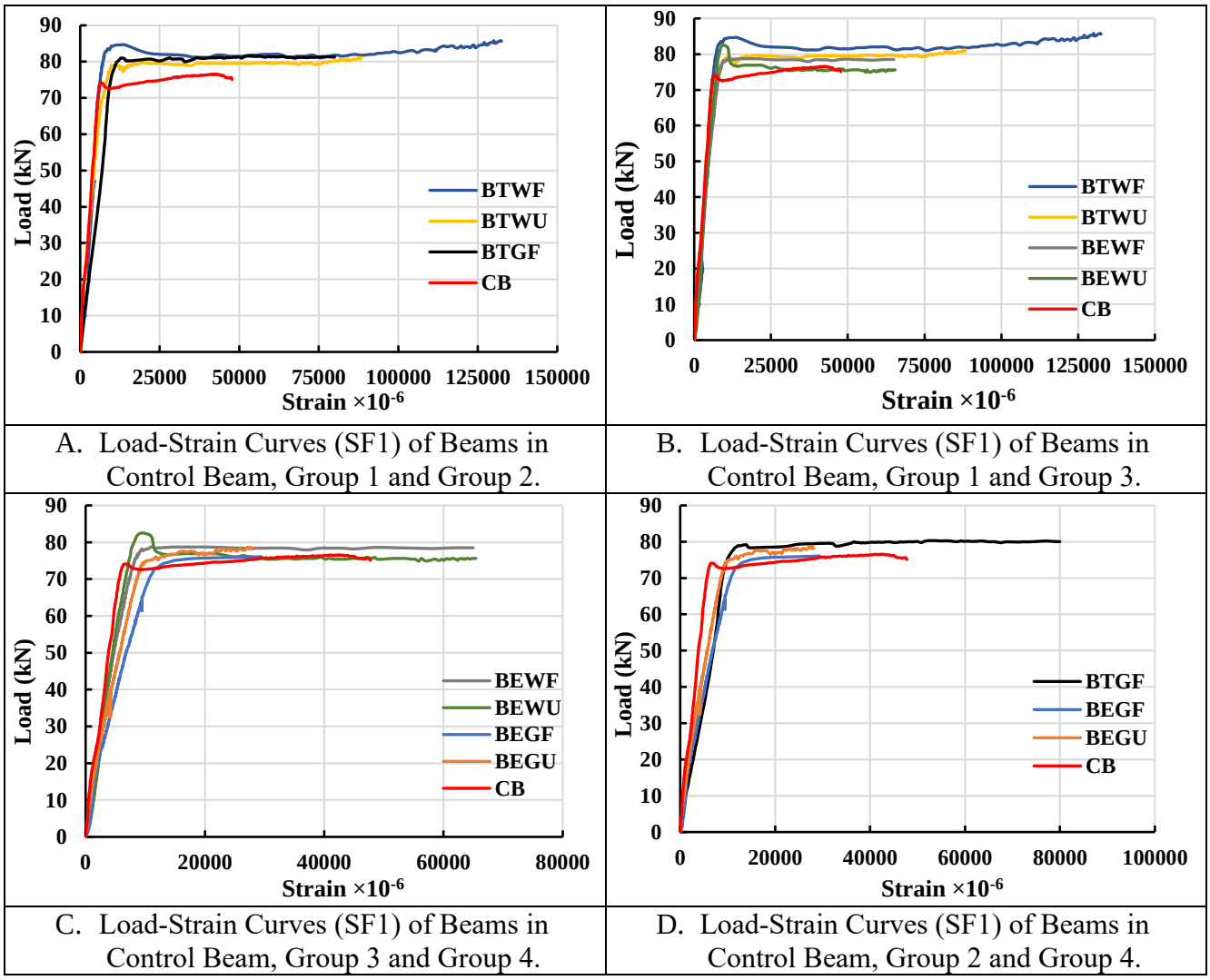

A. Load-Strain Curves (SF1) of Beams in Control Beam, Group 1 and Group 2.

B. Load-Strain Curves (SF1) of Beams in Control Beam, Group 1 and Group 3.

C. Load-Strain Curves (SF1) of Beams in Control Beam, Group 3 and Group 4.

D. Load-Strain Curves (SF1) of Beams in Control Beam, Group 2 and Group 4.

Figure (4.12): Comparison Between Load-Strain Curves of All Groups and Control Beam

4.4.5 Strain in Concrete

Strain gauges were placed at the center of the beam in the tension zone to measure the strain in ferrocement. However, their results were not discussed because they did not provide reliable information about the properties of the ferrocement. The reason is the

gauge's location at the center of the beam, which is susceptible to detachment due to cracks.

4.4.6 Crack Pattern and Mode of Failure

The stages of crack development for the test beams, including control beams and beams retrofitted, using traditional and sustainable mortar reinforced with either welded steel wire mesh or glass fiber mesh, are shown in the Figure (4.13). Crack initiation occurs when the tensile stresses in the beam exceed the modulus of rupture, causing hairline cracks to appear in the tension zone at mid-span of the beam. As the load increased, cracks propagated on both sides of the beam and continued towards the compression zone. At ultimate load, the failure occurred through a single wide crack in the middle of the beam, extending from the tension zone to the compression side.

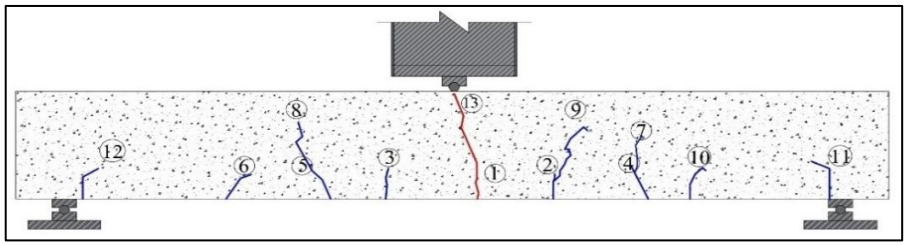

Figure (4.13): Process of Propagation of Cracks in All Beams

The crack patterns and modes of failure of all beams are described as follows.

In general, all retrofitted beams failed due to a single wide crack that occurred within the mid-span of beams in the tension zone and continued to the compression zone. The hairline cracks appeared on both sides of the beam when the loads increased; some of these beams were exposed to crushing in the compression zone at location of the applied load. Table (4.9) shows the failure mode and crack pattern for all beams.

Table (4.9): Mode of Failure of All Tested Beams

Specimen's Code	Mode of Failure
CB1	Flexural + Crushing
CB2	
BTWF	Flexural + Crushing
BTWU	Flexural
BTGF	Flexural + Crushing
BTGU	Flexural
BEWF	Flexural + Crushing
BEWU	Flexural + Crushing (Debonding in Ferrocement)
BEGF	Flexural + Crushing
BEGU	Flexural

Figure (4.14) (B-C) shows mode of failure and crack pattern of beams in Groups 1 and 2. The rate of crack growth in these beams was less than control beam. They also had fewer number of cracks with less width as compared to the control beam. This figure also shows that the wrapping configuration, whether full or U-shaped, did not significantly affect the width and number of cracks in the beams. A slight difference was noted in the number of cracks, with the U-shaped wrapping having slightly more cracks than the full wrapping. In addition, the full wrapping was exposed to the crushing in the compression zone.

Figure (4.14) (B-C), also shows that beams retrofitted, using ferrocement reinforced with welded wire mesh developed fewer and narrower cracks compared to the beams retrofitted using ferrocement and reinforced with glass fiber mesh. This outcome is attributed to the better capacity of welded wire mesh to control the crack width. These results are in consistent with findings reported in [97] and [98]. Also, weak bond between glass fiber mesh and mortar due to small opening size of these mesh. These results are consistent with the findings in [99] and [100].

Figure (4.14) (D-E) shows the mode of failure and crack pattern of beams in Groups 3 and 4. The comparison of the failure mode based on wrapping configuration and reinforcement type is consistent with the previous discussion. Beams in Groups 3 and 4 retrofitted using sustainable mortar result in the formation of more hairline cracks on the beam surface compared to the control beams and beams in Groups 1 and 2. This is likely due to improved stress distribution and a weak bond between sustainable materials and the beam surface. The use of waste plastic fiber caused a reduction in the crack width and enhanced tensile strength. These fibers acted as reinforcement, preventing the formation and propagation of cracks within the matrix. These results align with findings reported in [101] and [102].

Rupture of the welded steel wire and glass fiber mesh was observed, indicating that these meshes had reached their maximum tensile stress. After each test, the mortar cover was removed to expose the mesh. Visual check confirmed mesh rupture, as shown in Figure (4.14) (F).

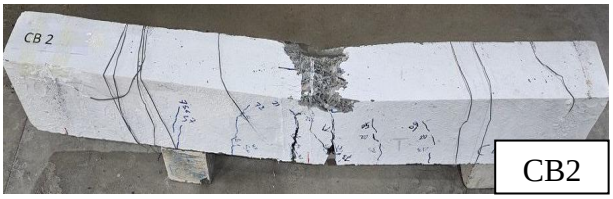

A. Failure Mode and Crack Pattern of Control Beams.

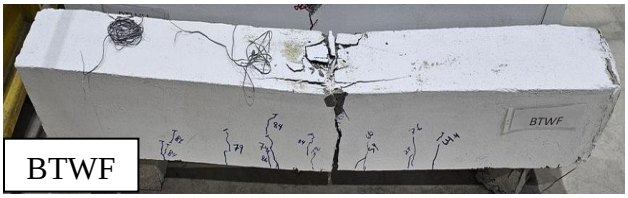

B. Failure Mode and Crack Pattern of Group 1.

C. Failure Mode and Crack Pattern of Group 2.

D. Failure Mode and Crack Pattern of Group 3.

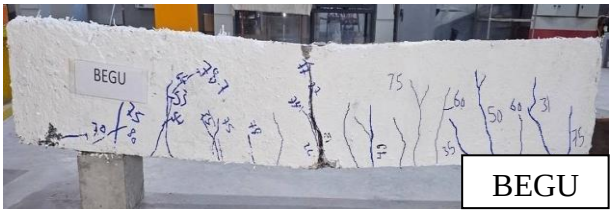

E. Failure Mode and Crack Pattern of Group 4.

Welded Steel Wire Mesh.

Glass Fiber Mesh.

F. Rupture of Mesh.

Figure (4.14): Crack Patterns and Modes of Failure for All Group

4.4.7 Ductility

Ductility refers to the ability of the structure to sustain applied loads after yielding without experiencing critical failure. It indicates how much plastic deformation the structure can endure before fracturing. The ductility index (μ) is defined as the deflection ratio at the ultimate load to the deflection at yield [96].

$$\mu = \frac{\delta_{\text{ult. load}}}{\delta_{\text{yielding}}} \quad \ldots\ldots\ldots\ldots (4.1)$$

Figure (4.15) shows the ductility index for all tested beams. The average ductility of the control beams was (2.05): Compared to the control beam, the retrofitted beams showed the following:

Group 1: The ductility index of beam BTWF was 3.06 and for beam BTWU was 2.84. The ductility index increased by 49.3% for the full wrapped beam and by 38.5% for the U-shape wrapped compared to the control beam.

Group 2: The ductility index was 2.79 for beam BTGF and 2.68 for beam BTGU. The ductility index increased by 36.1% for the fully wrapped beam and by 30.7% for the U-shape wrapped beam, compared to the control beam. The ductility index of beams in Group 1 was higher than that of beams in Group 2 by 9.7% and 5.97% for full and U-shape wrapping, respectively. Due to the use of welded wire mesh.

Group 3: The ductility index of beam BEWF was 3.17 with an increase of 54.63% and 3.6%, compared to the control beam and beam BTWF, respectively. For beam BEWU, ductility index was 1.0 with a decrease of 51.2% and 64.8%, compared to the control beam and beam BTWU, respectively. This decrease was due to a drop in load-carrying capacity that may caused due to weak bonding between sustainble materials, and crushing in the compression zone of beam BEWU. In addition, internal

debonding of ferrocement may have occurred, but it was not obvious. This occurred as a result of using sustainable material.

Group 4: The ductility index for beam BEGF was 2.94 with an increase of 43.4% and 5.4%, compared to the control and BTGF beams, respectively. For beam BEGU, the ductility index increased by 41% and 7.8% compared to the control and BTGU beams, respectively.

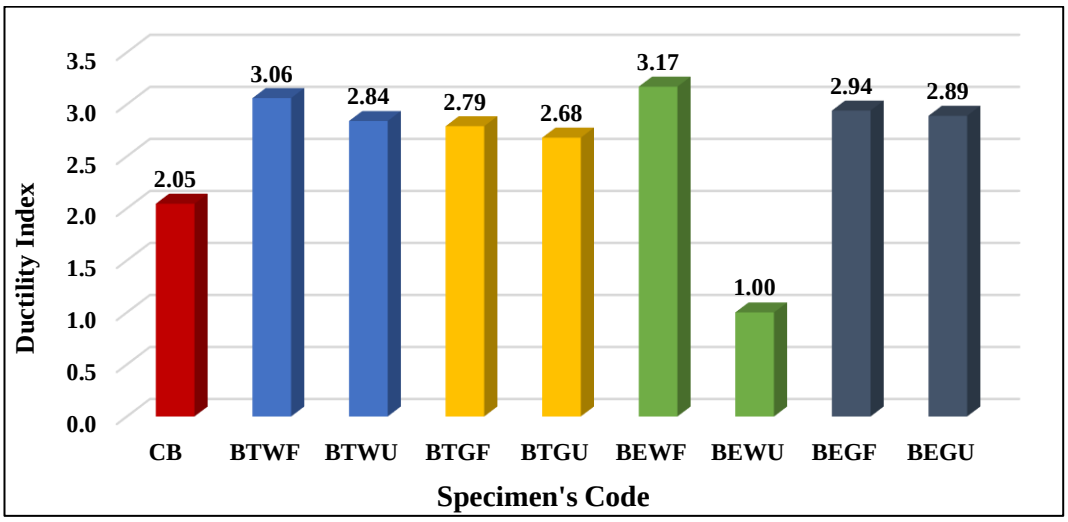

Figure (4.15): Ductility Index for the Tested Beams

4.4.8 Toughness

Toughness can be defined as the energy absorbed needed to fracture the sample. Toughness can be measured by calculating the area under the load-deflection curve up to the ultimate load [100], as shown in the Figure (4.16). AutoCAD software was used to determine the area under the load-deflection curve according to ASTM C1018 [103]. Figure (4.17) shows the toughness for all the tested beams and its increase or decrease as compared to the control beam. Also, Figure (4.17) shows that all retrofitted beam has toughness more than the control beam due to the increase in ultimate load and deflection except the toughness of beam BEWU was less than control beam due to drop

in the ultimate load as a result of using sustainable material may cause deboning of ferrocement layer.

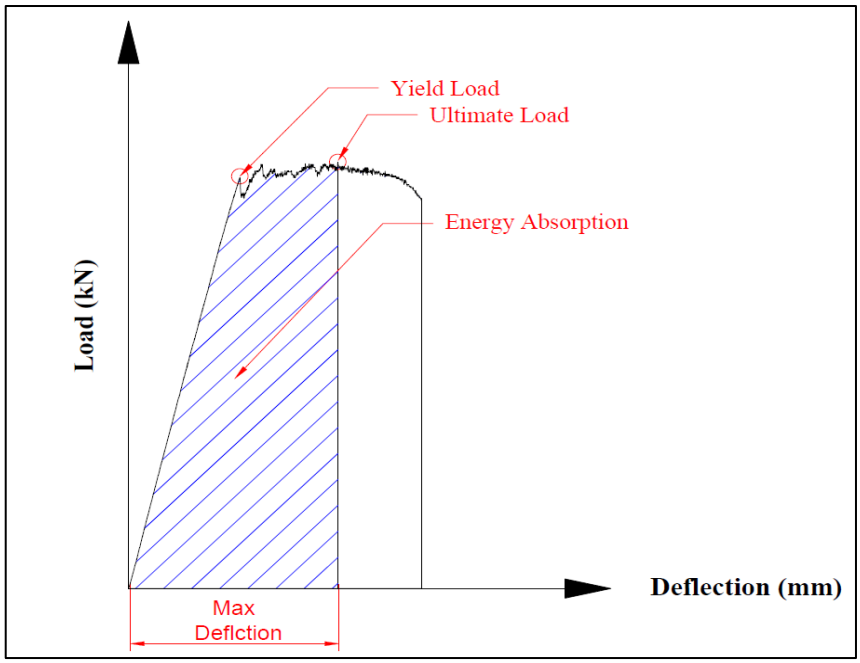

Figure (4.16): Calculation of Toughness

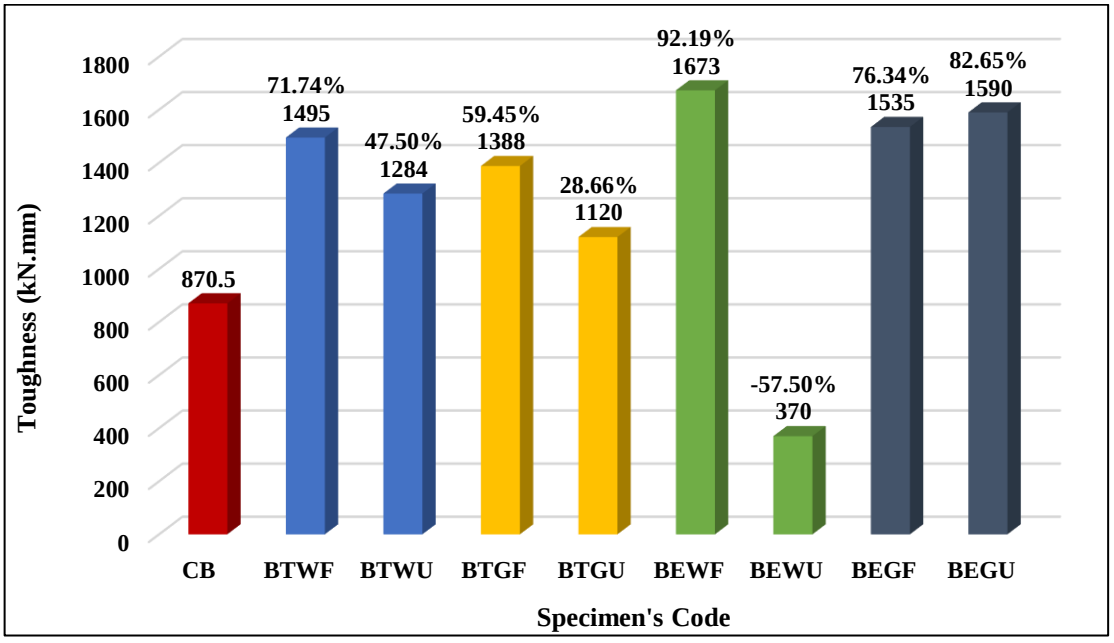

Figure (4.17): Toughness for the Tested Beams

4.4.9 Stiffness

Stiffness refers to the ability of a structural member to resist deformation within an approximately elastic range. Many factors influence stiffness, including material properties, deflection, ductility, and crack patterns. In this study, stiffness was determined as the slope of the load-deflection curve at the yield load. Table (4.10) lists the stiffness values for each beam. The results indicate that the beams retrofitted, using traditional mortar exhibited higher stiffness values, compared to the control beam. The increases were BTWF (22.9%), BTWU (12.5%), BTGF (9.9%), and BTGU (3.3%). In contrast, retrofitted beams using sustainable mortar exhibited lower stiffness, compare to the control beam. The decreases were BEWF (2.05%), BEWU (4.9%), BEGF (10.7%), and BEGU (10.9%). Stiffness in beams reinforced with welded steel wire mesh was higher than glass fiber mesh by BTWF (11.8%), BTWU (8.9%), BEWF (9.7%) and BEWU (6.8%) compared to BTGF, BTGU, BEGF and BEGU. Full wrapping beams has stiffness more than U-shape wrapping the increase were BTWF (9.2%), BTGF (6.3%), BEWF (2.98%) and BEGF (0.22%), compared to BTWU, BTGU, BEWU and BEGU respectively.

Table (4.10): Stiffness of All Tested Beams

Specimen's Code	Yielding Load (kN)	Deflection at Yield load (mm)	Stiffness (kN/mm)	% Increase & Decrease in Stiffness
CB	73.45	7.17	10.24	---
BTWF	84.3	6.7	12.58	22.9
BTWU	78.9	6.85	11.52	12.5
BTGF	81	7.2	11.25	9.9
BTGU	75.1	7.1	10.58	3.3
BEWF	78.2	7.8	10.03	-2.05
BEWU	82.8	8.5	9.74	-4.9
BEGF	74	8.1	9.14	-10.7
BEGU	76.6	8.4	9.12	-10.9

4.5 Effect of Key Parameters on Beam Behavior

4.5.1 Effect of Wrapping Types:

- **Load-Deflection Curve**

Two types of wrapping configurations were used: full and U-shaped wrapping. Both configuration types had a positive effect by enhancing the ultimate load, delaying the first cracking load, and reducing deflection. However, full wrapping using ferrocement with traditional mortar provided better confinement and improved the ultimate load compared to U-shape wrapping, as shown in Figure (4.18). At the corresponding load level, beams with full wrapping exhibited less deflection compared to U-shaped wrapped beams. This behavior is due to the increased effective depth of retrofitted beams as well as the ability of full wrapping to prevent the debonding of the ferrocement layer. These results are consistent with [38] and [104]. Their findings show that full wrapping results in higher ultimate load and less deflection compared to U-shape wrapping.

When using sustainable materials, beams with full wrapping showed a decrease in ultimate load compared to U-shaped wrapping. This is due to the lower compressive and flexural strength of sustainable mortar, as discussed in section (4.2.3), in addition to its weak bonding to the beam surface. These factors may lead to increased stress distribution at the edges, which causes early failure through cracks or debonding.

The U-shaped wrapping provides a higher ultimate load due to better stress redistribution. The free upper surface allows natural deformation, while other three wrapping sides enhance tensile strength. But the deflection in the full wrapping remained less compared to the U-shaped wrapping.

- **Strain in Steel Bars**

Full wrapping configuration results in higher strain values compared to the U-shaped wrapping configuration. This increase is due to better confinement and load distribution provided by full wrapping, which enhances stress transformation and increases the strain. These results are consistent with previous research [105], [106], [107] and [108].

- **Ductility**

Beams with full wrapping exhibits higher ductility than U-shape wrapped beams. This is due to full wrapping beams providing better confinement and more plastic deformation before failure. These results agree with the findings in [105], [107] and [109].

- **Toughness**

Full wrapping improved the toughness of the beams. This is because full wrapping provided better confinement and more uniform stress distribution, allowing the beam to sustain higher stresses before failure. In contrary, U-shaped wrapping can cause uneven stress distribution, leading to premature failure and lower overall toughness. These results align with [105] and [110].

In Group 3, the toughness of the fully wrapped beam with sustainable mortar was higher than U-shaped wrapping. This may be due to the drop in the load carrying capacity of the U-shaped wrapped beam. In Group 4, the toughness for both types of wrapping, full and U-shaped, was nearly the same, with a slight increase of 3.6% for U-shaped wrapping compared to full wrapping. This is due to a higher ultimate load and deflection for the U-shaped beam.

- **Stiffness**

Fully wrapped beams retrofitted, using either traditional or sustainable mortar exhibited higher stiffness than U-shaped wrapped beams. Full wrapping provides more uniform stress distribution, stronger bonding with the beams, and better confinement. These results align with the findings in [107] and [110].

4.5.2 Effect of Mortar Types:

- **Load-Deflection Curve**

The use of sustainable mortar resulted in lower ultimate loads, an increased number of cracks, reduced crack width, and greater deflection compared to beams retrofitted with traditional mortar. On the other hand, traditional mortar led to the delaying of the first cracking load, an increase in the ultimate load, and reduced deflection at the corresponding load levels. These results agree with [31] and [34].

Figure (4.18) shows that the ultimate load of beams retrofitted using sustainable mortar was lower than traditional mortar due to the weak bonding between sustainable materials that caused loss of strength. In addition, the sustainable material used has a smooth surface, which can make it difficult to adhere to the mortar itself. These results confirmed the testing results in this study and previous studies [95], [101] and [104]

- **Strain in Steel Bars.**

Beams retrofitted using sustainable mortar exhibited higher yield strain than those retrofitted using traditional mortar. This is due to the materials used in the sustainable mortar mix. The presence of silica fume improved the stiffness and increased the stress and strain. Furthermore, the presence of crumb rubber weakened the bond within

the mortar, leading to greater deformation and strain. Additionally, plastic fiber enhanced the tensile strength by bridging the cracks and increased the number of cracks by improving stress distribution, which also contributed to higher strain.

- **Ductility**

Sustainable mortar increased the ductility, compared to traditional mortar. This was due to the inclusion of crumb rubber and plastic fibers, which allowed for more deformation before failure. These results matched the findings in [111], [112] and [113].

- **Toughness**

The sustainable mortar has exhibited higher toughness than traditional mortar. This increase is due to the use of sustainable materials, such as silica fume, which enhances the bond strength between compounds and improves durability. Additionally, crumb rubber allows greater deformation before failure. At the same time, plastic fibers act as reinforcement in the material, reducing crack width and allowing a uniform distribution of stress across the beam and increasing tensile strength. This result is demonstrated in section (4.2.3) and aligns with the findings in [95] and [114].

- **Stiffness**

Beams retrofitted using sustainable mortar exhibited lower stiffness than traditional mortar. This behavior is due to the presence of crumb rubber and plastic fiber, which increases voids and gaps in the mix and reduces the cohesion between the mixture components and the beam surface. These results are consistent with [101] and [115].

4.5.3 Effect of Reinforcement Types:

- **Load-Deflection Curve**

Figure (4.18) shows that the beam retrofitted using traditional or sustainable mortar reinforced with welded steel wire mesh exhibited a higher ultimate load compared to the beam reinforced with glass fiber mesh. The reason is that the welded steel wire mesh had a higher ultimate load of 518 N, compared to 340 N for the glass fiber mesh. These results agree with [100] and [116], who reported that metallic mesh increases ultimate load compared to non-metallic mesh.

Beams retrofitted with traditional or sustainable mortar and reinforced with welded steel wire mesh showed lower deflection compared to those reinforced with glass fiber mesh. This behavior is attributed to several factors, such as the high stiffness and young modules of welded wire mesh and the weak bonding between mortar and glass fiber mesh due to its small opening size. This behavior agrees with [95] and [99] and with the results of the current study (section (3.4.2)).

- **Strain in Steel Bars.**

The strain in the longitudinal bars for beams retrofitted using traditional or sustainable mortar reinforced with welded steel wire mesh was lower than those reinforced with glass fiber mesh. This is because welded steel wire mesh exhibits higher stiffness and lower flexibility resulting in smaller deformation compared to the glass fiber mesh. This result is matches the results in section (3.4.2).

- **Ductility**

Beams retrofitted using either traditional or sustainable mortar and reinforced with welded steel wire mesh provided higher ductility compared to beams reinforced with glass fiber mesh because welded

steel wire mesh allows for gradual yielding and increases the energy absorption, helping the beam to carry load after yielding. Unlike glass fiber, which doesn't have a yield point, its behavior stays linear until failure. These results are consistent with the results in the section (3.4.2) and the findings in [95], [100] and [117]

- **Toughness**

Beams reinforced with welded steel wire mesh exhibited higher toughness than those reinforced with glass fiber mesh for both types of mortar (traditional and sustainable). This is due to the higher ductility of the welded steel wire mesh, which allows more plastic deformation before failure unlike glass fiber mesh, which fracture suddenly with minimal plastic deformation, resulting in a reduction in toughness. These results are consistence with [95] and [100].

- **Stiffness**

Beams retrofitted with either traditional or sustainable mortar and reinforced with welded steel wire mesh exhibited higher stiffness than those reinforced with glass fiber mesh. The welded steel wire mesh provides higher tensile strength, stronger bonding to the mortar, and more uniform stress distribution, which reduces deformation and increase stiffness.

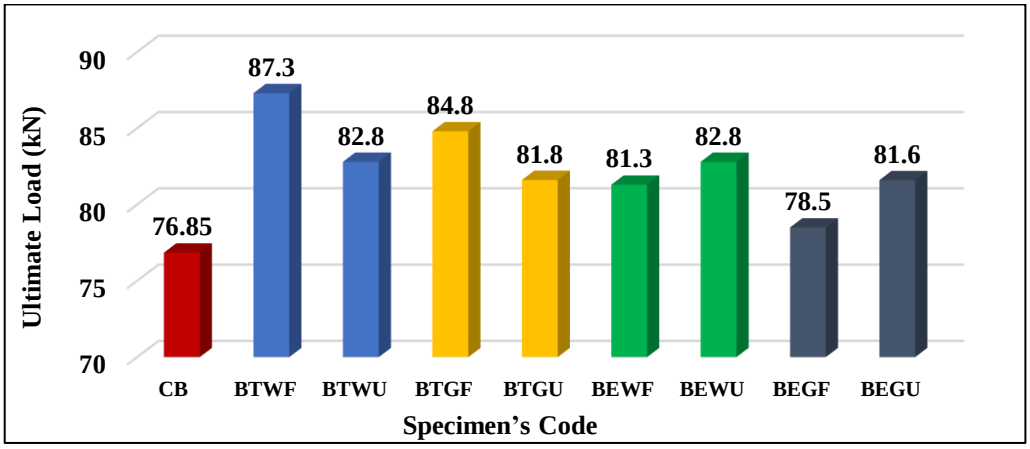

Figure (4.18): Ultimate Load for All the Tested Beams

4.6 Experimental and Theoretical Calculation of Ultimate Load

The expected failure load was calculated based on the ACI 549R-18 [9]. All calculated details are provided in Appendix C. The predicted load values are listed in Table (3.21) in Chapter 3.

Table (4.11) shows the failure load values based on the experimental test and predicted from the ACI 549R-18 [9]. The result shows that the experimental and predicted loads of the retrofitted beams, using either traditional or sustainable mortar reinforced with welded steel wire mesh or glass fiber mesh were quite close. The ratio of test to calculate ranged from 0.92 to 1.01. This agreement in the results is due to the use of the actual material properties in the calculation, including the compressive strength of both types of mortar, traditional and sustainable, and the yield and ultimate tensile strength of reinforcing steel bars, welded steel wire mesh, and glass fiber mesh.

Table (4.11): Comparison Between Theoretical and Experimental Ultimate Loads

Sample	Depth of neutral axis c (mm)	Ultimate load Pu (kN)		Pult. Exp/ Pult.Theo.
		Experimental	Theoretical	
CB	42.74	75.65	74.78	1.01
BTWF	34.36	87.3	91.52	0.95
BTWU	34.54	82.8	90.10	0.92
BTGF	33.42	84.8	88.31	0.96
BTGU	33.21	81.8	87.08	0.94
BEWF	44.80	81.3	88.31	0.92
BEWU	45.00	82.8	86.54	0.96
BEGF	42.93	78.5	83.96	0.93
BEGU	42.63	81.6	82.86	0.98

4.7 Estimating Stresses by Experimental Calculations

The stress values in the bar for each retrofitted beam were calculated based on the strain values obtained from the strain gauge, and according to the stress-strain curve of the steel reinforcement as shown in Figure (3.7), the stress values associated with each strain value were obtained.

Table (4.12) shows the experimental stress in the steel bars of the retrofitted beams. It was observed that the stress in the bars of beams retrofitted using sustainable mortar was higher than those retrofitted using traditional mortar. This was due to lower strength and stiffness of sustainable mortar in addition to weak bonding between sustainable mortar and the beam surface.

Table (4.12): Result of Experimental Strain and Stress in Steel Bars

Group	Specimen's Code	Strain at Yield $\times 10^{-6}$	Stress (MPa)
CB	**CB**	6462	655
Group 1	**BTWF**	9792	680
	BTWU	9500	670
Group 2	**BTGF**	12588	681
	BTGU	---	---
Group 3	**BEWF**	10131	685
	BEWU	9796	680
Group 4	**BEGF**	13000	---
	BEGU	11000	690

Chapter 5

Conclusions and Recommendations

Chapter Five

Conclusions and Recommendations

5.1 Introduction

The main objective of this study was to develop a mixture containing sustainable materials such as silica fume, crumb rubber, and waste plastic bottle fibers. This was accomplished by preparing, casting, and testing samples containing varying proportions of these materials to determine their compressive, flexural, and tensile strength and find the optimum mixture. Then, using the optimum mixture of sustainable mortar, in addition to traditional mortar, and reinforced with either welded steel wire mesh or glass fiber mesh to retrofit preloaded beams from full or U-shaped wrapping to find their effect on the structural behavior of the beams.

In this chapter, the conclusions drawn from the experimental results are described, and the suggestions for future works are also presented.

1. Using 8% silica fume (SF) as a partial replacement of cement in mortar improves its mechanical properties, compared to traditional mortar at ages 7 and 28 days.
2. Using crumb rubber (CR) as a partial replacement of sand in cement mortar caused a reduction in compressive, flexural, and tensile strength. The decrease in these strength properties increases with the increase of crumb rubber (CR) content. A 5% replacement of crumb rubber (CR) by sand was determined to be acceptable level.
3. Implementing 0.75% plastic fiber (PF) in a mortar containing 8% silica fume and 5% crumb rubber enhanced splitting tensile

strength, demonstrating the ability of plastic fibers (PF) to improve the tensile properties of sustainable mortar.

4. The mechanical performance of sustainable mortar is optimized by combining 8% silica fume, 5% crumb rubber, and 0.75% (PF) fiber, especially in terms of tensile strength.
5. Retrofitting of the RC beams, using either traditional or sustainable mortar, reinforced with welded steel wire mesh or glass fiber mesh in a full or U-shape wrapping configurations, effectively increased their ultimate load, compared to the reference beams.
6. Retrofitting RC beams, using either traditional or sustainable mortar reinforcement with welded steel wire mesh showed lower deflection than glass fiber mesh.
7. Retrofitting RC beams, using traditional mortar reinforced with either welded steel wire mesh or glass fiber mesh, with full wrapping or U-shape wrapping, resulted in increased ductility, stiffness and toughness, compared to reference beams
8. Retrofitting RC beams, using sustainable mortar and reinforced with either welded steel wire mesh or glass fiber mesh for U-shape wrapping, gives higher resistance than full wrapping.
9. Deflection in the beams retrofitted using sustainable mortar and reinforced with either welded steel wire mesh or glass fiber mesh for full and U-shape wrapping was higher, compared to traditional mortar.
10. The stiffness of the beams retrofitted using sustainable mortar reinforced with welded steel wire mesh or glass fiber mesh was lower than the beams retrofitted using traditional mortar and the reference beam.

11. The ductility and toughness of beams retrofitted using sustainable mortar reinforced with either welded steel wire mesh or glass fiber mesh with full and U-shaped wrapping was higher than traditional mortar.
12. Mode of failure for all retrofitted beams was flexural failure, and some of these beams were exposed to crushing in the compression zone at location of the applied load.

5.2 Recommendation for Future Works

The following recommendations are proposed for future researches:

1. Studying the effect of using a glass fiber mesh with the same dimension of the welded steel wire mesh in either traditional or sustainable mortar to retrofit RC beams.
2. Investigating the effect of testing RC beams retrofitting using sustainable mortar under two-point load on the ultimate strength.
3. Strengthening of RC beams using sustainable mortar.
4. Developing a sustainable mixture by adding SBR to increase the bonding strength of the mixture components.
5. Strengthening of RC beams reinforced with glass fiber bars instead of steel bars using traditional or sustainable mortar.
6. Developing a sustainable mortar by treatment the crumb rubber with NaOH and increase length of plastic fiber.

Refrences

References

[1] H. S. M. Al Saadi, H. P. Mohandas, and A. Namasivayam, "An Experimental Study on Strengthening of Reinforced Concrete Flexural Members Using Steel Wire Mesh," Curved Layer. Struct., Vol. 4, No. 1, PP. 31–37, 2017.

[2] A. Siddika et al., "Flexural Performance of Wire Mesh and Geotextile-Strengthened Reinforced Concrete Beam," SN APPl. Sci., Vol. 1, No. 11, PP. 1–13, 2019.

[3] M. M. A. Alhadid and M. A. Youssef, "Assessment of the Flexural Behavior of Reinforced Concrete Beams Strengthened with Concrete Jackets," Eng. Struct., Vol. 167, No. March, PP. 108–120, 2018.

[4] A. Si Larbi, R. Contamine, and P. Hamelin, "TRC and Hybrid Solutions for Repairing and/or Strengthening Reinforced Concrete Beams," Eng. Struct., Vol. 45, PP. 12–20, 2012.

[5] G. Xing, T. Wu, B. Liu, H. Huang, and S. Gu, "Experimental Investigation of Reinforced Concrete T-Beams Strengthened with Steel Wire Mesh Embedded in Polymer Mortar Overlay," Adv. Struct. Eng., Vol. 13, No. 1, PP. 69–79, Feb. 2010.

[6] C. K. Ma, N. M. Apandi, S. C. S. Yung, N. J. Hau, L. W. Haur, A. Z. Awang, W. Omar., "Repair and Rehabilitation of Concrete Structures Using Confinement: A Review," Constr. Build. Mater., Vol. 133, PP. 502–515, 2017.

[7] G. E. Thermou and A. S. Elnashai, "Seismic Retrofit Schemes for RC Structures and Local-Global Consequences," Prog. Struct.

Eng. Mater., Vol. 8, No. 1, PP. 1–15, 2006, doi: 10.1002/pse.208.

[8] N. Ganesan, P. V. Indira, and S. P. Thadathil, “Effect of Ferrocement Wrapping System on Strength and Behavior of RC Frames Under Reversed Lateral Cyclic Loading,” Exp. Tech., Vol. 35, No. 4, PP. 23–28, 2011.

[9] American Concrete Institute (ACI 549.1R-18), "State - of - the - Art Report on Ferro Cement". American Concrete Institute, Farmington Hills, Michigan, 2018.

[10] B. TABRAIZ, “Ferro-Cement Technology and Prospective Developments in Durability and Sustainability,” A Thesis Submitted to the Department of Environment, Land and Infrastructure Engineering, Politecnico Di Torino, Italy, 2019.

[11] P. P. Bansal, B. E. Civil, and C. Structures, “Effect of Wire Mesh Orientation on Strength of Beams Retrofitted Using Ferrocement Jackets,” Int. J., Vol. 5, No. 2, PP. 8–19, 2014.

[12] S. Tian, “Shear Behaviour of Ferrocement Deep Beams,” A thesis submitted to The University of Manchester for the degree of Doctor of Philosophy in the Faculty of Engineering and Physical Sciences, 2013.

[13] A. E. Naaman, “Ferrocement and Laminated Cementitious Composites”, Textbook, University of Michigan: Techno Press, America, 2000.

[14] M. A. Mansur and M. A. Aziz, “Study of Reinforced Cement Composites,” Int. J. Cem. Compos. Light. Concr., Vol. 5, No. 3, PP. 165–171, 1983.

[15] Maharashtra Engineering Research Institute, “Ferrocement technology,” Maharashtra Eng. Res. Inst., No. 1, PP. 1–152, 2018.

[16] A. Alexander, “Retrofitting of Reinforced Concrete Beam with Glass Fiber Reinforced Polymer Strips and Sheet,” Int. J. Eng. Res. Technol., Vol. 3, No. 29, PP. 1–6, 2015.

[17] R. P. Thangaraj and B. Shanmugam, “Performance of RC Beams Developed With ECC Layer and AR Glass Fiber Mesh Under Flexural Loading,” Rev. Mater., Vol. 29, No. 3, PP. 1–17, 2024.

[18] N. Mohamad, K. Muthusamy, R. Embong, A. Kusbiantoro, and M. H. Hashim, “Environmental Impact of Cement Production and Solutions: A review”, Mater. Today Proc., Vol. 48, PP. 741–746, 2021, doi: 10.1016/j.matpr.2021.02.212.

[19] T. Senthil Vadivel and R. Thenmozhi, “Experimental Study on Waste Tyre Rubber Replaced Concrete - An Ecofriendly: Construction material,” J. Appl. Sci. Res., Vol. 8, No. 6, PP. 2966–2973, 2012.

[20] American Concrete Institute (ACI), “234R-06 Guide for the Use of Silica Fume in Concrete,” Aci 234R-06, Vol. 96, No. Reapproved, PP. 0–64, 2006.

[21] M. K. Batayneh, I. Marie, and I. Asi, “Promoting the Use of Crumb Rubber Concrete in Developing Countries,” Waste Manag., Vol. 28, No. 11, PP. 2171–2176, 2008.

[22] C. E. Pierce and M. C. Blackwell, “Potential of Scrap Tire Rubber as Lightweight Aggregate in Flowable Fill,” Waste Manag., Vol. 23, No. 3, PP. 197–208, 2003.

[23] A. M. Ghaly and J. D. Cahill IV, “Correlation of Strength, Rubber Content, and Water to Cement Ratio in Rubberized Concrete”, Can. J. Civ. Eng., Vol. 32, No. 6, PP. 1075–1081, 2005, doi: 10.1139/l05-063.

[24] A. Mohajerani et al., “Recycling Waste Rubber Tyres in Construction Materials and Associated Environmental Considerations: A Review,” Resour. Conserv. Recycl., Vol. 155, PP. 104679, 2020, doi: 10.1016/j.resconrec.2020.104679.

[25] F. Mahdi, H. Abbas, and A. A. Khan, “Strength Characteristics of Polymer Mortar and Concrete Using Different Compositions of Resins Derived from Post-Consumer PET Bottles,” Constr. Build. Mater., Vol. 24, No. 1, PP. 25–36, 2010.

[26] L. Kumar, “Overviews on Recycling of Post-Consumer Pet Bottles and Applications of Rpet,” Int. J. Adv. Res., Vol. 10, No. 06, PP. 685–695, 2022, doi: 10.21474/ijar01/14937.

[27] S. Yang, X. Yue, X. Liu, and Y. Tong, “Properties of Self-Compacting Lightweight Concrete Containing Recycled Plastic Particles,” Constr. Build. Mater., Vol. 84, PP. 444–453, 2015.

[28] B. Harini and K. V Ramana, “"Use of Recycled Plastic Waste as Partial Replacement for Fine Aggregate in Concrete,” Int. J. Innov. Res. Sci. Eng. Technol., Vol. 4, No. 9, 2015.

[29] P. G. Prabhu, C. A. Kumar, R. Pandiyaraj, P. Rajesh and L. Sasi Kumar, “Study on Utilization of Waste Pet Bottle Fiber in Concrete,” IMPACT Int. J. Res. Eng. Technol. (IMPACT IJRET), Vol. 2, No. 5, PP. 233–240, 2014.

[30] L. A. Pereira De Oliveira and J. P. Castro-Gomes, “Physical and Mechanical Behaviour of Recycled PET Fibre Reinforced Mortar,” Constr. Build. Mater., Vol. 25, No. 4, PP. 1712–1717, 2011, doi: 10.1016/j.conbuildmat.2010.11.044.

[31] S. U. Khan, S. F. A. Rafeeqi, and T. Ayub, “Strengthening of RC Beams in Flexure Using Ferrocement,” Iran. J. Sci. Technol. - Trans. Civ. Eng.,Vol. 37, PP. 353–365, 2013.

[32] M. R. Alam, M. A. Hossain, R. Dey, and M. M. Uddin, “Flexural Retrofitting of Reinforced Concrete Beam Using Ferrocement,” 2nd Int. Conf. Advances in Civil Engineering (ICACE), Chittagong Univ. Eng. Technol., Bangladesh, Dec. 26–28, 2014.

[33] E. H. Fahmy, Y. B. I. Shaheen, A. M. Abdelnaby, and M. N. Abou Zeid, “Applying the Ferrocement Concept in Construction of Concrete Beams Incorporating Reinforced Mortar Permanent Forms,” Int. J. Concr. Struct. Mater., Vol. 8, No. 1, PP. 83–97, 2014, doi: 10.1007/s40069-013-0062-z.

[34] R. F. Makki, “Response Of Reinforced Concrete Beams Retrofitted By Ferrocement,” Int. J. Sci. Technol. Res., Vol. 3, No. 9, PP. 27–34, 2014.

[35] M. M. Vijayalakshmi and A. Vijayalakshmi, “Experimental Studies on Strengthening of Reinforced Concrete Beams Using Ferrocement Wraps For Energy Efficiency,” Key Eng. Mater., Vol. 692, PP. 38–44, 2016.

[36] T. A. El-Sayed and A. M. Erfan, “Improving Shear Strength of Beams Using Ferrocement Composite,” Constr. Build. Mater., Vol. 172, PP. 608–617, 2018.

[37] M. J. Miah, M. S. Miah, W. B. Alam, F. Lo Monte, and Y. Li, "Strengthening of RC Beams by Ferrocement Made With Unconventional Concrete," Mag. Civ. Eng., Vol. 89, No. 5, PP. 94–105, 2019, doi: 10.18720/MCE.89.8.

[38] S. Sirimontree, B. Witchayangkoon, K. Leartpocasombut, and C. Thongchom, "Flexural Behavior of Reinforced Concrete Beams Strengthened With Ferrocement," Int. Trans. J. Eng. Manag. Sci. Technol., Vol. 10, No. 9, PP. 1–9, Jul. 2019, doi: 10.14456/ITJEMAST.2019.11 July, 2019.

[39] J. Pragadhish and R. Jagadeesan, "Strengthening of RC Beam Using Ferro Cement Laminates," Int. Adv. Res. J. Sci. Eng. Technol., Vol. 7, No. 7, PP. 91–96, 2020.

[40] M. Soundararajan, S. Balaji, J. Sridhar, and G. Ravindran, "Sustainable Retrofitting and Moment Evaluation of Damaged RC Beams Using Ferrocement Composites for Vulnerable Structures," Sustainability., Vol. 14, No. 15, 2022.

[41] D. Živković, P. Blagojević, D. Kukaras, R. Cvetković, and S. Ranković,"Comprehensive Analysis of Ferrocement Strengthened Reinforced Concrete Beam," Buildings, Vol. 14, No. 4, 2024.

[42] R. Taha, M. AL Allaf, and I. Tarsha, "Experimental and Analytical Evaluation to Strengthened R.C Beams Using Ferrocement Under Torsion," Steps Civil, Constr. Environ. Eng., Vol. 2, No. 3, PP. 9–17, 2024, doi: 10.61706/sccee1201121.

[43] Y. B. I. Shaheen, B. A. Eltaly, and S. G. Abdul-Fataha, "Structural Performance of Ferrocement Beams Reinforced With Composite Materials," Struct. Eng. Mech., Vol. 50, No. 6, PP. 817–834, 2014.

[44] P. Tilekar, M. Chanra and K.Gowda, “Experimental Study on Strengthening of RC Beams Using Glass Fiber,” Int. J. Civ. Eng. Technol., Vol. 9, No. 11, PP. 959–965, 2017.

[45] A. Kumar and N. Modi, "Retrofitting of RCC Beams using FRP and Ferrocement Laminates," International Journal of Scientific Engineering and Research (IJSER), Vol. 5, No. 6, PP. 87-93, Jun. 2017. https://www.researchgate.net/publication/374337411

[46] H. S. Al-Rawe, S. Y. Ahmed, and S. M. Abdullah, “Retrofitting of Reinforced Concrete Columns Under Eccentric Loads Using Enhanced Ferrocement,” Asian J. Civ. Eng., 2024.

[47] H. U. Boiny, Y. M. Alshkane, and S. K. Rafiq, “Mechanical Properties of Cement Mortar By Using Polyethylene,” 5th Natl. 1st Int. Conf. Mod. Mater. Struct. Civ. Eng. 26-27 October 2016.

[48] M. H. Shukur, K. A. Ibrahim, S. Y. Al-Darzi, and O. A. Salih, “Mechanical Properties of Concrete Using Different Types of Recycled Plastic as an Aggregate Replacement,” Cogent Eng., Vol. 10, No. 1, PP. 1–21, 2023.

[49] E. T. Dawood, A. S. Shawkat, and M. H. Abdullah, “Flexural Performance of Ferrocement Based on Sustainable High-Performance Mortar,” Case Stud. Constr. Mater., Vol. 15, 2021.

[50] D. Sumanth, K. Gopal, G. Kartheek, K. Sai Kumar, T. Bhargav “An Experimental Study on Partial Replacement of Fine Aggregates by Crumb Rubber in Ferrocement,” Int. J. Multidiscip. Res., Vol. 5, No. 2, PP. 283–293, 2023.

[51] Iraqi Standard Specifications (IQS) No: 5 “Properties of Ordinary

Portland Cement", P.1-8, 2015.

[52] Iraqi Standard Specifications (IQS): 45 "Aggregate from Natural Sources for Concrete and Building Construction, 2016.

[53] ASTM International, "Standard Test Method for Relative Density (Specific Gravity) and Absorption of Fine Aggregate (ASTM C128-22)," PP. 1–4, 2022, doi: 10.1520/C0128-22.1.

[54] ASTM International, "Standard Test Method for Total Evaporable Moisture Content of Aggregate by Drying (ASTM C566-19)," PP. 1–3, 2019.

[55] ASTM International, "Standard Test Method for Relative Density (Specific Gravity) and Absorption of Coarse Aggregate (ASTM C127-15),", PP. 1–5, 2015, doi: 10.1520/C0127-15.2.

[56] ASTM International, , "Standard Test Method for Bulk Density ("Unit Weight") and Voids in Aggregate", ASTM:C29/C29M-09., PP. 1–5, 2009, doi: 10.1520/C0029.

[57] Iraqi Standard Specifications (IQS), No. 1703, "Water for Making Concrete, Ministry of Planning, Central Organization for Standardization and Quality Control,", 2016.

[58] MegaAdd MS (D), "MegaAdd MS (D)," D, PP. 10–11, 2015.

[59] ASTM International, "Standard Specification for Silica Fume Used in Cementitious Mixtures (ASTM C1240-20),", PP. 1–4, 2020.

[60] T. Sulaiman, I. Ja'e, Y. Yau, and Y. Hashim, "Investigation of Crumb Rubber Proportion on Compressive Strength and Water Absorption of Crumb Rubber Mortar Use of Recycled Fibres to

Develop Sustainable Concrete. View Project Reliability Assessment, Static and Dynamic Response of Transmission Line Tower: a Comparative Study View project," J. Sci. Technol. Educ., Vol. 8, No. 2, PP. 84–89. June, 2020.

[61] N. M. Mhedi, A. A. Hilal and A. Al-Hadithi, "Effect of Adding Waste Plastic Fibers on Properties of Modified Foamed Concrete at Various Densities," J. Sci. Technol. Educ.*, vol. 8, no. 1, PP. 372–381, 2019.

[62] ASTM International, "Standard Specification for Deformed and Plain Carbon-Steel Bars for Concrete Reinforcement (ASTM A615/A615M − 22),", Vol. 1, PP. 5–7, 2022.

[63] Salwa M., Bayer J., Mohammad N., "Strengthening of Eccentrically Loaded Reinforced Concrete Columns Using Ferrocement or Carbon Fibers". A Thesis Submitted to the Council of the College of Engineering, Civil Department, University of Mosul, Mosul, Iraq, 2013.

[64] ASTM International., "Compressive Strength of Hydraulic Cement Mortars (Using 2-in Cube Specimens ASTM C109/C109M)," Am. Soc. Test. Mater., PP. 1–9, 2023.

[65] ASTM International, "Flexural Strength Cement Mortars ASTM-C348-21," Vol. 04, PP.1–5, 2021.

[66] ASTM International, "Standard Test Method for Tensile Strength of Hydraulic Cement Mortars ASTM C 260-01,". PP. 1–8, 2001.

[67] ASTM International, "Standard Practice for Making and Curing Concrete Test Specimens in the Laboratory," Vol. 04, PP. 1–4,

2019, doi: 10.1520/C0192.

[68] ACI Committee 318, “Building Code Requirements for Structural Concrete (ACI 318-19),”American Concrete Institute, Farmington Hills, MI 48331, 2019.

[69] American Concrete Institute ACI Committee 211, “Selecting Proportions for Normal-Density and High-Density Concrete Guide (ACI PRC-211.1-22),”, PP. 1–38, 2022.

[70] ASTM International, “Standard Test Method for Slump of Hydraulic-Cement Concrete (ASTM C143/C143M-20),”, PP. 1–3, 2020, doi: 10.1520/C0143.

[71] B.S 1881: Part 116, “Method for Determination of Compressive Strength of Concrete Cubes,” Br. Stand. Inst., 2003.

[72] ASTM International, “Standard Test Method for Splitting Tensile Strength of Cylindrical Concrete Specimens ASTM C496,”, Stand. B., pp. 545-545–3, 2017.

[73] ASTM International, “Standard Test Method for Flexural Strength of Concrete (Using Simple Beam with Third-Point Loading ASTM C293M),”, PP. 1–5, 2016.

[74] H. M. Hamada et al., “Effect of Silica Fume on The Properties of Sustainable Cement Concrete”, J. Mater. Res. Technol., Vol. 24, No. 1, PP. 8887–8908, 2023, doi: 10.1016/j.jmrt.2023.05.147.

[75] P. Duan, Z. Shui, W. Chen, and C. Shen, “Effects of Metakaolin, Silica Fume and Slag on Pore Structure, Interfacial Transition Zone and Compressive Strengthof Concrete,” Constr. Build. Mater., Vol. 44, PP. 1–6, 2013.

[76] V. Bhikshma, K. Nitturkar, and Y. Venkatesham, “Investigations on Mechanical Properties of High Strength Silica Fume Concrete”, Asian J. Civ. Eng., Vol. 10, Vo. 3, PP. 335–346, 2009.

[77] P. Singh, M. A. Khan, and A. Kumar, “The Effect on Concrete by Partial Replacement of Cement by Silica Fume : A Review”, Irjet, Vol. 3, No. 3, PP. 118–121, 2016.

[78] B. Hanumesh, and B. Varun, B. H.-I. J. of, , “The Mechanical Properties of Concrete Incorporating Silica Fume as Partial Replacement of Cement”, International J. Emerg. Technol. Adv. Eng., Vol. 9001, No. 9, PP. 270, 2015.

[79] V. Preetha, S. Sathyapriyadharshini, S. Sarguna, and S. Senthamilselvan, “Studies on Effect of Silica Fume on Workability and Strength of Concrete”, Int. Res. J. Multidiscip. Technovation, Vol. 1, No. 6, PP. 165–171, 2019.

[80] L. N. Assi, A. Alsalman, Y. A. J. Al-Hamadani, R. Kareem, and H. M. Ashour Al Khuzaie, “Observations of Supplementary Cementitious Materials Effects on the Performance of Concrete Foundation,” IOP Conf. Ser. Earth Environ. Sci., Vol. 856, 2021.

[81] A. Samuel, “Mechanical Strength of Concrete with Crumb and Shredded Tyre as Aggregate Replacement,” Int. J. Eng. Res. Appl., Vol. 3, No. 2, PP. 1098–1101, 2013.

[82] Z. Muyen, F. Mahmud, and M. Hoque, “Application of Waste Tyre Rubber Chips as Coarse Aggregate in Concrete,” Progress. Agric., Vol. 30, No. 3, PP. 328–334, 2020.

[83] D. Z. A. Tudin and A. N. Rizalman, “Properties of Cement Mortar

Containing NaOH-Treated Crumb Rubber as Fine Aggregate Replacement," IOP Conf. Ser. Earth Environ. Sci., Vol. 476, No. 1, Montréal, Canada, Palais des Congrès de Montréal, 2020.

[84] M. A. Mutar, T. S. Hussein, and S. H. Malik, "Effect of Crumb Rubber Aggregates on the Characteristics of Cement Concrete as Partial Replacement," Int. J. Mech. Prod. Eng. Res. Dev., Vol. 8, No. 1, PP. 1327–1336, 2018.

[85] I. Mohammadi, H. Khabbaz, and K. Vessalas, "In-depth Assessment of Crumb Rubber Concrete (CRC) Prepared by Water-Soaking Treatment Method for Rigid Pavements," Constr. Build. Mater., Vol. 71, PP. 456–471, 2014.

[86] T. Gupta, S. Chaudhary, and R. K. Sharma, "Assessment of Mechanical and Durability Properties of Concrete Containing Waste Rubber Tire as Fine Aggregate," Constr. Build. Mater., Vol. 73, PP. 562–574, 2014.

[87] L. Gu and T. Ozbakkaloglu, "Use of Recycled Plastics in Concrete: A Critical Review," Waste Manag., Vol. 51, PP. 19–42, 2016.

[88] D. Foti, "Preliminary Analysis of Concrete Reinforced with Waste Bottles PET Fibers", Constr. Build. Mater., Vol. 25, No. 4, PP. 1906–1915, 2011, doi: 10.1016/j.conbuildmat.2010.11.066.

[89] O. Karahan and C. D. Atiş, "The Durability Properties of Polypropylene Fiber Reinforced Fly Ash Concrete," Mater. Des., Vol. 32, No. 2, PP. 1044–1049, 2011.

[90] R. A. Mahmood and N. U. Kockal, "Effects of Silica Fume and

Micro Silica on the Properties of Mortars Containing Waste PVC Plastic Fibers," Microplastics, Vol. 1, No. 4, PP. 587–609, 2022.

[91] M. S. Meddah and M. Bencheikh, "Properties of Concrete Reinforced with Different Kinds of Industrial Waste Fibre Materials," Constr. Build. Mater., Vol. 23, No. 10, PP. 3196–3205, 2009.

[92] J. M. Irwan, R. M. Asyraf, N. Othman, H. B. Koh, M. M. K. Annas, and S. K. Faisal, "The Mechanical Properties of PET Fiber Reinforced Concrete from Recycled Bottle Wastes," Adv. Mater. Res., Vol. 795, No. March, PP. 347–351, 2013.

[93] E. T. Dawood and T. W. Ghanim, "Mechanical Properties of Mortar Using Polypropylene Fibers," J. Civ. Eng. Res. Technol., Vol. 2, No. 1, PP. 1–4, 2020.

[94] L. A. Abdulateef, S. H. Hassan, and A. M. Ahmed, "Exploring the Mechanical Behavior of Concrete enhanced with Fibers derived from recycled Plastic Bottles," Eng. Technol. Appl. Sci. Res., Vol. 14, No. 2, PP. 13481–13486, 2024.

[95] Y. B. I. Shaheen and E. A. Eltehawy, "Structural Behaviour of Ferrocement Channels Slabs for Low-Cost Housing," Chall. J. Concr. Res. Lett., Vol. 8, No. 2, PP. 48, 2017, doi: 10.20528/cjcrl.2017.02.002.

[96] R. Park, "Ductility Evaluation from Laboratory and Analytical Testing," Proc. Ninth World Conf. Earthq. Eng., PP. 1–12, Tokyo-Kyoto, Japan, 1988.

[97] Y. Shaheen, N. Soliman, and F. El-Araby, “Repairing Reinforced Concrete Beams with Openings by Ferrocement Laminates,” Int. Conf. Civ. Archit. Eng., Vol. 12, No. 12, PP. 1–20, Cairo, Egypt 2018.

[98] I. Bin Muhit, N. E. T. Jitu, and M. R. Alam, “Structural Shear Retrofitting of Reinforced Concrete Beam: Multilayer Ferrocement Technique,” Asian J. Civ. Eng., Vol. 22, No. 2, PP. 191–203, 2021, doi: 10.1007/s42107-020-00306-3.

[99] Q. N. Abdullah and A. I. Abdulla, “Flexural Behavior of Hollow Self-Compacted Mortar Ferrocement Beam Reinforced by GFRP Bars”, Case Stud. Constr. Mater., Vol. 17, No.1, August, PP. e01556, 2022, doi: 10.1016/j.cscm. 2022.e01556.

[100] Q. N. Abdullah, A. I. Abdulla, and M. Al-Mashaykhi, “Shear Behavior of Hollow Ferrocement Beam Reinforced by Steel and Fiberglass Meshes,” Tikrit J. Eng. Sci., Vol. 29, No. 4, 2022.

[101] A. Jawhar, A. Al-Hadithi, and Y. Mansoor, “Investigate the Fresh and Hardened Properties of Shotcrete Concrete Contains Different Types of Plastic Fibers,” Iraqi J. Civ. Eng., Vol. 16, No. 2, PP. 90–100, 2023, doi: 10.37650/ijce.2022.160209.

[102] A.M. Ramadan, “Repair and Strengthening of Rc Slabs Using Ferrocement Layers Reinforced with Different Frp Meshes,” ERJ. Eng. Res. J., Vol. 40, No. 1, PP. 47–57, 2017.

[103] ASTM International, “Standard Test Method for Flexural Toughness and First-Crack Strength of Fiber-Reinforced Concrete (Using Beam with Third-Point Loading) ASTM C1018,”., Vol. 04, PP. 1–8, 1998.

[104] M. B. Zisan, B. K. Biswas, M. A. Hasan, M. Chanda, and A. Dhar, “Flexural Performance of Reinforced Concrete Beams Retrofitted Using Ferrocement Wire Mesh,” Archit. Eng., Vol. 8, No. 1, PP. 71–81, 2023.

[105] T. F. Yuan, S. H. Hong, H. O. Shin, and Y. S. Yoon, “Bond Strength and Flexural Capacity of Normal Concrete Beams Strengthened with No-Slump High-Strength, High-Ductility Concrete,” Materials (Basel)., Vol. 13, No. 19, 2020.

[106] W. Iesa, M. Alferjani, N. Ali, and A. Abdul Samad, “Study on Shear Strengthening of RC Continuous Beams with Different CFRP Wrapping Schemes,” Int. J. Integr. Eng., Vol. 2, No. 2, PP. 1–10, 2010.

[107] S. M. Alzabidi, G. Diaa, A. A. Abadel, K. Sennah, and H. Abdalla, “Rehabilitation of Reinforced Concrete Beams Subjected to Torsional Load Using Ferrocement,” Case Stud. Constr. Mater., Vol. 19, No. August, PP. e02433, 2023.

[108] W. M. Iesa, M. B. S. Alferjani, N. Ali, and A. A. Abdul Samad, "Study on Shear Strengthening of RC Continuous Beams with Different CFRP Wrapping Schemes," Int. J. Integr. Eng., Vol. 2, No. 2, PP. 35–42, Jan. 2010.

[109] K. I. Mohammad, “Behavior of Rc Beams Strengthened With CFRP Under Combined Actions,” Dr. Philos. Thesis Univ. Mosul, March, 2011.

[110] A. M. Hussein and A. Abdul-Ameer, “Torsional Response Forecasting of Reinforced Concrete Beams Strengthened with Ferrocement,” AIP Conf. Proc., Vol. 3219, PP. 3291–3299, 2024.

[111] A. J. Kilani, B. D. Ikotun, and R. Abdulwahab, “Effect of Crumb Rubber on Concrete’s and Mortar’s Structural Properties: A Review”, Iran. J. Sci. Technol., Trans. Civ. Eng. Vol. 49, No. 2. Springer International Publishing, 2024.

[112] M. M. Al-Tayeb, and H. Md Akil, “Effect of Partial Replacement of Sand by Fine Crumb Rubber on Impact Load Behavior of Concrete Beam: Experiment and Nonlinear Dynamic Analysis,” Mater. Struct. Constr., Vol. 46, No. 8, PP. 1299–1307, 2013.

[113] B. S. Mohammed, M. Adamu, and N. Shafiq, “A Review on the Effect of Crumb Rubber on the Properties of Rubbercrete,” Int. J. Civ. Eng. Technol., Vol. 8, No. 9, PP. 599–615, 2017.

[114] A. A. Jawhar, "Properties and Flexural Behavior of Reinforced Shotcrete Concrete One-Way Slabs Containing Different Types of Fibers," M.S. thesis, Dept. Civil Eng., Univ. Anbar, 2022.

[115] A. M. Enad, Y. A. Mansoor, and A. I. Al-Hadithi, "Flexural Behaviour of Reinforced Shotcrete Beams Comprehending Waste Plastic Fiber," Wasit J. Eng. Sci., Vol. 12, No. 1, PP. 66–75, 2024.

[116] A.M. Ramadan, ‘Repair and Strengthening of Rc Slabs Using Ferrocement Layers Reinforced with Different FRP Meshes’, ERJ. Eng. Res. J., Vol. 40, No. 1, PP. 47–57, 2017, doi: 10.21608/erjm.2017.66332.

[117] I. G. Shaaban, E. L. Elsayed, O. A. Kamal, and P. A. Adesina, “Flexural Characteristics of Lightweight Ferrocement Beams With Various Types of Core Materials and Mesh Reinforcement,” Constr. Build. Mater., Vol. 171, PP. 802–816, 2018.

Appendix- A

Analysis of Simply Supported Beam

Appendix- A

Analysis of Simply Supported Beams

The beams used in this study were analyzed based on ACI 318 M-2019. Take fy= 580 MPa, f'c = 30 MPa and cover= 20 mm. Beam cross section were width=150 mm, height=250 mm and length= 1800 mm, d=215 mm, d′=35 mm and reinforced as shown in Figure (A-1).

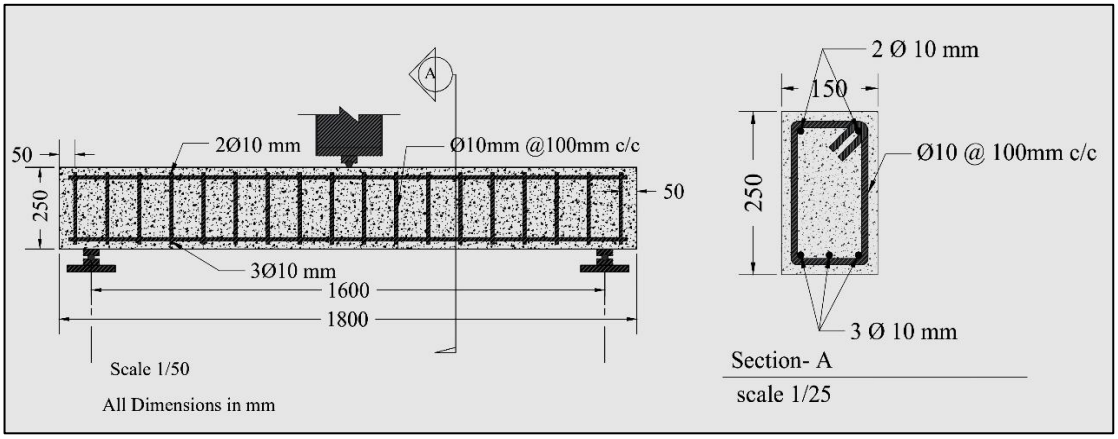

Figure (A-1): Details of Beam

For Flexural

As= 3×78.54=235.62mm^2

$\rho max=0.85\times\beta1\times\frac{f'_c}{f_y}\times\frac{\epsilon_u}{\epsilon_u+0.004}$ where ϵ_u=0.003

when 28<f'_c<50 MPa

$\beta1=0.85-\frac{0.05(f'_c-28)}{7}\Rightarrow 0.836$

$\rho_{max}=0.85\times0.836\times\frac{30}{580}\times\frac{0.003}{0.003+0.004}\Rightarrow 0.01575$

$\rho=\frac{As}{b.d}\Rightarrow\frac{235.62}{150\times215}=7.3\times10^{-3}<\rho max=0.01575\ \therefore$ under reinforced section

$$\omega=\frac{\rho f_y}{f'_c} \Longrightarrow \frac{7.3\times10^{-3}\times580}{30}=0.1412$$

$$\frac{Mn\times10^6}{f'_c.\ b.\ d^2}=\omega-0.59\omega^2$$

$$\frac{Mn\times10^6}{30\times150\times215^2}=0.1412-0.59\times0.1412^2 \Longrightarrow Mn=26.92\ kN.m$$

$$a=\frac{As\ f_y}{0.85\ f'_c\ b} \Longrightarrow \frac{235.62\times580}{0.85\times30\times150}=35.73mm$$

$$c=\frac{a}{\beta1} \Longrightarrow \frac{35.73}{0.836}=42.74\ mm$$

$$\epsilon t=\frac{d-c}{c}\times0.003 \Longrightarrow \frac{215-42.74}{42.74}\times0.003=0.0121>0.005 \therefore \text{Ø}=0.9$$

$$Mn=\frac{P_n\times L_n}{4}$$

$$\text{Max load (Pu)}=\frac{\frac{26.92}{0.9}\times4}{1.6}=74.78\ kN$$

For shear

$$Vc=\frac{\sqrt{f'_c}}{6}\ b\times d \Longrightarrow \frac{\sqrt{30}}{6}\times150\times0.215=29.44\ kN$$

By using Ø10mm@100mm c/c

Av = 2×Ab by using Ø10mm

$Av=2\times78.54=157.08\ mm^2$

$$Vs=\frac{A_v\times f_{y_t}\times d}{s}$$

$$Vs=\frac{157.08 \times 580 \times 215}{100}$$

Vs= 195.8 kN

Vn = Vs + Vc

Vn = 195.8+ 29.44= 225.2 kN

ØVn = 0.75× 225.2→168.9 kN

$$Vu = \frac{P_u}{2} \Longrightarrow \frac{74.78}{2} = 37.39 \text{ kN}$$

If ØVn > Vu ∴ No shear failure is expected.

$$\rho_{Stirrup} = \frac{Av}{b \times s} \Longrightarrow \frac{157.08}{150 \times 100} = 0.010466$$

Deflection calculation.

$$fr = 0.62\lambda\sqrt{f'_c} = 0.62\sqrt{30} = 3.396 \text{ MPa}$$

$$E = 4700\sqrt{f'_c} \Longrightarrow 4700 \times \sqrt{30} = 25742.96 \text{ MPa}$$

$$Ig = \frac{bh^3}{12} \Longrightarrow \frac{150 \times 250^3}{12} = 195312500 \text{ mm}^4$$

$$fr = \frac{Mcr \times y}{Ig}$$

$$3.396 = \frac{Mcr \times 125}{195312500} \Longrightarrow Mcr = 5.306 \text{ kN.m}$$

$$n = \frac{E_S}{E_c} \Longrightarrow \frac{200000}{25742.96} \Longrightarrow 7.77$$

$$\frac{b\times c^2}{2} - \left(n\times As\times(d-c)\right)= 0$$

$$\frac{150\times c^2}{2} - \left(7.77\times 235.62\times(215-c)\right)=0$$

$c= 61.26$ mm

$$I_{cr}=\frac{b\times c^3}{3} + (n\times As\times(d-c)^2)$$

$$I_{cr}=\frac{150\times 61.26^3}{3} + (7.77\times 235.62\times(215-61.26)^2)$$

$I_{cr}=54.766\times10^6$ mm^4

$$Ma=\frac{P_u\times L_n}{4} \Longrightarrow \frac{74.78\times 1.6}{4}$$

$Ma=29.912$ kN.m > $Mcr = 5.306$ kN. m $\therefore$ use I_{eff}

$$I_{eff}=\left(\frac{M_{cr}}{M_a}\right)^3\times I_g+\left[1-\left(\frac{M_{cr}}{M_a}\right)^3\right]\times I_{cr}$$

$$I_{eff} = \left(\frac{5.306}{29.912}\right)^3 \times 195312500 + \left[1-\left(\frac{5.306}{29.912}\right)^3\right]\times 54.766 \times 10^6$$

$$I_{eff} = 55.5505 \times 10^6 \text{ mm}^4$$

$$\Delta \text{ mid}=\frac{5\times M_d\times L_n^{\,2}}{48\ EI_{eff}}$$

$$\Delta \text{ mid}=\frac{5\times 29.912\times 10^6\times 1600^2}{48\times 25742.96\times 55.5505\times 10^6}=5.6 \text{ mm}$$

First Cracking Load of RC Beam.

$$M_{cr}=\frac{f_r \times I_g}{y_b}$$

$$fr = 0.62\lambda\sqrt{f'_c}= 0.62\sqrt{30}=3.396 \text{ MPa}$$

y_b = Distance from the neutral axis to the bottom of the specimen.

$\bar{y}$ =125 mm

$$Ig=\frac{bh^3}{12} \Longrightarrow \frac{150\times250^3}{12}=195312500 \text{ mm}^4$$

$$M_{cr}=\frac{3.396\times 195312500}{125}=5.30625 \text{ kN.m}$$

$$M_{cr}=\frac{P_{cr} \times L}{4} \Longrightarrow 5.30625=\frac{P_{cr}\times 1.6}{4} \Longrightarrow P_{cr}=13.267 \text{ kN}$$

Cracking load of RC beam strengthened with ferrocement from three side with welded wire mesh.

$$M_{cr}=\frac{f_r \times I_g}{y_b}$$

$$fr = \text{ for crack} = 0.62\lambda\sqrt{f'_c} = 0.62\sqrt{30} = 3.396 \text{ MPa}$$

y_b = Distance from the neutral axis to the bottom of the specimen.

$$A.\bar{y}=\sum a.y$$

$$[(150\times250)+(25\times200)+ (2\times25\times250)]\bar{y}$$

$$=(150\times250\times150)+(25\times200\times12.5)+(2\times25\times250\times150)$$

$\bar{y}$ =137.5 mm

$Ig=I+Ad^2 \Longrightarrow$

$$\frac{150\times250^3}{12}+\left(150\times250\times12.5^2\right)+\frac{200\times25^3}{12}+(200\times25\times125^2)+$$

$$2\times(\frac{25\times250^3}{12}+(25\times250\times12.5^2))$$

$=346786458.3\ mm^4$

$$M_{cr}=\frac{3.396\times\ 346786458.3}{137.5}=8.56\ kN.m$$

$$M_{cr}=\frac{p_{cr}\times L}{4}\Longrightarrow 8.56=\frac{P_{cr}\times 1.6}{4}\Longrightarrow P_{cr}=21.412\ kN$$

Cracking load of RC beam strengthened with ferrocement from four side welded wire mesh

$$M_{cr}=\frac{f_r\times I_g}{y_b}$$

$$fr = \text{ for crack} = 0.62\lambda\sqrt{f'_c} = 0.62\sqrt{30} = 3.396\ \text{MPa}$$

y_b = Distance from the neutral axis to the bottom of the specimen

y_b =150 mm

$$Ig=I+Ad^2\Longrightarrow\frac{200\times300^3}{12}=450\times10^{\ 6}mm^4$$

$$M_{cr}=\frac{3.396\times\ 450\times10^{\ 6}}{150}=10.2\ kN.m$$

$$M_{cr}=\frac{p_{cr}\times L}{4}\Longrightarrow 10.2=\frac{P_{cr}\times 1.6}{4}\Longrightarrow P_{cr}=25.5\ kN$$

Appendix- B

Mix Design

Appendix- B

Mix Design

The target 28-day compressive strength is 30 MPa. Based on aggregate properties in the table below, the mix was designed according to ACI 211.1-22.

Table (B.1): Properties of Aggregate

Properties	Coarse Aggregate	Fine Aggregate
Specific Gravity (SSD)	2.691	2.6042
Absorption %	0.662	2.46
Surface Moisture %	1.5	1.53
Fineness Modulus	6.7	2.61
Dry rodded unit weight (Kg/m^3)	1626	---
Max aggregate sizes (mm)	19	---

Cement Specific Gravity= 3.15

Step 1 – Slump

Use slump = (75-130) mm

Step 2 – Max. Agg. Size

Use the max aggregate size available = 19 mm

Step 3 – Water Content and Air Content

Use non- air-entrained concrete.

Weights of water = 205 Kg/m^3

Air content = 2%

Step 4 – Water Cementitious Material

Target compressive strength = 30 MPa

w/c = 0.5387

Step 5 – Cement Content

From w/c = 0.5387 and Weights of water = 205

$C=\frac{205}{0.5387} \rightarrow C\ 380.55\ Kg/m^3$

Step 6 – Weight of Course Aggregates.

Use fineness modulus = 2.61 and M.A.S = 19 mm,

Get: - Volume of course agg. = 0.639

Weight of course agg. = $0.639 \times 1626 = 1039\ Kg/m^3$

Step 7 – Weight of Fine Agg.

Using Volume Method: -

Volume of water= $\frac{205}{1000} \Longrightarrow 0.205 m^3$

Volume of Cement= $\frac{380.55}{1000 \times 3.15} \Longrightarrow 0.1208\ m^3$

Volume of Coarse agg.= $\frac{1039}{1000 \times 2.691} \Longrightarrow 0.3861\ m^3$

Volume of Air=$0.02\ m^3$

Total volume =$0.7319\ m^3$

Volume of fine agg. = 1 – 0.7319=$0.2681\ m^3$

Weight of fine agg. = $0.2681 \times 1000 \times 2.6042 = 698\ Kg/m^3$

Correct unit to S.S.D

1- Weight of Course agg. = $1039 \times 1.02162 = 1061.5\ Kg/m^3$

2- Weight of Fine agg. = $698 \times 1.0399 = 726\ Kg/m^3$

3- Weight of water=205- (1039 ×0.015)- (698×0.0153) =$178.74\ Kg/m^3$

Based on estimated concrete weight for 1 m^3

Water 179 Kg/m^3

Cement 381 Kg/m^3

Fine agg. wet 726 Kg/m^3

Coarse agg. wet 1062 Kg/m^3

The Mix Proportions 1: 1.906: 2.787 / 0.47

Appendix- C

Estimate the Ultimate Load by Theoretical Calculations

Appendix- C

Estimate the Ultimate Load by Theoretical Calculations

Many studies utilized finite element simulation, numerical solutions, and mathematical modeling to estimate the ultimate loads of ferrocement structural elements. This study used a method established by ACI 549R-18, Qutaiba et al. (2022) and Shaaban et al. (2018) to calculate the theoretical ultimate load. The following fundamental assumptions are employed in the computation of the ultimate load.

1. As illustrated in Figure (C-1), strains in the reinforcement and mortar matrix are proportional to distance from the neutral axis.
2. When strain reached to 0.003 indicated that failure occurs in ferrocement.
3. The tensile contribution of the mortar matrix is ignored at ultimate load and the compressive contribution is equal to (0.85fc′. a. b) as shown in the Figure (C-1).

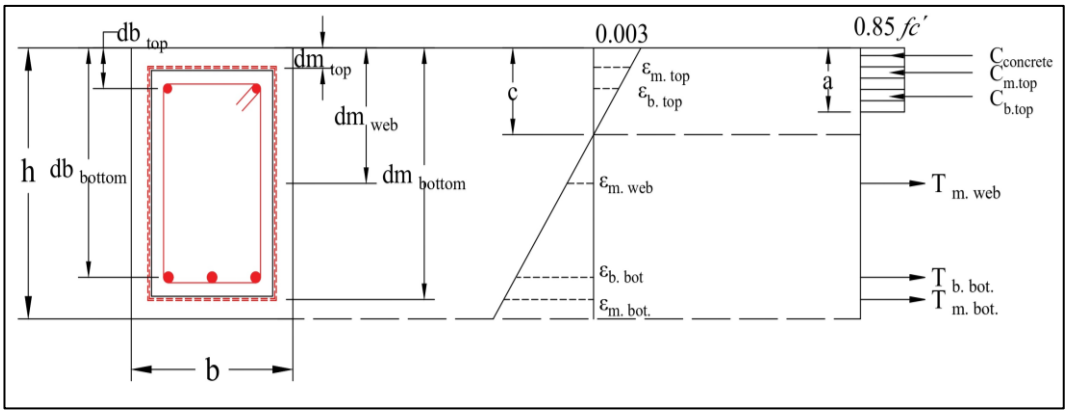

A. Full Wrapping

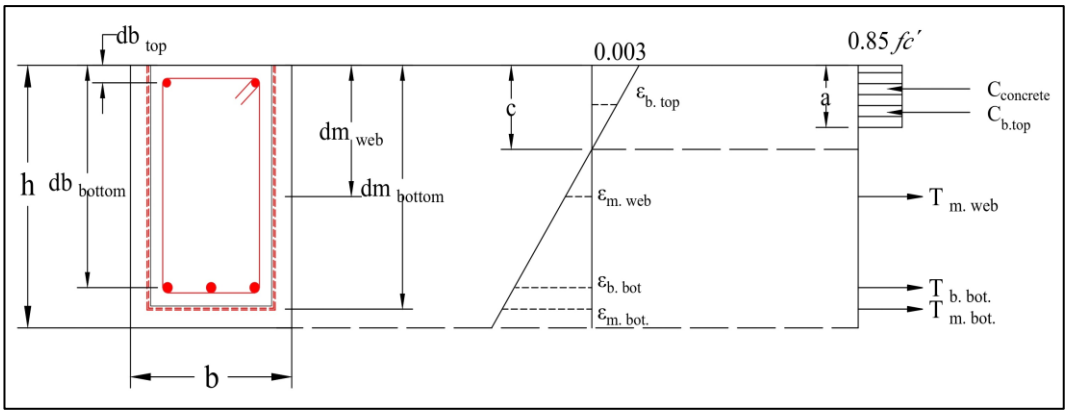

B. U Shape Wrapping

Figure (C-1): Stress-Strain Distribution of Beam with Ferrocement

From Figure (C- 1) shows that the strain and internal force in the steel bars, mesh reinforced, mortar and concrete are at equilibrium.

$$C = T \quad \text{(C-1)}$$

$$C = 0.85 \times fc' \times a \times b \quad \text{(C-2)}$$

$$\text{Where } a = \beta 1 \times c \quad \text{(C-3)}$$

$$\beta 1 = 0.85 - \frac{0.05}{7}(fc' - 28) \geq 0.65 \quad \text{(C-4)}$$

$$T = \sum T + C = C_{m\ top} + C_{b\ top} + T_{m.web} + T_{b.bot.} + T_{m.bot.} \quad \text{(C-5)}$$

$$C_{m\ top} = (\sigma - 0.85 \times fc')\times A)_{m\ top} \text{ (Compression)} \quad \text{(C-6)}$$

$$C_{b\ top} = (\sigma \times A)_{b\ top} \quad \text{(Compression)} \quad \text{(C-7)}$$

$$T_{m\ web}=(\sigma\times A)_{m\ web}\times \text{No. of webs} \quad \text{(C-8)}$$

$$T_{m\ bot.}=(\sigma\times A)_{m\ bot.} \quad \text{(C-9)}$$

$$\sigma_{m\ top}=E_m\times\varepsilon_{m\ top}\leq F_{u\ m} \quad \text{(C-10)}$$

$$\sigma_{b\ top}=E_b\times\varepsilon_{b\ top}\leq F_{u\ b} \quad \text{(C-11)}$$

$$\sigma_{m\ web}=E_m\times\varepsilon_{m\ web}\leq F_{u\ m} \quad \text{(C-12)}$$

$$\sigma_{b\ bot.}=E_b\times\varepsilon_{b\ bot.}\leq F_{u\ b} \quad \text{(C-13)}$$

$$\sigma_{m\ bot.}=E_m\times\varepsilon_{m\ bot.}\leq F_{u.m} \quad \text{(C-14)}$$

Where:

$A_{m\ top}$ = Area of the welded steel wire or glass fiber mesh at top.

$A_{b\ top}$ = Area of the steel bars at top of the beams.

$A_{m\ web}$ = Area of the welded steel wire or glass fiber mesh at web.

$A_{b\ bot.}$ = Area of the steel bars at bottom of the beams.

$A_{m\ bot.}$ = Area of the welded wire or glass fiber mesh at bottom.

a = Depth of the compression zone.

b = Width of the beam.

c = Depth of neutral axis from the top of the beam.

E_b = Modulus of elasticity of the steel bars.

E_m = Modulus of elasticity of the welded wire or fiber glass mesh.

$F_{u\ b}$ = Ultimate strength of the steel bars.

$F_{u\ m}$ = Ultimate strength of the mesh.

f_c' = Compressive strength of ferrocement matrix.

C = Internal forces in compression zone.

T_i = Internal forces in tension zone.

$\sigma_{m\ top}$, $\varepsilon_{m\ top}$ = Stress and strain of mesh at the top of the beam.

$\sigma_{b\ top}$, $\varepsilon_{b\ top}$ = Stress and strain steel bars.

$\sigma_{m\ web}$, $\varepsilon_{m\ web}$ = Stress and strain of mesh at the sides of the beam.

$\sigma_{b\ bot.}$, $\varepsilon_{b\ bot.}$ = Stress and strain of bottom steel bars.

$\sigma_{m\ bot}$, $\varepsilon_{m\ bot.}$= Stress and strain of mesh at the bottom of the beam.

The strain at the top, bottom and web mesh, top and bottom bars, can be determined based on the geometry of the strain distribution as shown in Figure (C-1). Excel sheet is used by trial and error method to determine the location of the neutral axies (c). After that, calculation of the ultimate moment (Mu) by taking the moment about the point of application of the compressive force is done as follows:

$$M_{ult.}=\sum C \text{ or } T\times\left(d_i-\frac{a}{2}\right) \qquad \text{(A-16)}$$

The ultimate load (P_{ult}) of beam tested under center point loading can be determined from

$$M_u=\frac{P_{ult}\times L}{4} \qquad \text{(A-17)}$$

Where L = the clear span of beam

P_{ult} = the ultimate load for flexure failure

الخلاصة

تهدف هذه الدراسة إلى ايجاد تأثير استخدام مونة الفيروسمنت المستدامة وتقييم كفاءتها مقارنةً بالمونة التقليدية، وكذلك إيجاد تأثير استخدام أنواع مختلفة من التسليح في الفيروسمنت لإعادة تأهيل العتبات الخرسانية المغلفة من أربع جوانب او من ثلاث جوانب. قسم البرنامج العملي الى ثلاث اجزاء: يتضمن القسم الأول البرنامج التجريبي المُعد لدراسة تأثير استخدام مواد اسمنتية تكميلية مثل دخان السيليكا ومخلفات الإطارات المطاطية وألياف المخلفات البلاستيكية على الخواص الميكانيكية للمونة الفيروسمنت المستدامة. أشارت النتائج إلى أن إضافة ٨٪ من دخان السيليكا، و٥٪ من المخلفات الاطارات المطاطية، و٠.٧٥٪ من ألياف المخلفات البلاستيكية يتمثل بالخليط الأمثل. وبالمقارنة مع الخلطة المرجعية عند عمر ٢٨ يوم، انخفضت مقاومة الانضغاط بنسبة ٤٢,٧٪، ومقاومة الانحناء بنسبة ٢٥,٢٦٪، ومقاومة الشد بنسبة ١,٩٧%.

يتناول القسم الثاني العتبات المحملة مسبقًا. تم اختبار عتبتين الى حد الفشل تحت حمل نقطي مركز وتم تحميل العتبات الثمانية الأخرى بنسبة ٧٠٪ من الحمل الأقصى الناتج عن العتبات المرجعية. في القسم الثالث، أُجرى عمل تجريبي للتحقيق من أداء العتبات الخرسانة المسلحة المعاد تأهيلها باستخدام مونة الفيروسمنت التقليدية او المستدامة والمسلحة باستخدام (شبكة سلكية ملحومة او شبكة من الألياف الزجاجية). التغليف الذي كان تغليفًا كاملاً للعتبة من أربعة جوانب او من ثلاث جوانب.

أظهرت النتائج أن استخدام الفيروسمنت أدى إلى تحسين فعال في الحمل الأقصى وتأخير ظهور التشققات مقارنةً بالعتبات المرجعية. كان أعلى تحسن في الحمل الاقصى (١٣,٦) ٪ للعتبة المغلفة من أربعة جوانب باستخدام المونة التقليدية والمسلحة بشبكة سلكية ملحومة، بينما ازداد الحمل الاقصى للعتبة المسلحة بشبكة الألياف زجاجية بنسبة (١٠,٣) ٪.

كانت المطيلية للعتبات المُعاد تأهيلها باستخدام المونة المستدامة أعلى من المونة التقليدية بنسبة (٣,٦, ٥,٤) ٪، وازداد امتصاص الطاقة بنسبة (١١,٩, ١٠,٦) ٪ للعتبات المُغلّفة بالكامل والمسلحة بشبكة سلكية ملحومة وشبكة من الألياف الزجاجية، على التوالي.

انخفضت صلابة العتبات المؤهلة باستخدام المونة المستدامة والمغلفة من أربع وثلاث جوانب والمسلحة بشبكة سلكية ملحومة بنسبة (٢٠,٣, ١٥,٤٥) ٪ مقارنة بالمونة التقليدية، كما انخفضت الصلابة عند التسليح بشبكة الألياف الزجاجية انخفضت الصلابة بنسبة (١٨,٧٥, ١٣,٨) ٪ مقارنة بالمونة التقليدية، على التوالي.

كان الانحراف في العتبات المعاد تأهيلها باستخدام المونة التقليدية أقل من الانحراف في العتبات المرجعية والعتبات المعاد تأهيلها باستخدام المونة المستدامة.

شكر وتقدير

بدايةً، أتقدم بالشكر والامتنان لله تعالى على نعمه التي لا تُحصى، وعلى توفيقه لي في إتمام هذا العمل.

ثم أتقدم بالشكر الجزيل للأستاذ المساعد الدكتورة سلوى مبارك عبد الله، وللدكتورة منى مبارك عبد الله، على دعمهما وإرشادهما المتواصل. فلولا عنايتهما الكبيرة وأمانتهما العلمية، لما كان هذا العمل ممكنًا.

كما أتقدم بالشكر الجزيل للأستاذ المساعد عمر محمد حمدون، عميد كلية الهندسة، والأستاذ المساعد الدكتور براء جبار محمود الدكتور، رئيس قسم الهندسة المدنية. كما أتقدم بالشكر الجزيل لأعضاء هيئة التدريس الذين أرشدوني طوال فترة دراستي، وخاصةً الدكتور خلف إبراهيم، والأستاذ الدكتور معتز العبيدي، والأستاذ المساعد الدكتور سفيان يونس أحمد، وفريق مختبر فحص المواد في قسم الهندسة المدنية على دعمهم القيّم.

شكر خاص لوالدي العزيز، ووالدتي الفاضلة، وإخوتي وأخواتي الأعزاء على تشجيعهم ودعمهم المتواصل خلال مسيرتي الدراسية.

أود أن أعرب عن حبي وشكري الخاص لزوجتي الرائعة وبناتي، وأنا ممتن للغاية لوجودكم بجانبي. لقد ساهم صبركم وتفهمكم ودعمكم الكبير في تحقيق هذه الرحلة.

إلى أصدقائي الأعزاء، الذين كانوا بجانبي في كل خطوة: لطفكم ودعمكم يعنيان لي الكثير، وأقدر كل واحد منكم تقديرًا كبيرًا.

إقرار المشرف

نشهد أن إعداد هذه الرسالة الموسومة " **أداء العتبات الخرسانية المسلّحة المقواة بمونة الاسمنت المُعزز المستدامة** " جرى بإشرافنا في جامعة الموصل / كلية الهندسة وهي جزء من متطلبات نيل شهادة الماجستير علوم في الهندسة المدنية / انشاءات.

التوقيع: **التوقيع:**

المشرف: أ.م.د. سلوى مبارك عبدالله **المشرف: م.د. منى مبارك عبدالله**

التاريخ: / / **التاريخ: / /**

إقرار المقوم اللغوي

أشهد أن إعداد هذه الرسالة الموسومة " **أداء العتبات الخرسانية المسلّحة المقواة بمونة الاسمنت المُعزز المستدامة** " تمت مراجعتها من الناحية اللغوية وتصحيح ما ورد فيها من أخطاء لغوية وتعبيرية وبذلك أصبحت الرسالة مؤهلة للمناقشة بقدر تعلق الأمر بسلامة الأسلوب وصحة التعبير.

التوقيع:

الاسم: أ.م.د. علي حمادة مكلد

التاريخ: / /

إقرار رئيس لجنة الدراسات العليا

بناءً على توصيتي المشرف والمقوم اللغوي، أرشح هذه الرسالة للمناقشة.

التوقيع:

الاسم: أ.د. معتز عبد الجبار العبيدي

التاريخ: / /

إقرار رئيس القسم

بناءً على توصيات المشرف والمقوم اللغوي ورئيس لجنة الدراسات العليا، أرشح هذه الرسالة للمناقشة.

التوقيع:

الاسم: أ.م.د. براء جبار محمود

التاريخ: / /

إقرار لجنة المناقشة

نشهد نحن أعضاء لجنة التقويم والمناقشة الموقعون أدناه إننا قد اطلعنا على رسالة الطالب **(جون مازن فرج عبوش)** والموسومة **(أداء العتبات الخرسانية المسلّحة المقواة بمونة الاسمنت المُعزز المستدامة)** وناقشناها في محتوياتها وفيما له علاقة بها بتاريخ ١/ ٩ /٢٠٢٥ وقررنا إنها جديرة لنيل شهادة ماجستير علوم في الهندسة المدنية / انشاءات.

التوقيع:	التوقيع:	التوقيع:
رئيس اللجنة:	عضو اللجنة:	عضو اللجنة:
أ.م. د. سفيان يونس احمد	أ.م.د. عمر محمد عبد الكريم	م. د. ايمان خالد إبراهيم
المرتبة العلمية: أستاذ مساعد	المرتبة العلمية: أستاذ مساعد	المرتبة العلمية: مدرس
التاريخ: / /٢٠٢٥	التاريخ: / /٢٠٢٥	التاريخ: / /٢٠٢٥

التوقيع:	التوقيع:
عضو اللجنة (مشرف اول): أ.م.د. سلوى مبارك عبدالله	عضو اللجنة (مشرف ثاني): م.د. منى مبارك عبدالله
المرتبة العلمية: أستاذ مساعد	المرتبة العلمية: مدرس
التاريخ: / /٢٠٢٥	التاريخ: / /٢٠٢٥

إقرار مجلس الكلية

اجتمع مجلس كلية الهندسة بجلسته ( ) المنعقدة في ( )
وقرر الاتي :
يوصي المجلس بمنح شهادة ماجستير علوم في الهندسة المدنية / انشاءات.

أ. م. د. ايمن طالب حميد	أ.م.د. عمر محمد حمدون
مقرر مجلس الكلية	**عميد الكلية**
/ /	/ /

جامعة الموصل

كلية الهندسة

أداء العتبات الخرسانية المُسلّحة المقواة بمونة الاسمنت المُعزز المستدامة

رسالة ماجستير علوم في الهندسة المدنية / انشاءات

جون مازن فرج عبوش

إلى

مجلس كلية الهندسة في جامعة الموصل كجزء من متطلبات نيل شهادة ماجستير علوم في الهندسة المدنية / الانشاءات

بإشراف

الأستاذ المساعد الدكتور

سلوى مبارك عبدالله

المدرس الدكتور

منى مبارك عبدالله

١٤٤٧هـ

٢٠٢٥م

جامعة الموصل

كلية الهندسة

أداء العتبات الخرسانية المُسلّحة المقواة بمونة الاسمنت المُعزز المستدامة

جون مازن فرج عبوش

رسالة ماجستير علوم في الهندسة المدنية / الانشاءات

بإشراف

الأستاذ المساعد الدكتور

سلوى مبارك عبدالله

المدرس الدكتور

منى مبارك عبدالله

١٤٤٧هـ

٢٠٢٥م